INTEGRATED DESIGN AND CONTROL UNDER UNCERTAINTY

INTEGRATED DESIGN AND CONTROL UNDER UNCERTAINTY

by

Rohil Jaydeep, BASc

A Thesis
Submitted to the School of Graduate Studies
in Partial Fulfillment of the Requirements
for the Degree
Master of Applied Science

McMaster University

MASTER OF APPLIED SCIENCE (2018) McMaster University

(Chemical Engineering) Hamilton, Ontario, Canada

TITLE:	Integrated Design and Control under Uncertainty
AUTHOR:	Rohil Jaydeep, BASc
	(University of Toronto, Toronto, ON)
SUPERVISOR:	Dr. Christopher L.E. Swartz
NUMBER OF PAGES:	xiv, 93

ABSTRACT

Market variation such as changing utility price or demand can lead to non-static operation of chemical plants, such as in cases where new objectives must be met, or varying operating conditions can be taken advantage of to increase operational profit. Integrated design and control (where both the design and operation are considered simultaneously when the design of the plant is being formulated) can be used to address the challenges that plants that operate under uncertainty may face. When considering demand uncertainty for a plant, not only must the different realizations of demand be considered, but how the plant transitions from one demand to another is also of interest.

Ideally when transitioning, the plant must quickly and feasibly transition from one operating point to another. In the first study of this thesis we consider the benefit of taking into account the demand transitions a plant must undergo; compared to only considering the final operating states. In this study we examine an air separation unit (ASU) since in industrial practice ASUs can often be subject to demand uncertainty. Assessing the impact that an ASU design has on its dynamic response characteristics motivates us to include plant dynamics in the design formulation. Using a two-stage stochastic optimization framework, the optimal design parameters are found for a nitrogen plant operating under uncertain demand. Three design paradigms are explored and compared - a nominal steady-state design, a flexible design that maintains steady-state feasibility, and a dynamically operable design that enforces feasibility of dynamic transitions. The designs obtained are subjected to random demand changes to evaluate the expected economic return under transitions not directly designed for. From this study we see that when the dynamically operable design and the flexible design are both subject to dynamic transitions, the dynamically operable design in certain cases can provide more economic benefit during transition and at the final steady state.

In the second study of this thesis we address an important issue that arises when uncertainty in the plant operation is captured by utilizing two-stage stochastic optimization. If the optimization formulation can see the uncertainty profile in its entirety, then it can make control moves and design decisions based on the fact that the optimization problem knows what operating conditions it transitions between. This may not however be a realistic assumption to operate under, as future uncertainty is unknown. Given lack of foresight into future uncertainties it is logical to currently operate at the the optimal steady-state. This poses a bilevel problem for the design and control of a plant because the feasible region is determined by an inner optimization. In this study the Karush-Kuhn-Tucker conditions are incorporated into a two-stage stochastic optimization formulation for a dynamic model of chemical plant to generate a design. This design is then compared to a design generated from an optimization formulation where future knowledge of uncertainty is assumed and it is seen that the former design can provide greater economic benefit.

ACKNOWLEDGEMENTS

I would like to thank my academic supervisor, Dr. Christopher L.E. Swartz, who has guided me throughout the entirety of my graduate studies and I have learned so much from. I would also like to acknowledge Yanan Cao and Praxair Inc. for their advice and financial support. I am also grateful to the McMaster Control Consortium and Department of Chemical Engineering at McMaster University for both their personal and financial support.

Table of Contents

List of Figures

List of Tables

Chapter 1

Introduction

Chemical processes are often subject to uncertainty from several different sources. This can include parametric uncertainty, disturbances to the process feeds and uncertainty in the economics of the process such as utility costs and market demand. Particularly in the case of economic uncertainty it may be necessary or beneficial to for a process to switch from one operating point to another. A process plant transitioning between operating points poses its own complexities as operating constraints must be maintained during the transition and ideally the transition should happen as quickly as possible. To find the designs and operating conditions of a plant that are conducive to the optimal transition, a dynamic optimization of the differential-algebraic equations (DAEs) that define the chemical process can be implemented.

In this thesis we examine paradigms and benefits of utilizing dynamic optimization for chemical processes under uncertainty. The main objectives and contributions of the studies presented in this thesis are as follows:

1. Demonstrate the benefits of dynamic optimization compared to optimization formulations that only consider the final steady-states when applied to large

scale industrial processes under uncertainty, with regards to the design and operation of the process.

2. Identify operating conditions that should be considered when dynamic optimization is used for processes under uncertainty, with regards to the design and operation of the process.

In presenting the studies done, the thesis is organized in the following manner:

Chapter 2: A literature review giving a general overview of dynamic optimization, optimization under uncertainty and integrated design and control, which are underlying concepts to the studies done in this thesis.

Chapter 3: A study that investigates the integrated design and control of nitrogen plant subject to demand uncertainty. In this study the design of the nitrogen plant given by a dynamic optimization (that takes into account transition from one demand to another) is compared and contrasted to designs generated from steady-state optimizations (which do not consider plant transitions).

Chapter 4: A study that examines how the assumptions for the initial and final operating conditions of a CSTR in series affect the design and operation of the CSTRs generated from dynamic optimization.

Chapter 5: A summary of the work done in this thesis and the takeaways and insights that have been generated from the studies done.

Chapter 2

Literature Review

2.1 Dynamic Optimization

Changing operating conditions are important to consider for chemical plants. Adjusting plant operation depending on demands or other market conditions can be used to increase operating profit or may be necessary. Thus given a plant at an operating point, ideally it should be able to transition as close to optimally as possible while maintaining feasibility. Optimal transition could consist of several metrics such operating profit during the transition or meeting the operating change as quickly as possible. Operating at an initial point and finding a time dependent control profile that meets some metric of transition poses an open loop optimal control problem, or a dynamic optimization [Chachuat, 2007].

The general form of a dynamic optimization problem as given in Barton *et al.* [1998] is:

$$\begin{aligned}
&\min_{u(t)} \int_0^{t_f} \phi(\mathbf{x}(t), \mathbf{y}(t), \mathbf{u}(t), \mathbf{p}) \\
&\text{s.t} \\
&\mathbf{f}(\dot{\mathbf{x}(t)}, \mathbf{x}(t), \mathbf{y}(t), \mathbf{u}(t), \mathbf{p}) = 0 \\
&\mathbf{h}(\mathbf{x}(t), \mathbf{y}(t), \mathbf{u}(t), \mathbf{p}) = 0 \\
&\mathbf{g}(\mathbf{x}(t), \mathbf{y}(t), \mathbf{u}(t), \mathbf{p}) \leq 0 \\
&\boldsymbol{\kappa}(\mathbf{x}(t_i), \mathbf{y}(t_i), \mathbf{u}(t_i), \mathbf{p}) \leq 0 \quad \forall i \in \{0, ...n\} \\
&\mathbf{x}(0) = \mathbf{x_o}
\end{aligned}$$

where $\mathbf{x}$, $\mathbf{y}$ and $\mathbf{u}$ are the differential, algebraic and control variables respectively, and $\mathbf{p}$ are parameters in the optimization. $\mathbf{f}$ and $\mathbf{h}$ are the differential and algebraic equations that make up the differential algebraic equations (DAE) that govern the system being optimized. $\mathbf{g}$ and $\boldsymbol{\kappa}$ are the path constraints and point constraints respectively.

Solving dynamic optimization can be categorized into two methods, variational or indirect solution methods and direct methods [Chachuat, 2007]. In the variational method a solution is obtained from the first order necessary conditions for optimality from Pontryagin's maximum principle [Cervantes and Biegler, 2009]. The first order necessary conditions is a DAE that poses a two point boundary value problem (TPBVP) to solve. Methods such as single, shooting, multiple shooting and collocation on finite elements can be used to solve the TPBVP [Cervantes and Biegler, 2009]. Incorporating inequality constraints poses problems for indirect methods, because this requires some knowledge of the variable trajectories before hand as well as causing discontinuities of the trajectories of the adjoint variables [Chachuat, 2007].

Thus there are several issues that need to be addressed when dealing with indirect methods, that can be avoided when using direct methods.

In direct methods, the optimal control problem is either partially or fully discretized and NLP methods are used to solve a dynamic optimization [Chachuat, 2007].

2.1.1 Partial Discretization

In a direct method utilizing partial discretization, only the control variables are discretized and the state variables are found by solving the DAE using integrators. Three techniques that involves partial discretization are iterative dynamic programming (IDP), single shooting and multiple shooting [Biegler, 2007].

From Luus [1993], in IDP the time horizon is split into P intervals (where P is chosen) of equal length, where the control variable is represented by either a piecewise linear or piecewise constant function on each interval. An initial profile for each interval is initially chosen and the DAE for the system is then integrated. A new profile for the control variables in interval P is then selected to find the optimal trajectory starting from the state conditions at the end interval $P-1$. We then repeat this for interval $P-1$, where we select a new control profile that optimizes the trajectory over intervals P and $P-1$. We repeat this for all the intervals in the control horizon, moving back one control interval at at time (thus we integrate one more interval every iteration). This entire procedure is repeated for a chosen number of iterates. From this an optimal profile is determined. A benefit of the IDP method is that sensitivity equations for the DAE are not needed; however IDP can only be used for smaller problems, and any constraints must be formulated as penalty terms in the objective function [Cervantes and Biegler, 2009].

In the single shooting method (which is a sequential method) the control variable is

discretized using piecewise constant or linear functions or by polynomial functions. This method is also known as control vector parametrization (CVP) [Feehery and Barton, 1999]. Given a discretized control profile, the resulting DAE is then integrated to find the state variables of the system. Thus an NLP solver is used to solve the dynamic optimization (obtaining the control profile that optimizes the objective function). However for each iteration of the NLP a DAE must be solved and this can require a lot of computational effort and the solution can be affected by the stability of the DAE [Biegler, 2007].

In the multiple shooting method we again use CVP but instead of integrating the DAE over the entire time horizon, the time horizon is split into periods, and the DAE is only integrated over each period. The initial conditions for the DAE at the start of each period are decision variables. However continuity constraints are imposed such that the initial conditions at the start of each period must be equal to the final state of the system in the previous period. This means that during the iterations to solve the dynamic optimization the state variable of the system can be discontinuous (only the optimal solution must be continuous) [Chachuat, 2007].

In the sequential methods, to the NLP solver only the control variables, constraints and objective functions exist. Gradient information is provided to the solver via sensitivity or adjoint equations [Biegler, 2007]. These equations provide the gradients of the constraints and objective functions (which are expressed in terms of the state and control variables) with respect to the control variables to the NLP solver. Sequential methods are advantageous as only an initial guess for the control profile needs to be given to the NLP solver. Because sequential methods use an integrator to find the state profiles, the accuracy of the profiles is high as the error is controlled by the integrator [Chachuat, 2007]. In the sequential method both state variable bounds and path constraints are enforced using integral square error terms for the constraints (that must be approximately zero for the entire integration horizon). Integrators that

are commonly used in sequential methods are CVODES and IDAS.

2.1.2 Full Discretization

An alternative to the sequential method is the simultaneous method. In this method the entire dynamic optimization is discretized. Thus both the state and control variables are discretized. The horizon is divided into several discrete time points and the values for the state variables at each of these time points represent the profile of the state variables. The value of the state variable at each time point is considered a separate optimization variable (as opposed to a time dependent state variable we see for sequential methods). Derivatives can be estimated using numerical integration techniques such as Runge-Kutta methods [Chachuat, 2007]. As the entire DAE is now represented as a system of algebraic variables, the entire optimization is formulated as a NLP [Cervantes and Biegler, 2009]. The path constraints are turned into point constraints enforced at each discretized time point in the horizon. While we do not have to perform integrations to find the state variables, the simultaneous method does require a large initial guess. Initial guesses must be given for both control and state variables at every time point and we see that the discretization of a dynamic optimization can lead to large scale NLPs [Biegler *et al.*, 2002].

A common approach to full discretization of the dynamic optimization is to estimate the state and control variables profiles using polynomial interpolation in what is know as the collocation method [Cervantes and Biegler, 2009]. In time collocation, the time horizon is divided into finite elements and each finite element contains several collocation points. Polynomial interpolation (using the values of the state and control variables at the collocation points) is used to generate a profile for the state variables for each finite element [Biegler, 2007]. It is the variables that represent the value of the state and control variables at each collocation point that make up the variables

of the NLP. As the state variables are estimated using polynomials, the derivative at a given collocation point can be expressed algebraically as the derivative of the polynomial [Biegler *et al.*, 2002]. In the NLP created, path constraints are enforced at each collocation point and continuity is enforced for the polynomials that represent the differential variables (thus the final value of the polynomial at the end of a finite element must match the initial value of the new polynomial for the next finite element) [Biegler, 2007].

Common algorithms to solve NLPs include interior point methods and sequential quadratic programming (SQP). In both methods the Karush -Kuhn-Tucker (KKT) conditions for the NLP are solved iteratively. In interior points methods the complementarity conditions of the KKT conditions are initially relaxed and the KKT system is solved [Nocedal and Wright, 2006]. The relaxed complementary conditions are tightened with each iteration until the original KKT conditions are solved. For the SQP method the KKT conditions are solved for by solving an equivalent quadratic program [Nocedal and Wright, 2006]. Both the sequential and simultaneous methods are used to solve dynamic optimization problem in this thesis, and both interior point and SQP methods are used to solve the NLPs formulated.

2.2 Optimization under Uncertainty

A design for a chemical process plant must not only be able to transition from one operating point to another as quickly and feasibly as possible, but it must also be able to do this for transitions between several different operating points. Thus a design must accommodate several different operating scenarios, and the optimization must be able to include uncertain parameters such as product demand or utility costs. There are several methods that are used to capture uncertainty in an optimization formulation.

One of the most common ways to incorporate uncertainty in optimization is to utilize a two-stage stochastic optimization.

The formulation for two-stage stochastic optimization as given in Pistikopoulos and Ierapetritou [1995] takes the form:

$$\max_{\mathbf{z},\mathbf{d},\mathbf{x}} \underset{\boldsymbol{\theta}\in\mathbf{R}}{\mathbf{E}}\left[P(\mathbf{x},\mathbf{z},\mathbf{d},\boldsymbol{\theta})\right]$$

$$\text{s.t}$$

$$\mathbf{h}(\mathbf{x},\mathbf{z},\mathbf{d},\boldsymbol{\theta}) = \mathbf{0}$$

$$\mathbf{g}(\mathbf{x},\mathbf{z},\mathbf{d},\boldsymbol{\theta}) \leq \mathbf{0}$$

In this formulation , $\underset{\boldsymbol{\theta}\in\mathbf{R}}{\mathbf{E}}\left[P(\mathbf{x},\mathbf{z},\mathbf{d},\boldsymbol{\theta})\right]$ is the expected value of the objective function over the uncertainty $\boldsymbol{\theta}$ in $\mathbf{R}$. $\mathbf{d}$ is the first-stage decision variables that are common to all realizations of $\boldsymbol{\theta}$. $\mathbf{x}$ and $\mathbf{z}$ are the second-stage decision or recourse variables which can be adjusted depending on the realization of $\boldsymbol{\theta}$. Finding a design that is feasible for all realizations of $\boldsymbol{\theta}$ poses a feasibility problem for an infinite number of constraints [Halemane and Grossmann, 1983]. To make the problem more tractable, a multiperiod or multiscenario approach can be used, where the uncertainty set is reduced to a number of discrete points, and hence $\underset{\boldsymbol{\theta}\in\mathbf{R}}{\mathbf{E}}\left[P(\mathbf{x},\mathbf{z},\mathbf{d},\boldsymbol{\theta})\right]$ can be expressed in a discrete form and feasibility only needs to be applied for a finite number of realizations of uncertainty [Paules IV and Floudas, 1992].

In Halemane and Grossmann [1983] it shown that for a multiperiod approach assuming a convex feasible region, if the discrete uncertainty set chosen contains all the vertices of the uncertainty domain ($\mathbf{R}$), then the design generated will be feasible for all $\boldsymbol{\theta}$ in $\mathbf{R}$. This concept is applied for dynamic processes in Dimitriadis and Pistikopoulos [1995] where for a given design and a given range of uncertainty for

a process, the uncertainty profile that maximizes constraint violations is found in a formulation called the *dynamic feasibility problem*. In addition to this, the maximum deviation in nominal uncertainty (the uncertainty range) that the design can undergo is known as the *dynamic flexibility index*. The concept of the *dynamic feasibility problem* is applied to a two-stage stochastic optimization for a dynamic problem in Mohideen *et al.* [1996] and Bansal *et al.* [2002]. In these studies, to find a design that is feasible over an uncertainty range, a design is subject to the *dynamic feasibility problem*. If an uncertainty profile is found that can violate the operating constraints, this uncertainty profile is added to the set of uncertainty profiles that are considered when the optimal design is found. This process is repeated until a design is found where no realization of uncertainty causes infeasible operation for the design.

Instead of enforcing feasibility for all uncertainty scenarios (or the entire uncertainty domain), enforcing feasibility up to a certain probability is known as chance-constrained programming [Sahindis, 2004]. A general form for a linear program using chance constrained programming from Sahindis [2004] is given below:

$$\begin{aligned} \max \ & \mathbf{c}^T\mathbf{x} \\ \text{s.t} & \\ P(A\mathbf{x} \geq b) & \geq p \end{aligned}$$

In this formulation there is uncertainty in both the matrix A and the vector b, where $\mathbf{x}$ is the set of decision variables. P is the probability distribution of the uncertainty and p is a given probability that is required to be met. An example of chance-constrained programming used in a process engineering optimization is seen in Zhu, Yu, Laird [2011] where the optimal operation of an air separation unit (ASU) is examined. In this study the air separation unit operates under uncertain demand, where the

demand has a given probability distribution, average and standard deviation. Instead of being forced to be able to meet all realizations of the demand, the ASU only needs to make sure the expected value of the amount of product it produces exceeds a given fraction of the average demand.

2.3 Integrated Design and Control

Given varying market conditions, disturbances and parameter uncertainty, it is important for a process plant to be able accommodate for these conditions, often through the operation and design of the plant. Even for plants operating at steady-state, the dynamics of the process should be taken into account in order to reject disturbances and account for parametric uncertainty. Thus the concept of integrated design and control is applicable to almost any chemical process. Integrated design and control can improve plants in several different aspects, two important factors being the economic operation of the plant (as well as the capital costs) and the ability to quickly transition between operating points and to reject disturbances (dynamic resilience) [Morari, 1983]. The above factors are commonly used in multi-objective approaches for integrated design and control, often when utilizing steady-state optimizations where the dynamics are not inherent in the objective function. Pareto optimality is considered when using multi-objective approaches to find the optimal design and operation of chemical processes. Objectives being traded off can include the capital and operational cost versus several controllability indicators such as RGA, minimum singular value and condition number [Luyben and Floudas, 1994] or operational costs versus the integral square error around a set-point [Lenhoff and Morari, 1982].

When dynamic models are incorporated into processes operating at a steady-state, the dynamic operation of the process when subject to disturbances can now be accounted for in an economic objective function (as opposed to using a multi-objective

function). When operating at steady-state, the concept of "back-off" arises where the steady-state operating point is selected to avoid constraint violations given a disturbance. Thus studies look to minimize the "back-off" necessary through design and control, such as the finding the optimal plant layout [Narraway *et al.*, 1991] or minimizing the operational losses due to "back-off" by the optimal pairing of measured and controlled variables for a flotation circuit (optimal control structure)[Narraway and Perkins, 1993]. As opposed to just examining how "back-off" affects operational and capital costs, Figueroa *et al.* [1996] maximized operational profit, and investigated how various control-schemes affect the "back-off" necessary within a range of disturbance and uncertainty. This was extended for the same process by considering optimal design parameters, plant layout and control structure in Bahri *et al.* [1997]. Applications of MPC to steady-state "back-off" have been investigated using mixed-integer formulations [Soliman *et al.*, 2008] and interior point methods [Baker and Swartz, 2008].

While the previous studies mentioned generally considered disturbances to steady-state processes, we see in current operating paradigms such as deregulated electricity markets (where the variation of electricity price can be taken advantage of and future electricity prices are uncertain) uncertainty in operation such as demand, must be taken into account. Using dynamic optimization to study switches between operating points is studied in White *et al.* [1996] where a reduced dynamic model of a distillation column is used to find the optimal design that allows the column to transition as quickly as possible from one purity set-point to another. Mohideen *et al.* [1996] utilized a dynamic optimization to find the optimal design, control structure and operational profile for chemical process subject to an uncertain process flow profile over a given time period. The benefit of utilizing a dynamic model under uncertain operating conditions was observed in Cao *et al.* [2016b]. In this study various operating paradigms were explored for an air separation unit (ASU) under varying electricity price over a given period. It was seen that operational profit can be increased by

overproducing and under producing product depending on the electricity price. Using a dynamic model prevents constraint violations when the ASU transitions from one operating point to another.

Two-stage stochastic formulations are commonly used in integrated design and control. They can be used to optimize large industrial processes such as in Ierapetritou and Pistikopoulos [1996] and Zhu *et al.* [2010]. In Zhu *et al.* [2010] the optimal design (1st stage decision variables such as column diameter and heat exchanger surface area) and operation of a steady-state model of an ASU are found that provides feasible operation over many discrete uncertainty scenarios. The studies in this thesis will use two-stage stochastic optimization to find the optimal design and operation of dynamic processes under uncertainty.

Chapter 3

Design of a Dynamically Operable Air Separation Plant

3.1 Introduction

Cryogenic air separation plants or air separation units (ASUs) produce both liquid and gaseous high purity nitrogen, oxygen and argon from air that is fed to a distillation column. As ASUs take air from the atmosphere, electricity costs comprise the majority of the ASU operational cost [Miller *et al.*, 2008b]. Energy markets in the US are encouraged to reduce electricity consumption during times of high demand or poor grid reliability [US Department of Energy, 2006]. Price-based demand response is a practice employed by energy markets to reduce electricity consumption where the electricity prices for consumers vary during the day [US Department of Energy, 2006]. Demand response of this type can thus be utilized during ASU operation to reduce electricity cost. The operation of ASUs utilize demand response by allowing for product storage thus allowing for overproduction relative to demand when electricity prices are low. Given that there will be changes in production due to electricity

prices, the ASU must transition from one operating point to another and there are dynamics in the process that are not taken into account using steady-state models of the ASU.

Dynamics can be estimated in a steady model of an ASU by establishing minimum time periods that the ASU must be producing or be shut down for [Ierapetritou *et al.*, 2002]. The transition from one operating point to another in a steady state model is modelled in Zhu, Yu, Laird [2011] as a linear profile where the slope is determined by the steady state end points. To more accurately capture the dynamics of an ASU when operating under varying electricity price and production, dynamic models of an ASU can be used. Using a data driven low-order dynamic model, it has been shown that by utilizing a storage tank to allow for overproduction (so product can be stored), the operational costs of an ASU can be reduced compared to operating at a constant production rate [Pattison *et al.*, 2016]. Examining several paradigms involving different storage practices and additional reflux for an ASU under varying electricity price and demand showed that utilizing a dynamic model of a nitrogen plant is necessary to observe certain operational limitations and economic benefits [Cao *et al.*, 2016b].

From the above examples we see the importance of being able to accurately capture dynamics of an ASU when operating under demand uncertainty. Frequently changing demand can mean frequently changing operating points for the ASU. Transition between operating points is integral to the operation of the ASU as operating constraints may still need to be met during the transition. Hence it is imperative to transition between operating points economically and feasibly. Miller *et al.* [2008a] investigated improving plant flexibility by introducing additional feed into the column during start-up. With regards to operating an ASU under varying electricity price and demand, it has been found that using stored product as additional reflux as opposed to selling the product can reduce operating costs even further [Cao *et al.*,

2016b]. In addition to operational strategies to reduce operational costs for an ASU under varying demand and electricity, we must also consider design parameters. Design parameters such as the diameter of the column will also have an effect of the dynamics and optimal operation of the ASU. Considering the design of the ASU is imperative to recognize that an ASU may not be able to transition from one set point another under a given design. Thus the design must reflect the variation of demand that the ASU undergoes.

Incorporating long term uncertainties, capital expenditure decisions (integer decisions), weekly, seasonal, yearly demand and electricity price variation to find the optimal design and operation of an ASU was studied in Mitra *et al.* [2014]. However in this formulation the operation of the ASU is represented through inventory and operational constraints as opposed to a mathematical model of an ASU. The design of an ASU subject to uncertainty in argon demand and a given thermodynamic parameter was studied in Zhu *et al.* [2010]. Given a steady state model of an ASU, based on these uncertainties optimal column diameters, compressor power and heat exchanger area were found, and it was shown that the more uncertainty scenarios included, the more conservative the design. However when designing an ASU, the dynamics of the plant must also be taken into account [Cao *et al.*, 2015]. In this study it was shown that direct step changes (which would be assumed by a steady state design) in the column can lead to the column violating operational constraints. Design under uncertainty utilizing dynamic optimization has been studied previously in Mohideen *et al.* [1996] using a mixed integer dynamic optimization (MIDO) formulation. However the uncertainties considered were disturbances in the process. Schenk *et al.* [2002] studied finding the optimal design of an ASU (including mixed-integer decisions such as the number of trays and control schemes) allowing the ASU to provide greater profit over a wide range of disturbances (uncertainties) compared to a steady-state design. In these studies by utilizing dynamic optimization, operational feasibility can be maintained throughout the operation as opposed to just the endpoint (which

occurs if a steady state designed was used).

Hence in this chapter, two-stage stochastic dynamic optimization for a nitrogen plant will be conducted using several different demand scenarios. It is expected that the dynamically operable design produced will be more conservative than the flexible and nominal designs. However when each design is required to maintain feasibility during the transition between operating points, we would expect that the dynamically operable design will provide more operational profit in these cases. This would illustrate that finding a dynamically operable design for a nitrogen plant subject to uncertainty can provide economic benefits that may not be realized using less conservative formulations.

3.2 Process Description and Mathematical Model

To conduct the investigation set out in this study, we will use a first-principles dynamic model of an N_2 plant based on that utilized in Cao *et al.* [2016b]. The N_2 plant (whose configuration is shown Figure 3.1) utilizes both full order and collocation modelling for the units that make up the plant model. The plant takes in air from the atmosphere, which is removed of impurities in an upstream section that is outside the scope of the present study, and then passes through a compressor. The stream is then sent through a counter-current plate and fin primary heat exchanger (PHX), within which the stream is split into a liquid air feed and vapor air feed, which enter the column at different tray locations. Before the gaseous air is sent to the column, it is sent to the turbine for additional cooling. The feed to the column is separated into high purity nitrogen gas product (leaving at the top of the column) and a crude oxygen stream. A portion of the gas product (GN2) leaves the plant for sale, while the remainder enters the integrated reboiler/condenser where it is condensed against the crude oxygen stream to return to the column as reflux. The GN2 product stream and

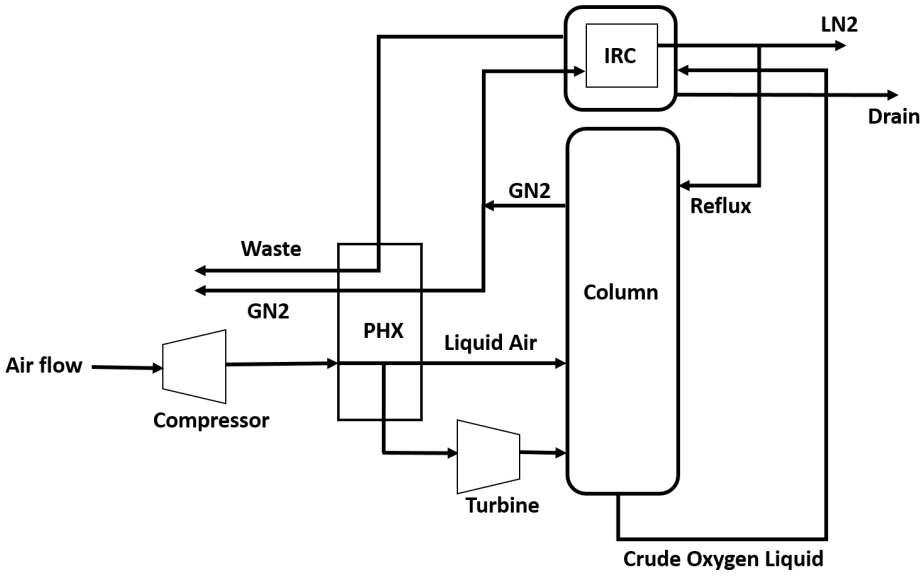

Figure 3.1: Schematic of the N_2 plant configuration used in this study

vapor waste from the reboiler that leave the plant pass through the PHX where they provide cooling to the air feed.

The distillation column is represented by material and energy balances for each tray that take the following form,

$$\begin{aligned} \frac{dm_{n,i}}{dt} &= x_{n+1,i}L_{n+1} + y_{n-1,i}V_{n-1} - x_{n,i}L_n - y_{n,i}V_n \\ \frac{dE_n}{dt} &= h_{n+1}^{Liq\,Mix}L_{n+1} + h_{n-1}^{Vap\,Mix}V_{n-1} - h_n^{LiqMix}L_n - h_n^{VapMix}V_n - Q^{Leakage} \end{aligned} \quad (3.1)$$

where $m_{n,i}$ is the molar holdup of component i on tray n, x and y are the liquid and vapor mole fractions, and L and V are the liquid and vapor flow rates from each tray. In the energy balance, E is the energy holdup for a given tray and h is the molar enthalpy for the associated vapor and liquid streams. While these equations are for a full-order model, they are identical when a collocation based model is implemented, where n then represents a collocation point and $n+1$ and $n-1$ represent "one tray above" and "one tray below" the collocation point, respectively [Cao *et al.*, 2016a][Swartz and Stewart, 1986] (the collocation point can be a non-integer value,

unlike the the tray number). Reduced order modelling utilizing collocation is used to model a section of the distillation column and the entirety of the primary heat exchanger (PHX). In the column, low-order Lagrange polynomials are used to interpolate the material and energy flows between collocation points. In a full-order model, the PHX was divided into cells to develop temperature and pressure profiles, where dynamic energy balances were performed around each cell [Cao *et al.*, 2015]. In a collocation approach, the balances are confined to collocation pints that are spatially distributed along the length of the PHX [Cao *et al.*, 2016a]. Fewer collocation points are used than the number of cells or trays, thus reducing the size of the model. The collocation methods used in this model are explained in greater detail in Cao *et al.* [2016a].

The plant model is also governed by several other principles. The thermodynamics of the distillation column utilize modified Raoult's Law, Margules equations, the Antoine equation and the Peng-Robinson equation of state. The characteristics of the distillation trays are captured through the Francis Weir equation and Murphree tray efficiencies. In previous versions of this nitrogen plant model, the pressure drop was assumed to be constant throughout the column [Cao *et al.*, 2015], leading to an index-2 DAE that required the application of index reduction techniques. However in the present model, the pressure drop is a function of flow rates and vapor and liquid densities in the column, which results in an index-1 DAE system that can be handled directly by standard DAE solvers.

The turbine and compressor in this plant model are systems of algebraic equations that use polytropic relations and regressions from compressor mappings to determine the operating states and operating constraints (such as surge) of each unit. Equations estimating valve dynamics are used to capture how the control variables change within the plant. The overall plant model comprises 148 differential equations and 1903 algebraic equations. A summary of the model structure of each unit in the plant is

Table 3.1: A summary of units that comprise the N_2 plant model

Unit	Model Structure
Compressor	System of Algebraic Equations
Turbine	System of Algebraic Equations
Primary Heat Exchanger	DAE utilizing spatial collocation
Distillation Column	DAE utilizing first principles and collocation
Integrated Reboiler and Condenser	DAE utilizing first principles

given in Table 3.1. Further detail regarding the model of the N_2 plant may be found in Cao *et al.* [2016a] and Appendix A.

3.3 Optimization Formulation

The goal is to determine a design that accounts for the dynamics of plant transitions in response to uncertain demand changes. The design problem is consequently formulated as a stochastic dynamic optimization problem. A two-stage stochastic optimization approach is followed, in which the uncertain parameter set is discretized into N_s trajectories, $\{\theta_i(t)\} \in \Gamma$, each of which generates an uncertain scenario. The design optimization problem takes the form,

$$\begin{aligned}
\min_{\mathbf{d},\mathbf{u}_i(t)} \quad & E_{\theta_i(t)\in\Gamma}\{\phi(\mathbf{x}_i(t_f), \mathbf{z}_i(t_f), \mathbf{u}_i(t_f), \mathbf{d}, \theta_i(t), t_f)\} \\
\text{st:} \quad & \dot{\mathbf{x}}_i(t) - \mathbf{f}_d(\mathbf{x}_i(t), \mathbf{z}_i(t), \mathbf{u}_i(t), \mathbf{d}, \theta_i(t), t) = \mathbf{0} \\
& \mathbf{f}_a(\mathbf{x}_i(t), \mathbf{z}_i(t), \mathbf{u}_i(t), \mathbf{d}, \theta_i(t), t) = \mathbf{0} \\
& \mathbf{g}(\mathbf{x}_i(t), \mathbf{z}_i(t), \mathbf{u}_i(t), \mathbf{d}, \theta_i(t), t) \leq \mathbf{0} \\
& t \in T = [t_0, t_f], \quad \dot{\mathbf{x}}_i(t) = \mathbf{0} \\
& \theta_i(t) \in \Gamma, \quad i = 1, \ldots, N_s
\end{aligned} \tag{3.2}$$

where $\mathbf{x}_i(t) \in \Re^{n_x}$, are differential states, $\mathbf{z}_i(t) \in \Re^{n_z}$ are algebraic states, $\mathbf{u}_i(t) \in \Re^{n_u}$

are inputs, and $\mathbf{d} \in \Re^{n_d}$ are design variables. ϕ represents the objective function whose expected value is to be minimized, $\mathbf{f}_d$ and $\mathbf{f}_a$ are the differential and algebraic functions, respectively, of the DAE model in semi-explicit form, and $\mathbf{g}$ represents a set of path constraints. E represents the expectation operator.

In two-stage stochastic programming, the variables are partitioned into two sets: first-stage decisions (here and now) that are made prior to uncertainty realizations being revealed, and second-stage, or recourse, decisions (wait and see) that are dependent on the uncertainty realizations. A detailed description of stochastic optimization is given in Birge and Louveaux [1997]. In the present formulation, the design variables, $\mathbf{d}$, constitute the first-stage decisions, and are common to all uncertainty scenarios, whereas the input and state variables comprise the second-stage decisions associated with the uncertainty scenarios, i.

Our study will also consider two steady-state design formulations, namely, a nominal design and a flexible design. These may be derived from problem (3.2) be setting $\dot{\mathbf{x}}_i(t)$ to zero, and for the nominal design, considering only a single scenario with the parameter $\theta_i(t)$ set at a prescribed nominal value.

The following subsections will describe the various components of the formulation in more detail as they relate to the ASU design problem under consideration. All optimizations are performed in gPROMS 4.2 which utilizes the sequential method and the SQP algorithm to solve the NLP. Steady-state optimization is used for the nominal and flexible designs, and dynamic optimization is used for the dynamically operable formulation. All optimization studies were executed on a Dell Optiplex 7020 with 16GB of RAM.

3.3.1 Objective Function

The objective function is an annualized profit expressed as

$$\underset{\theta_i}{E}[\phi] = \text{Annualized profit} = \sum_{1}^{N_s} w_i(R_i - C_i^{op}) - C^{cap}/T \tag{3.3}$$

where R_i and C_i^{op} represent the revenue and operating cost, respectively, for demand scenario i, w_i represents the probability of occurrence of scenario i. C^{cap} represents the total capital cost and T represents the amortization period. For the ASU system under consideration, the revenue, R_i, comprises the gaseous nitrogen product flow multiplied by the associated price and the operating cost, C_i^{op}, is taken as the cost of the compressor power utilized. The equipment costing formulae utilized are given below; an amortization period of 6 years is used.

The capital cost formulation of the distillation column is taken from Douglas [1988]:

$$\begin{aligned} \text{Column Shell Capital Cost} &= (\frac{\text{CEPCI}}{113.6}) \cdot 101.9 D_{col}^{1.066} H_{col}^{0.802} (2.18 + F_{c1}) \\ \text{Column Trays Capital Cost} &= (\frac{\text{CEPCI}}{113.6}) \cdot 4.7 D_{col}^{1.55} H_{col} F_{c2} \end{aligned} \tag{3.4}$$

where D_{col} is the diameter of the column and H_{col} is the height of the column (calculated from the number of trays and tray spacing). F_{c1} is a correction factor based on pressure rating and column shell material and F_{c2} is a correction factor based on tray material, tray type and tray spacing. The CEPCI index is used to account for inflation in costs from 1988 to 2015. The sum of the shell and tray costs gives the total capital cost of the distillation column.

The capital cost formulation of the compressor is taken from Turton [1998]:

$$\begin{aligned}\log_{10}(\text{Compressor Capital Cost}) = \ & \log_{10}(2.5 \cdot (\frac{\text{CEPCI}}{360})) \\ & +(K_1 + K_2 \log_{10}(W_{max}) + K_3(log_{10}(W_{max}))^2) \\ \log_{10}(\text{Compressor Drive Capital Cost}) = \ & \log_{10}(1.5 \cdot (\frac{\text{CEPCI}}{360})) \\ & +(K_4 + K_2 \log_{10}(W_{max}) + K_6(\log_{10}(W_{max}))^2)\end{aligned} \tag{3.5}$$

where W_{max} is the maximum power of the compressor. K_{1-6} are correlation coefficients depending on the type of compressor and compressor drive used . The CEPCI index is used to account for inflation in costs from 1998 to 2015. The sum of the compressor and compressor drive costs gives the total capital cost of the compressor.

The capital cost of the plate and fin heat exchanger given by Najafi *et al.* [2011] is used.

$$Cost\ of\ PHX\ = \ C_s S_A \tag{3.6}$$

where C_s is the cost per m^2 of heat exchange area and S_A is the surface area of the heat exchanger.

3.3.2 Decision Variables and Constraints

The optimization decision variables considered are listed in Table 3.2. To perform the dynamic optimization, the inputs are parametrized as piecewise constant trajectories. For each demand change, the input horizon is partitioned into five control intervals, one control interval for each of the initial and final steady states, and three 5 minute control intervals during transition. An example of the control vector parametrization used is given in Figure 3.2 (in the actual 12 hr horizon, the periods of steady-state are longer, but the transition is still effected through three 5 minutes control intervals). Each demand scenario involves three demand changes over a 12 hr period, which

Table 3.2: A summary of decision variables used in the optimization

First-stage decision variables (design variables)	**Second-stage decision variables (operational variables)**
Column Diameter	GN2 produced for sale
Primary Heat Exchanger Length	Air feed to N2 plant
Maximum Compressor Power	Liquid air fed to column
PHX air withdrawal point	

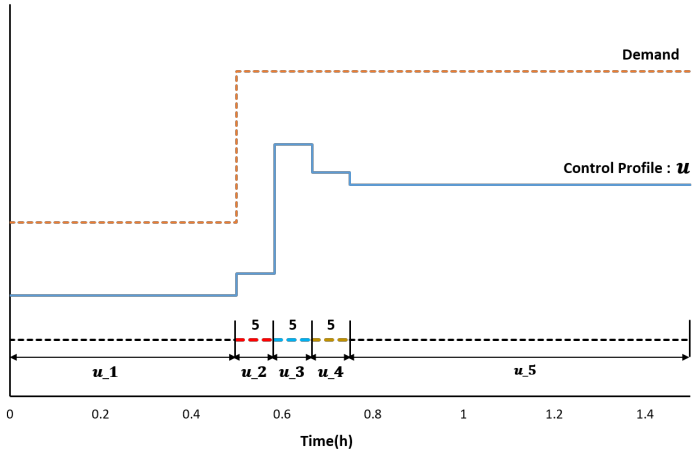

Figure 3.2: The control interval structure for the dynamic optimization

using the above input partitioning, requires 13 control intervals.

The path constraints imposed are described in Table 3.3. Given a constraint variable v_c and maximum value of the variable v_m, which v_c cannot exceed over an optimization horizon, the path constraint can formulated as follows, where ϵ is a sufficiently small tolerance:

$$\int_{t_o}^{t_f} \{\max[\ 0\ ,(\ v_c - v_m)\ ]\}^2\, dt\ \leq\ \epsilon \tag{3.7}$$

An endpoint constraint is also present when $\frac{dx(t)}{dt}\ =\ 0$ to ensure a final steady state.

Table 3.3: The path constraints that are used in the optimization formulation

Path Constraints	Condition to satisfy constraints
Compressor Surge	Air flow to column must not drop below a certain flow rate
Column Flooding	Vapor velocity in column must not exceed flooding velocity
Reboiler Level	Liquid in reboiler must vary between certain levels
Sump Level	Liquid in sump must vary between certain levels
Product Purity	Parts per million oxygen (PPMO) must not exceed 5 PPMO at steady state and must not exceed 10 PPMO during transition
Turbine Dewpoint	The pressure of the vapour air entering and exiting the turbine must be lower than the dew point pressure
PHX Bubble point	The pressure of the liquid in the PHX must be higher than the bubble point pressure
Maximum Compressor Power	The power output of the compressor must be less than maximum design power (a decision variable)

3.3.3 Demand Scenarios

In this study, the plant must be able to meet the demand required and cannot buy additional product to meet unmet demand. Given this, the electricity price is fixed throughout the horizon and is the same for all the uncertainty scenarios (the variation in electricity price paradigm allows the plant to not meet demand by utilizing already stored product). Thus the uncertainty set consists of six 12-hr horizons with varying demand where the demand changes every four hours. This uncertainty set can be seen in Figure 3.3. When the demand changes, the plant operating point must also move to meet this demand. The demand profiles are based on data provided by our industrial partner. Thus the second-stage decision variables will be the control variables for the plant. The variables that are common to each uncertainty scenario are selected design parameters, which will act as our first-stage decision variables.

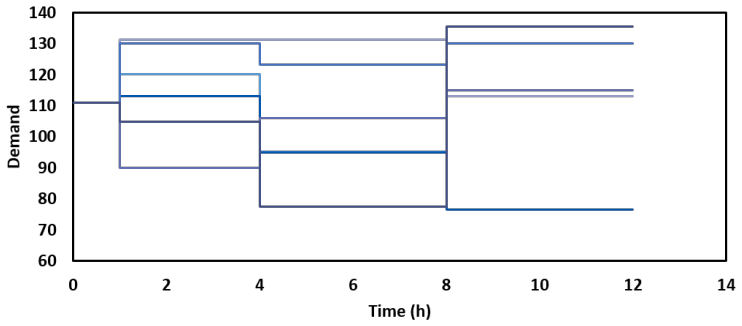

Figure 3.3: The six scenarios that comprise the uncertainty set used in this study

3.4 Design Comparison Studies

In this case study, we will compare three different design paradigms - nominal, flexible and dynamically operable designs. For the nominal design, the steady-state analog of Eq. 3.2 is solved for a single, constant nominal demand scenario. The flexible design maintains steady-state feasibility under uncertainty, without consideration of transition dynamics, whereas the dynamically operable design maintains feasibility of the dynamic response trajectories of the system. The flexible design utilizes a steady-state version of Eq. 3.2 in which the constant portions of the six demand scenarios described in the previous subsection are considered as individual static scenarios. The length of time the plant spends at each static demand scenario (required for the profit and operating cost evaluation) is taken from the dynamic demand profiles; thus the flexible and dynamically operable designs can be compared on a consistent basis.

The difference between the flexible and dynamically operable design paradigms is illustrated in Figure 3.4. We see that the dynamically operable design includes the transitions between steady states which is not captured in the flexible design formulation. In addition, the flexible design does not consider the permutation of the plant transitions. Given this, we expect the dynamically operable design to be more conservative than the flexible design. This would translate to the flexible design appearing to be a more attractive decision; however plant operation using the dynamically op-

erable design may be more profitable over the long run. The dynamically operable design may provide better operational profit as a plant based on the flexible design would typically still have to undergo transitions from one operating point to another. Because the flexible design used does not take into account transition between operating points, when it finally does have to transition, it may not be as quick compared to the dynamic design leading to lost revenue over the transition period (since when demand is not met, revenue is lost or the plant is forced to acquire product from an outside source).

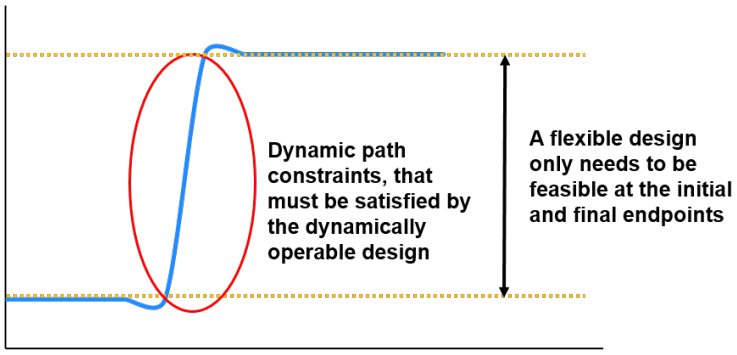

Figure 3.4: The difference in operational profile between a dynamically operable and flexible design

In order to compare the design of the N_2 plant generated by different formulations, random demand scenarios are created to test each design (moving from a lower demand to a higher demand or vice versa). A demand scenario is constructed from an initial demand point ($D_{initial}$) and a demand change (ΔD), which determines the final demand (D_{final}). The initial demand level and magnitude of the change are generated based on the average demand and the average change in demand in the uncertainty set. The range of the change in demand and initial demand point used

to construct the random demand scenario is given below.

$$\begin{aligned} \mu_{change} - 2\sigma_{change} \;\leq\; \Delta D \;\leq\; \mu_{change} + 2\sigma_{change} \\ \mu_{demand} - 2\sigma_{demand} \;\leq\; D_{initial} \;\leq\; \mu_{Demand} + 2\sigma_{demand} \\ D_{final} \;=\; D_{initial} \;\pm\; \Delta D \end{aligned} \tag{3.8}$$

The demand change and initial demand are assumed to be uniformly distributed within their ranges, and thus to construct a random demand scenario, a random point is selected between these ranges for both the demand change and initial demand. The direction of the change is also randomly selected.

The nominal, flexible, and dynamically operable designs are evaluated by applying the random demand scenarios to the N_2 plant, where the design parameters have been fixed at the nominal, flexible, and dynamically operable designs respectively. An optimization is performed to find the operational profile that maximizes the profit given the random demand scenario. The scenario is a 4 hr horizon formulated such that the initial demand spans a 1 hr horizon and then steps to the final demand for the remaining 3 hrs. The initial operating point for a given random demand scenario is a fixed point and not determined by the optimization. Instead this initial fixed point is determined by a steady-state optimization for the N_2 plant at the initial demand, where the demand parameters are fixed at the design being used for the random demand scenario. The reason this is done is because in practice the plant is operating at a steady-state point with no knowledge of future demand.

To compare the economic benefits of each design, given the average operational profit from the 10 random scenarios we can calculate the annualized profit as in Eq. 3.3, using the average operational profit of the 10 random scenarios.

3.5 Results and Discussion

The design parameters and optimal objective function values found from the three optimization formulations are given in Table 3.4. The nominal design is generated by finding the average demand over all six demand scenarios, which is then used in a single scenario steady-state optimization. The results have been scaled relative to the nominal design for confidentiality reasons.

Table 3.4: Optimization results for the six scenario two-stage stochastic optimization. Values are scaled relative to the nominal design as a baseline (100)

Design Parameters	**Nominal Design**	**Flexible Formulation**	**Dynamically Operable Formulation**
Column Diameter	100	105.2	103.2
PHX Length	100	106.7	108.6
Compressor Power	100	117.0	117.1
Objective Function	100	98.9	98.6

The dynamically operable design also yields input trajectories (second stage decisions) corresponding to each uncertain demand scenario; one such set of profiles is shown in Figure 3.5.

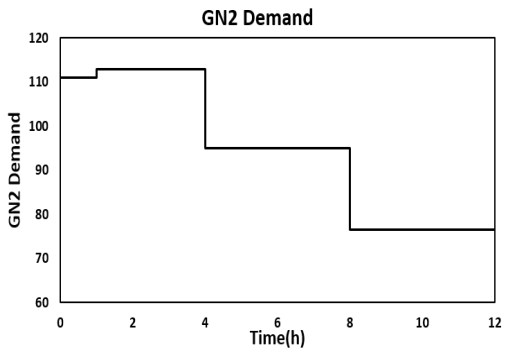

(a) GN2 Demand

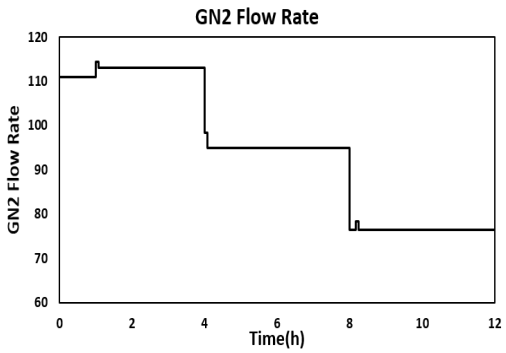

(b) GN2 production control moves

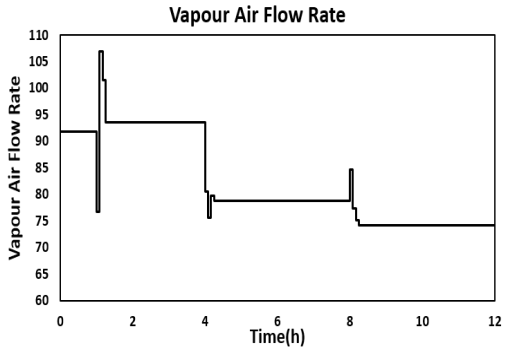

(c) Air flow to compressor control moves

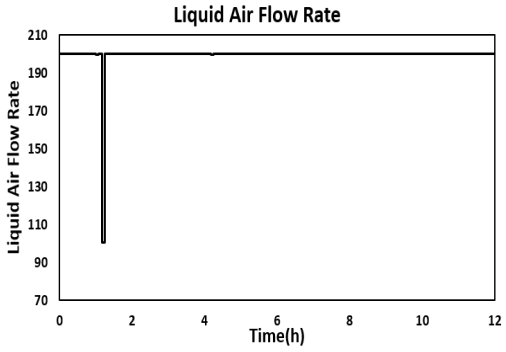

(d) Liquid air to column control moves

Figure 3.5: Demand profile (a) and optimal input trajectories (b)-(d) for a scenario in the two-stage stochastic dynamic optimization

From Table 3.4, we see that the flexible design provides the higher objective function, suggesting that adopting a flexible design may lead to higher profits. Examining the design parameters, it seems counter intuitive that the flexible design has a larger column diameter. This is due to fact there is an economic and operational trade-off between the column diameter and maximum compressor power. When the column diameter is increased this reduces the pressure drop along the column, and the compressor can use less power. This reduces the operational costs (lower compressor power uses less electricity) as well as the capital cost (lower maximum compressor power). Thus there is a trade-off between increasing the capital cost of the compressor or the column. The dynamics of the column are such that given the objective

function Eq. 3.3, it is more profitable in the dynamic optimization to have a lower column diameter compared to the flexible design. The reason the dynamically operable design requires a higher maximum compressor power can be explained with the aid of Figure 3.6, which shows a segment of one of the demand scenarios and profiles related to the compressor operation. For this demand scenario, there is a period of time for which the transient profiles of the compressor air flow and power exceed the final steady-state values. This phenomenon is not captured in the flexible design, and is why the dynamically operable design has a more conservative compressor design and lower objective function.

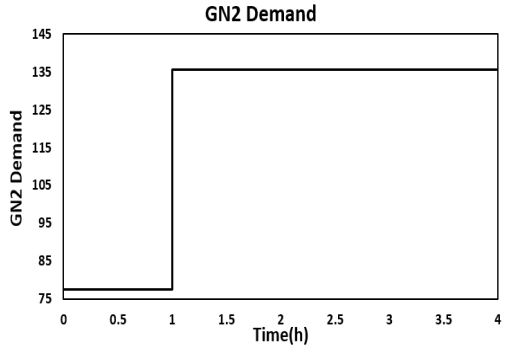

(a) GN2 Demand

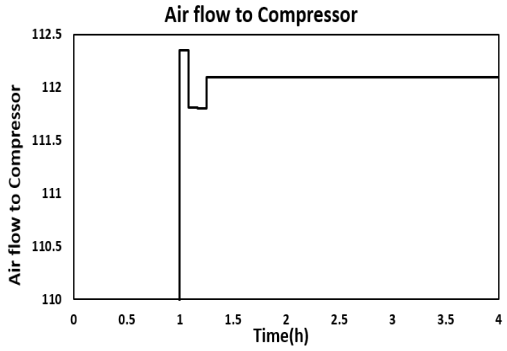

(b) Air flow to compressor

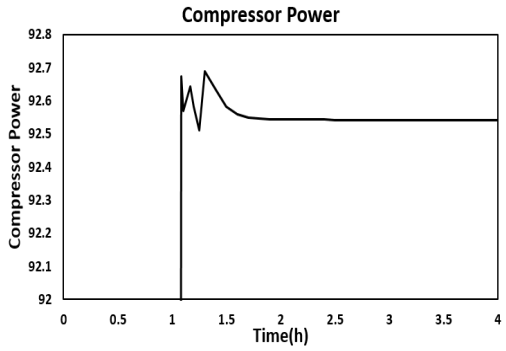

(c) Compressor power needed during operation

Figure 3.6: Profiles illustrating the need for incorporating dynamics into the design. These profiles are a 4 hr interval taken from a given 12 hr demand scenario

To further examine this effect, the trade-off between column diameter and compressor

Table 3.5: The single scenario optimization where the compressor power is fixed and not a design variable.

Design Parameters	**Flexible Formulation**	**Dynamically Operable Formulation**
Column Diameter	100	100.5
PHX Length	100	107.4
Objective Function	100	99.49

power is removed by fixing the compressor power. Flexible and dynamically operable designs are determined using the single demand profile shown in Figure 3.7. The results are shown in Table 3.5, where the dynamically operable design is now more conservative in all design parameters.

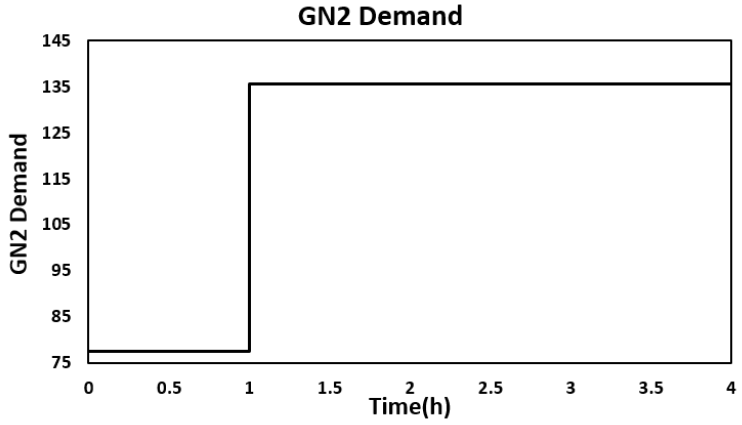

Figure 3.7: Demand change used to examine the trade-off between column diameter and maximum compressor power

3.5.1 Evaluation of Designs for Random Demand Scenarios

As discussed in the previous section, the nominal, flexible and dynamically operable designs will be subjected to ten random demand change scenarios generated using the approach described earlier. For each scenario, the plant design parameters were

fixed at either the nominal, flexible or dynamically operable design. The optimal operational profit and the annualized profit were then calculated for dynamic transition between the two demands. Unlike the optimization where the design is found, when testing the design we allow for unmet demand to occur. The results are presented in the Table 3.6.

Table 3.6: The average operating profit for 10 random scenarios when the plant design is fixed at the nominal, flexible and dynamically operable designs, generated from the six scenario two-stage stochastic optimization

Design	**Nominal Design**	**Flexible Formulation**	**Dynamically Operable Formulation**
Average Operational Profit	100	105.9	106.5
Annualized Profit	100	102.2	102.8

From Table 3.6 we can see that the dynamically operable design on average provides greater operational profit. However, the difference in operational profit is rather slight. This is because for most of the random scenarios the operational profit is very similar. But for scenarios where the demand change is relatively large (≥ 30) the dynamically operable design generates an operating profit that can be up to 5 percent greater than flexible design. In these cases we find that the dynamically operable design is able to meet the final demand while the flexible design does not. Thus in certain cases it is fairly evident that utilizing the dynamic design allows the plant to generate higher profits. The difference in average operational profit is small as most of the 10 random scenarios do not have a very large demand change, and both the dynamic and flexible design are able to transition from the change equally well. The nominal design performs significantly worse compared both other designs. This is because the nominal design takes into account only one demand and it is not able to exceed this when subjected to the random scenarios. Hence profit is lost, since in many cases the nominal design is not able to meet the demand. Factoring the capital cost of each design into the economic performance is done by the annualized profit. Here

we can see that even though the nominal design is much less conservative (the capital cost is about 13 percent less than the flexible and dynamically operable designs), its annualized profit is lower than the other two designs, as it performs poorly in the 10 random scenarios. The capital costs of the flexible and dynamically operable design are very close with the dynamically operable design only being about 0.6 percent greater in capital cost. The difference in performance between the two designs is more due to how the capital cost is distributed (with the flexible design utilizing a more expensive column design and the dynamically operable design utilizing a more expensive compressor and PHX design) as opposed to the difference in capital cost.

Figure 3.8 illustrates some differences in the dynamic performance between the flexible and dynamically operable designs, where comparisons of the GN2 flow for two demand changes are shown. There are cases in the random 10 scenarios where the flexible design is not able to meet the endpoint demand. Such a case is shown in Figure 3.8(c), in contrast to Figure 3.8(d) where the same endpoint demand can be met by the dynamically operable design. In other cases, the flexible design is able to meet the demand, but is not able to track the demand change during the transition as well as the dynamically operable design. This is shown in Figures 3.8(a) and (b). .

From Figure 3.9 we see that when we relax the lower bound of the reboiler liquid level, the flexible design is able to meet the demand both at the endpoint and during transitions. This suggests that the reason the flexible design cannot meet demand is because it cannot meet the demand within the purity (PPMO) specifications both during endpoint and transition. When the lower reboiler level lower bound is relaxed, this allows for more reflux to enter the column and increase the nitrogen purity of the product. The same effect is seen when the endpoint purity is lowered (a higher PPMO is allowed), which allows the flexible design to meet the demand without violating the original reboiler level constraint.

Even though the flexible and dynamically operable designs from the six scenario

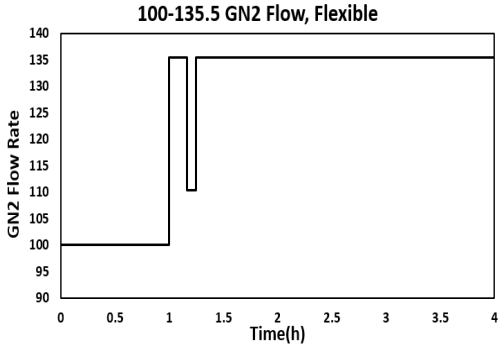

(a) A scenario where the endpoint demand is met by the flexible design, but during transition demand is not met

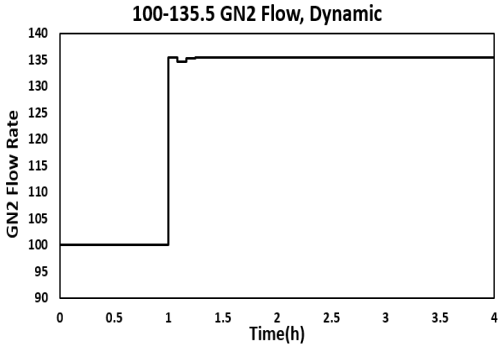

(b) Demand is met by the dynamically operable design compared)

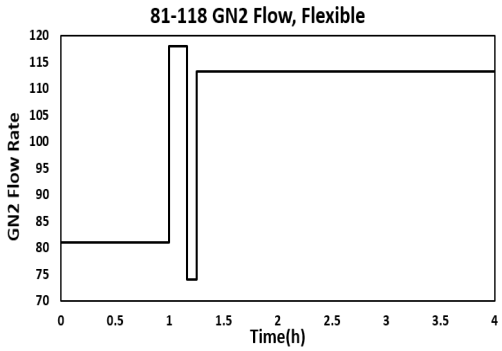

(c) A scenario where the flexible design cannot meet the demand

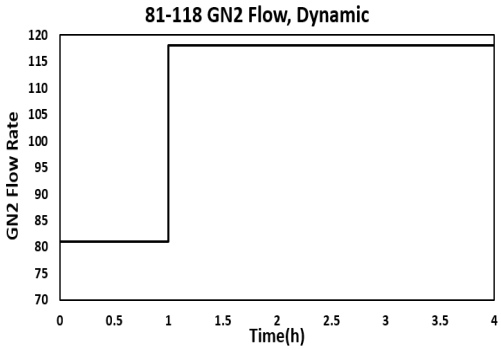

(d) The dynamically operable design in able to meet demand unlike the flexible design

Figure 3.8: Selected random scenarios showing the advantages of the dynamically operable design over the flexible design

optimization are somewhat similar, we have seen that this difference is still enough see differences in operational performance. In our experience with this study we have seen that the average demand change of the demand profiles affects the difference we see in the flexible and dynamically operable design. The larger the average change in demand, the more different the designs. To illustrate this, we did three single scenario optimizations, where the demand change was varied. The three scenarios were 85-125, 90-110 and 90-100. The results are seen in Tables 3.7, 3.8 and 3.9.

From Tables 3.7, 3.8 and 3.9 we can see that as the demand change decreases the

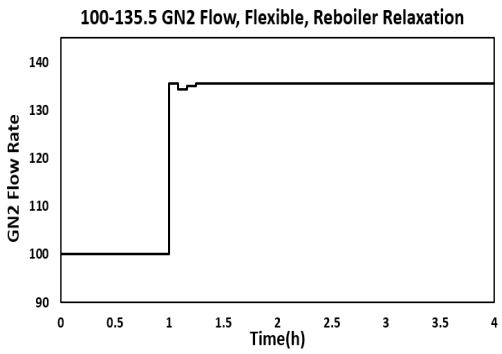

(a) The flexible design is very close to meeting demand completely during the transition when the reboiler constraint is relaxed

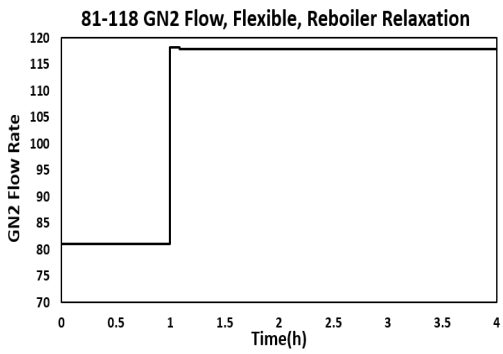

(b) The flexible design is able to meet endpoint demand, when the reboiler constraint is relaxed

Figure 3.9: The effect of constraint relaxation on the ability of the flexible design to meet demand

difference between the flexible and dynamically operable design also decreases. In addition to this, we see as the demand change decreases the difference in objective function value between the flexible and dynamically operable design also decreases. For 90-100 demand change we see that the dynamically operable and flexible design are almost identical. This shows that the flexible and dynamically operable design are highly dependent on the demand scenarios, and that the difference in the dynamically operable and flexible design may increase by choosing demand profiles that have greater demand changes on average.

Table 3.7: The results of single scenario optimization where demand changed from 85 to 125

Design Parameters	**Flexible Formulation**	**DO Formulation**
Column Diameter	100	98.0
PHX Length	100	99.8
Compressor Power	100	100.3
Objective Function	100	99.2

Table 3.8: The results of single scenario optimization where demand changed from 90 to 110

Design Parameters	**Flexible Formulation**	**DO Formulation**
Column Diameter	100	99
PHX Length	100	98.4
Compressor Power	100	100.2
Objective Function	100	99.5

Table 3.9: The results of single scenario optimization where demand changed from 90 to 100

Design Parameters	**Flexible Formulation**	**DO Formulation**
Column Diameter	100	99.4
PHX Length	100	100.04
Compressor Power	100	100.05
Objective Function	100	99.8

3.6 Conclusions and Future Work

This study considered the design of an air separation unit in which uncertain demand changes are taken into account. Three optimization-based design paradigms were explored. These comprised a steady-state design under a nominal static demand, a flexible design in which the expected economics are optimized subject to steady-state feasibility with respect to static demand levels in a specified uncertainty set, and a dynamically operable design in which feasibility of dynamic transitions between steady-states is additionally imposed. The latter two designs were formulated as two-stage stochastic programming problems.

Given the same uncertainty set, the flexible design provided a better annualized cost and lower operational costs over the uncertainty set than the dynamically operable design. However, when both designs were subjected to random demand scenarios and had to transition dynamically between the initial and final demand, the dynamically operable design provided superior operational profit on average. There were demand scenarios for which the nominal and flexible designs, under transient operation, were either unable to meet the final demand for the allowed number of input changes, and/or were unable to meet the demand during transition as well as the dynamically operable design. Thus when conducting design under uncertainty, the dynamics of the process should be taken into account.

An interesting trade-off between column diameter and maximum compressor power was observed. Focusing solely on the objective function as a metric for comparison can mask the differences between the designs. In this application, there is a shift in the distribution of costs between the flexible and dynamically operable designs. The difference between the flexible and dynamically operable designs was also shown to be impacted by the magnitude of the demand changes. It is therefore important that expected demand changes be carefully considered in the design problem formulation.

A useful configuration for ASU demand response operation is the inclusion of product storage in order to adjust production levels in response to electricity price changes, with demand in excess of production being met by stored product [Cao *et al.*, 2016b]. Design for this configuration under varying electricity prices would be a useful avenue for further study. The uncertainty in our case study was also limited to variation in demand. A useful extension would be consideration of additional sources of uncertainty, including short-term fluctuations (disturbances).

Chapter 4

A Bilevel Formulation for Integrated Design and Control under Uncertainty

4.1 Introduction

Motivated by the non-static operation ASUs may face from demand uncertainty, Chapter 3 used a two-stage stochastic optimization to find the optimal design and operation (to find the annualized profit) for a nitrogen plant operating under discrete demand uncertainty (several different demand scenarios). This study used a dynamic model of an ASU, as the dynamics of the plant should be taken into account given the plant is transitioning from one operating point to another. A characteristic of the formulation in Chapter 3, is that the optimization problem is allowed to choose the initial steady-state operating point. Thus the optimization could "back-off" from the optimal steady-state operating point (in terms of operational profit) to potentially reduce operational and capital costs over a future horizon that includes transitions.

This is a common paradigm in design and control studies where a nominal operating point is calculated such that feasibility can be maintained in the presence of disturbances. This however may be an unrealistic operation condition, as in an industrial setting you may not know future demand patterns and thus may choose to operate at the optimal steady-state instead. In this study we investigate optimal design and control of a chemical process, subject to demand uncertainty where several optimal steady-state points must be calculated with the plant subject to dynamic transitions between them.

Finding the optimal objective function (in this study annualized profit) while also ensuring that the initial and final operating points are at the steady-state optimum poses a bilevel problem. This is because the feasible region of the optimization is partly defined by maximizing the operating profit for the initial and final operating points. Bilevel problems are a common occurrence when finding an optimal design under uncertainty, where the uncertainty is a domain as compared to discrete values. This is seen in Mohideen *et al.* [1996] and Bahri *et al.* [1997] where optimization algorithms are used where an outer loop finds the optimal design, with a given disturbance or uncertainty set, and an inner loop is used to update the disturbance or uncertainty set (where the inner loop attempts to find a disturbance or uncertainty that maximizes the constraint violation for a given design). A common method used to transform a bilevel optimization into a single-level optimization, is to represent the inner most optimization in terms of its Karush-Kuhn-Tucker (KKT) conditions. This is applied in Pistikopoulos and Ierapetritou [1995] where determining the feasible region of an optimal design under uncertainty is posed as an optimization problem. The outer optimization finds the expected profit over an uncertainty set and the inner optimization determines the uncertainty set for a given design. The inner optimization problem is represented by its KKT conditions to transform the overall problem into a single level optimization. This method is also used in studies such as Baker and Swartz [2008] and Soliman *et al.* [2008] considering applications of MPC, where the

inner QP subproblem posed in MPC optimizations is replaced by its KKT conditions to again transform a bilevel optimization problem into a single level. Representing the inner optimization problem by its KKT conditions is the method used in this study to deal with the bilevel optimization investigated. This method will also be compared to a brute-force method applied to the bilevel problem. In the brute-force method, the optimal design is found by fixing the design and letting the optimization choose only the 2nd-stage decision variables. This is done for a range of designs to find which design provides the optimal overall objective value.

In this study using two-stochastic optimization we will find the optimal design and operation of chemical plant when the initial and final operating points must be at the steady-state optimum. We will compare this to the design where the optimization can choose the final and initial points. We will also look at various optimization formulations (that represent changes in operating conditions) that affect the designs. The expected difference in performance when subjected to certain operating conditions may elucidate why it is good design practice to incorporate optimal final and starting operating points for a chemical process.

4.2 Model Description

The model used in this study is based on the CSTRs in series utilized in Loeblein and Perkins [1998]. A diagram of the system is shown in Figure 4.1. In this model a the first order reaction A $\rightarrow$ B takes place in each CSTR. An additional side reaction B $\rightarrow$ C also takes place in each reactor. Fresh feed of pure A is fed to the first CSTR, and the exiting stream is sent to a mixer. The exiting stream from the first CSTR is mixed with additional feed of pure A and this is the feed sent to the second reactor. Each reactor is surrounded by a cooling jacket to remove excess heat. In Loeblein and Perkins [1998] the objective was to maximize the operating profit of the system (the

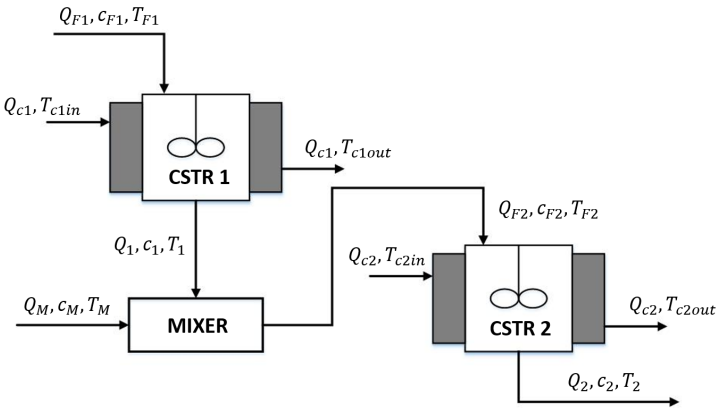

Figure 4.1: A schematic of the model used in this study

profit by selling product B) and this is also considered in this study. The model used in Loeblein and Perkins [1998] is a steady state model, but the model in this study is based on the dynamic model of the CSTR system used in Li and Swartz [2018]. The equations defining the model are as follows:

$$\frac{dc_{A1}}{dt} = Q_{F1}c_{A,F1} - Q_1 c_{A1} - c_{A1}V_d k_{0,I} e^{(-\frac{E_I}{RT_1})} \tag{4.1}$$

$$\frac{dc_{B1}}{dt} = Q_{F1}c_{B,F1} - Q_1 c_{B1} + c_{A1}V_d k_{0,I} e^{(-\frac{E_I}{RT_1})} - c_{B1}V_d k_{0,II} e^{-\frac{E_{II}}{RT_1}} \tag{4.2}$$

$$\frac{dc_{C1}}{dt} = Q_{F1}c_{C,F1} - Q_1 c_{C1} + c_{B1}V_d k_{0,II} e^{(-\frac{E_{II}}{RT_1})} \tag{4.3}$$

$$\frac{dT_1}{dt} = Q_{F1}T_{F1} - Q_1 T_1 - \frac{\Delta H_{R,I}}{\rho c_p} c_{A1}V_d k_{0,I} e^{(-\frac{E_I}{RT_1})} - \frac{\Delta H_{R,II}}{\rho c_p} c_{B1}V_d k_{0,II} e^{(-\frac{E_{II}}{RT_1})} - q_{cool,1} \tag{4.4}$$

$$\frac{dc_{A2}}{dt} = Q_{F2}c_{A,F2} - Q_2 c_{A2} - c_{A2}V_d k_{0,I} e^{(-\frac{E_I}{RT_2})} \tag{4.5}$$

$$\frac{dc_{B2}}{dt} = Q_{F2}c_{B,F2} - Q_2 c_{B2} + c_{A2}V_d k_{0,I} e^{(-\frac{E_I}{RT_2})} - c_{B2}V_d k_{0,II} e^{-\frac{E_{II}}{RT_2}} \tag{4.6}$$

$$\frac{dc_{C2}}{dt} = Q_{F2}c_{C,F2} - Q_2 c_{C2} + c_{B2}V_d k_{0,II} e^{(-\frac{E_{II}}{RT_2})} \tag{4.7}$$

$$\frac{dT_2}{dt} = Q_{F2}T_{F2} - Q_2 T_2 - \frac{\Delta H_{R,I}}{\rho c_p} c_{A2}V_d k_{0,I} e^{(-\frac{E_I}{RT_2})} - \frac{\Delta H_{R,II}}{\rho c_p} c_{B2}V_d k_{0,II} e^{(-\frac{E_{II}}{RT_2})} - q_{cool,2} \tag{4.8}$$

with the following algebraic equations:

$$q_{cool,i} = U_{a,i}\Delta T_{ln,i} \qquad i = 1,2 \tag{4.9}$$

$$\Delta T_{ln,i} = \frac{T_{ci,\text{out}} - T_{ci,\text{in}}}{ln(T_i - T_{ci,\text{in}})/(T_i - T_{ci,\text{out}})} \qquad i = 1,2 \tag{4.10}$$

$$q_{cool,i} = Q_{c,i}(T_{ci,\text{out}} - T_{ci,\text{in}}) \qquad i = 1,2 \tag{4.11}$$

$$Q_{F2} = Q_1 + Q_M \tag{4.12}$$

$$Q_{F2}c_{i,F2} = Q_1 c_{i,1} + Q_M c_{i,M} \qquad i = A,B,C \tag{4.13}$$

$$Q_{F2}T_{F2} = Q_1 T_1 + Q_M T_M \tag{4.14}$$

Table 4.1: The variables present in the two CSTR system

Variable	Description
Q_{Fi}	Feed to Reactor i
Q_i	Flow from Reactor i
Q_M	Feed to Mixer
c_{Ai}, c_{Bi}, c_{Ci}	Concentration of species A,B and C for reactor i respectively
$c_{AF2}, c_{BF2}, c_{CF2}$	Concentration of species A,B and C in the feed entering reactor 2 respectively
T_i	Temperature of reactor i
$T_{ci,out}$	Temperature of stream exiting cooling jacket of reactor i
$\Delta T_{ln,i}$	Log-mean temperature difference for reactor i and its cooling jacket
$q_{cool,i}$	Heat transfer between reactor i and its cooling jacket
V_d	Design volume for Reactor 1 and Reactor 2

The following constraints are also imposed:

$$T_1 \leq 350 \text{ K}, \quad T_2 \leq 350 \text{ K} \tag{4.15}$$

$$Q_{F1} + Q_M \leq 0.8 \text{ m}^3/\text{s} \tag{4.16}$$

$$T_{c1,\text{out}} \leq 330 \text{ K}, \quad T_{c2,\text{out}} \leq 300 \text{ K} \tag{4.17}$$

$$Q_{F1} \geq 0.05 \text{ m}^3/\text{s}, \quad Q_M \geq 0.05 \text{ m}^3/\text{s} \tag{4.18}$$

$$c_{A2} \leq 0.3 \text{ kmol/m}^3 \tag{4.19}$$

The state, control and design variables are defined in Table 4.1:

The parameters used in this model are provided in Appendix B.

4.3 Bilevel Formulation

As previously mentioned, when future operational points are uncertain due to factors such as uncertain demand or electricity price, it is logical for the current operating point to be at the steady-state optimum (the operational profit is optimal for a given design). Furthermore when transition does occur from one point to another, the final operating point can be considered the new operating point until further notice and thus should also be at the steady-state optimum. Thus a general integrated design and control problem where the initial and final point are optimal can be expressed in Equation 4.20.

$$
\begin{aligned}
\max_{\mathbf{d},\mathbf{u}(t)} \quad & [\phi(\mathbf{d},\mathbf{x}(t),\mathbf{y}(t),\mathbf{u}(t)) - f(\mathbf{d})] \\
\text{s.t} \quad & \mathbf{z}(\mathbf{d},\dot{\mathbf{x}}(t),\mathbf{x}(t),\mathbf{y}(t),\mathbf{u}(t)) = \mathbf{0} \\
& \mathbf{h}(\mathbf{d},\mathbf{x}(t),\mathbf{y}(t),\mathbf{u}(t)) = \mathbf{0} \\
& \mathbf{g}(\mathbf{d},\mathbf{x}(t),\mathbf{y}(t),\mathbf{u}(t)) \leq \mathbf{0} \\
\max_{\mathbf{x}(0),\mathbf{y}(0),\mathbf{u}(0)} \quad & \phi_{ss}(\mathbf{d},\mathbf{x}(0),\mathbf{y}(0),\mathbf{u}(0)) \\
\max_{\mathbf{x}(t_f),\mathbf{y}(t_f),\mathbf{u}(t_f)} \quad & \phi_{ss}(\mathbf{d},\mathbf{x}(t_f),\mathbf{y}(t_f),\mathbf{u}(t_f)) \\
& \dot{\mathbf{x}}(0) = \mathbf{0} \\
& \dot{\mathbf{x}}(t_f) = \mathbf{0} \\
& t_o \leq t \leq t_f
\end{aligned}
\tag{4.20}
$$

Where $\phi(\mathbf{d},\mathbf{x}(t),\mathbf{y}(t),\mathbf{u}(t))$ is the operational profit, $\mathbf{d}$, $\mathbf{x}(t)$, $\mathbf{y}(t)$ and $\mathbf{u}(t)$ are the design, differential, algebraic and control variables and $f(\mathbf{d})$ is the capital cost. $\mathbf{z}$ and $\mathbf{h}$ are the differential algebraic equations (DAEs) that define the system and $\mathbf{g}$ are the constraints for the optimization. $\dot{\mathbf{x}}(0) = \mathbf{0}$ is our initial condition for the system,

where the system is initially at steady-state. $\dot{\mathbf{x}}(t_f) = \mathbf{0}$ ensures that our system is at steady-state at the final time point. ϕ_{ss} is the equation for operational profit at a given time point (since for a dynamic optimization, objective functions are integrated over time). We see from the formulation that the initial and final operating points must be steady-state optimal for the operational profit at that point. Thus we have a bilevel formulation. In this section we deal with the bilevel formulation in two ways, using a brute-force method and replacing the inner optimizations with their KKT conditions. To compare these two methods we consider a dynamic optimization problem where a single demand change takes place. The objective used here is to minimize unmet demand in addition to minimizing the operational and capital costs. This is expressed in Equation 4.21:

$$\min_{Q_{F1},Q_M,V_d} \int_0^{t_f} [100(\, Q_2 c_{B2} - \mathit{Demand\ Setpoint})^2 + 0.01 q_{cool,1} + q_{cool,2} + 0.1 Q_{F1} + 0.1 Q_M] + 10 V_d \tag{4.21}$$

In Equation 4.21, $Q_2 c_b$ is the molar flow of species B from Reactor 2, and the fresh feed to Reactor 1 and the fresh feed to the Mixer are the control variables (Q_{F1} and Q_M). The fresh feed to Reactor 1 and to the the Mixer, as well as the cooling required for both tanks are our operational costs. The volume of both CSTRs (which are the same value, V_d) is our design variable. This is a rudimentary objective function used to examine the methods used to solve the bilevel problem. More rigorous profit based objective functions will be used later when a more formal design problem is considered. The demand step change used is shown in Figure 4.2.

In the dynamic optimization study used to compare the brute force method to the KKT methods, the operation horizon is 16 seconds, with there being 10 control intervals. The first control interval is 2 s (the initial steady state), the following 8 control intervals are 0.5 s in length and the final control interval is 10 s long. Thus our dy-

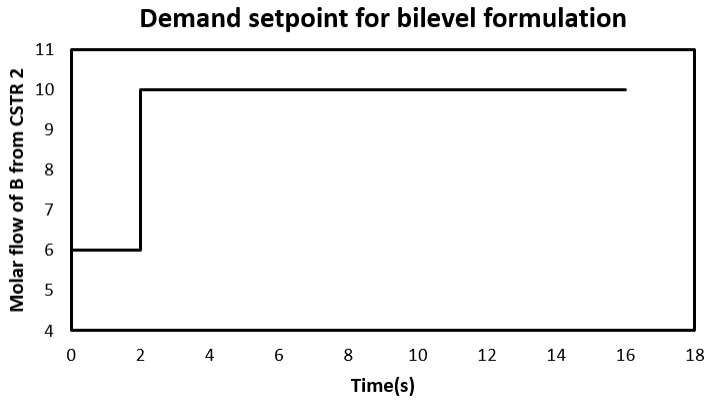

Figure 4.2: The demand scenario used in the dynamic optimization to compare bilevel solution methods

namic optimization is defined by the DAE in Equations 4.1 to 4.14, the constraints in Equations 4.15 to 4.19, the formulation in Equation 4.20 and the objective function in Equation 4.21. To integrate the DAE we use the Backward Euler discretization method and use the simultaneous method to solve the dynamic optimization. See Appendix B for further detail on the Backward Euler method.

The steps for the brute force method to find a bilevel solution are given below:

1. Choose a set design of variables (in this example, a specific value for volume V_d) for the system within a selected range of designs
2. At the chosen design, find the steady-state optimal operating point for the initial and final points
3. In a dynamic optimization, fix the final and initial points at the optimal operating points found in Step 2 (in this example, Q_{F1} and Q_M at t = 0 and t = t_f are fixed) and set the design variables to the design chosen in Step 1
4. Find the optimal operating trajectories via dynamic optimization
5. Repeat Steps 1-4 for all other design variables within the selected range

Thus for the brute force method we simply just pick a range of designs and enumerate through all of them to find the optimal solution. By removing the design as a decision variable we reduce the problem to a single level optimization. This is because we can find the optimal steady-states for the initial and final points beforehand, as opposed to in the bilevel formulation.

4.3.1 KKT Conditions

As shown in Soliman *et al.* [2008], a bilevel optimization can be reduced to a single level optimization where the inner optimization is replaced by its KKT conditions. If the inner optimization problem is convex, as in the case in Soliman *et al.* [2008], then the KKT conditions are necessary and sufficient for optimality. For the problem considered in this work, the KKT conditions are in general necessary but not sufficient for optimality, but numerical experiments indicate that the replacement of the inner optimizations with their KKT conditions does indeed yield a solution of the bilevel problem. The inner optimization is a steady-state optimization that can be formulated in Equation 4.22. In this formulation we have a steady state model of the dynamic optimization problem presented in Equation 4.20. Equation 4.22 shows the equations governing the steady-state optimal operating point with respect to the initial time point t = 0; however Equation 4.22 can also be applied to the final operating point by letting t = t_f. Equation $\mathbf{z_{ss}}$ are the set of differential equations $\mathbf{z}$, where the derivatives have been set to 0 and applied to only a single point in time. $\mathbf{h_{ss}}$ and $\mathbf{g_{ss}}$ are the set of algebraic equations $\mathbf{h}$ and constraints $\mathbf{g}$ that are applied to a single point in time ($\mathbf{g_{ss}}$ has no path constraints). From Equation 4.22 we can

derive the KKT conditions and Equation 4.20 can be reformulated as Equation 4.23.

$$\begin{aligned} \max_{\mathbf{x}(0),\mathbf{y}(0),\mathbf{u}(0)} \quad & [\phi_{ss}(\mathbf{d},\mathbf{x}(0),\mathbf{y}(0),\mathbf{u}(0))] \\ \text{s.t} \quad & \mathbf{z_{ss}}(\mathbf{x}(0),\mathbf{y}(0),\mathbf{u}(0)) = \mathbf{0} \\ & \mathbf{h_{ss}}(\mathbf{x}(0),\mathbf{y}(0),\mathbf{u}(0)) = \mathbf{0} \\ & \mathbf{g_{ss}}(\mathbf{x}(0),\mathbf{y}(0),\mathbf{u}(0)) \leq \mathbf{0} \end{aligned} \tag{4.22}$$

$$\begin{aligned} \max_{\mathbf{d},\mathbf{u}(t)} \quad & [\phi(\mathbf{d},\mathbf{x}(t),\mathbf{y}(t),\mathbf{u}(t)) - f(\mathbf{d})] \\ \text{s.t} \quad & \mathbf{z}(\mathbf{d},\dot{\mathbf{x}}(t),\mathbf{x}(t),\mathbf{y}(t),\mathbf{u}(t)) = \mathbf{0} \\ & \mathbf{h}(\mathbf{d},\mathbf{x}(t),\mathbf{y}(t),\mathbf{u}(t)) = \mathbf{0} \\ & \mathbf{g}(\mathbf{d},\mathbf{x}(t),\mathbf{y}(t),\mathbf{u}(t)) \leq \mathbf{0} \\ & \nabla_{[\mathbf{x}(0),\mathbf{y}(0),\mathbf{u}(0)]}\mathcal{L}(\mathbf{d},\mathbf{x}(0),\mathbf{y}(0),\mathbf{u}(0),\boldsymbol{\nu_0},\boldsymbol{\lambda_0}) = \mathbf{0} \\ & \nabla_{[\mathbf{x}(t_f),\mathbf{y}(t_f)\mathbf{u}(t_f)]}\mathcal{L}(\mathbf{d},\mathbf{x}(t_f),\mathbf{y}(t_f),\mathbf{u}(t_f),\boldsymbol{\nu_f},\boldsymbol{\lambda_f}) = \mathbf{0} \\ & \boldsymbol{\lambda_0}^T\mathbf{g_{ss}}(\mathbf{d},\mathbf{x}(0),\mathbf{y}(0),\mathbf{u}(0)) = 0 \\ & \boldsymbol{\lambda_f}^T\mathbf{g_{ss}}(\mathbf{d},\mathbf{x}(t_f),\mathbf{y}(t_f),\mathbf{u}(t_f)) = 0 \\ & \dot{\mathbf{x}}(0) = \mathbf{0} \\ & \dot{\mathbf{x}}(t_f) = \mathbf{0} \\ & \boldsymbol{\lambda_0} \geq \mathbf{0} \\ & \boldsymbol{\lambda_f} \geq \mathbf{0} \\ & t_o \leq t \leq t_f \end{aligned} \tag{4.23}$$

$\boldsymbol{\nu_0}$ and $\boldsymbol{\nu_f}$ are the Lagrange multipliers for the equality constraints of the steady-state optimization at the initial and final time points respectively. $\boldsymbol{\lambda_0}$ and $\boldsymbol{\lambda_f}$ are the

Lagrange multipliers for the inequality constraints of the steady-state optimization at the initial and final time points respectively. $\mathcal{L}$ is the Lagrangian function that is defined in Equation 4.24. $\nabla_{[\mathbf{x}(0),\mathbf{y}(0),\mathbf{u}(0)]}\mathcal{L}(\mathbf{d},\mathbf{x}(0),\mathbf{y}(0),\mathbf{u}(0),\boldsymbol{\nu_0},\boldsymbol{\lambda_0}) = \mathbf{0}$ and $\nabla_{[\mathbf{x}(t_f),\mathbf{y}(t_f)\mathbf{u}(t_f)]}\mathcal{L}(\mathbf{d},\mathbf{x}(t_f),\mathbf{y}(t_f),\mathbf{u}(t_f),\boldsymbol{\nu_f},\boldsymbol{\lambda_f}) = \mathbf{0}$ are the stationarity constraints for the KKT conditions at the initial and final time points respectively. ${\boldsymbol{\lambda_0}}^T\mathbf{g_{ss}}(\mathbf{d},\mathbf{x}(0),\mathbf{y}(0),\mathbf{u}(0)) = 0$ and ${\boldsymbol{\lambda_f}}^T\mathbf{g_{ss}}(\mathbf{d},\mathbf{x}(t_f),\mathbf{y}(t_f),\mathbf{u}(t_f)) = 0$ are the complementarity constraints of the KKT conditions at the initial and final time points respectively. $\mathbf{h_{ss}}$ and $\mathbf{g_{ss}}$ that are part of the KKT conditions are implicit, since they are included in the constraints $\mathbf{h}$ and $\mathbf{g}$. The complementarity constraints as they are formulated currently can pose numerically difficulties for standard NLP solvers. Techniques for dealing with these constraints are seen in Soliman *et al.* [2008] where the complimentary conditions are posed as mixed-integer constraints. In this study we use the technique implemented in Jamaludin and Swartz [2017] where the complementarity constraints are formulated as penalty functions in the objective function. With Equation 4.25 being the new objective function, Equation 4.23 can then be reformulated as Equation 4.26 where ρ_0 and ρ_f are the weights for the penalty functions.

$$\begin{aligned}\mathcal{L}(\mathbf{d},\mathbf{x}(t),\mathbf{y}(t),\mathbf{u}(t),\boldsymbol{\nu},\boldsymbol{\lambda}) =& \phi_{ss}(\mathbf{d},\mathbf{x}(t),\mathbf{y}(t),\mathbf{u}(t)) - \boldsymbol{\nu}^T\mathbf{h_{ss}}(\mathbf{d},\mathbf{x}(t),\mathbf{y}(t),\mathbf{u}(t)) \\ &- \boldsymbol{\lambda}^T\mathbf{g_{ss}}(\mathbf{d},\mathbf{x}(t),\mathbf{y}(t),\mathbf{u}(t))\end{aligned} \tag{4.24}$$

$$\begin{aligned}\phi_{kkt}(\mathbf{d},&\mathbf{x}(t),\mathbf{y}(t),\mathbf{u}(t),\boldsymbol{\lambda_0},\boldsymbol{\lambda_f}) = \phi(\mathbf{d},\mathbf{x}(t),\mathbf{y}(t),\mathbf{u}(t)) - f(\mathbf{d}) \\ &- \rho_0[{\boldsymbol{\lambda_0}}^T\mathbf{g_{ss}}(\mathbf{d},\mathbf{x}(0),\mathbf{y}(0),\mathbf{u}(0))] - \rho_f[{\boldsymbol{\lambda_f}}^T\mathbf{g_{ss}}(\mathbf{d},\mathbf{x}(t_f),\mathbf{y}(t_f),\mathbf{u}(t_f))]\end{aligned} \tag{4.25}$$

$$
\begin{aligned}
\max_{\mathbf{d},\mathbf{u}(t),\boldsymbol{\lambda_0},\boldsymbol{\lambda_f}} \quad & \phi_{kkt}(\mathbf{d},\mathbf{x}(t),\mathbf{y}(t),\mathbf{u}(t),\boldsymbol{\lambda_0},\boldsymbol{\lambda_f}) \\
\text{s.t} \quad & \mathbf{z}(\mathbf{d},\dot{\mathbf{x}}(t),\mathbf{x}(\mathbf{t}),\mathbf{y}(\mathbf{t}),\mathbf{u}(\mathbf{t})) = \mathbf{0} \\
& \mathbf{h}(\mathbf{d},\mathbf{x}(t),\mathbf{y}(t),\mathbf{u}(t)) = \mathbf{0} \\
& \mathbf{g}(\mathbf{d},\mathbf{x}(t),\mathbf{y}(t),\mathbf{u}(t)) \leq \mathbf{0} \\
& \nabla_{[\mathbf{x}(0),\mathbf{y}(0)\mathbf{u}(0)]}\mathcal{L}(\mathbf{d},\mathbf{x}(0),\mathbf{y}(0),\mathbf{u}(0),\boldsymbol{\nu_0},\boldsymbol{\lambda_0}) = \mathbf{0} \\
& \nabla_{[\mathbf{x}(t_f),\mathbf{y}(t_f)\mathbf{u}(t_f)]}\mathcal{L}(\mathbf{d},\mathbf{x}(t_f),\mathbf{y}(t_f),\mathbf{u}(t_f),\boldsymbol{\nu_f},\boldsymbol{\lambda_f}) = \mathbf{0} \\
& \dot{\mathbf{x}}(0) = \mathbf{0} \\
& \dot{\mathbf{x}}(t_f) = \mathbf{0} \\
& \boldsymbol{\lambda_0} \geq \mathbf{0} \\
& \boldsymbol{\lambda_f} \geq \mathbf{0} \\
& t_o \leq t \leq t_f
\end{aligned}
\tag{4.26}
$$

Thus now with the KKT conditions formulated to solve the bilevel problem as a single level optimization problem we can compare the KKT and brute force methods. It should be noted that in this formulation for the 2 CSTR model, the final steady-state is almost identical to the optimal steady-state regardless whether optimality for the final steady-state is enforced. Thus for the sake of simplicity in our comparison we only enforce steady-state optimality for the initial point (in later formulations, where integrated design and control is the focus, we do enforce the KKT conditions at the initial and final time points). The brute force method was implemented for a tank volume (where both CSTR tanks have the same tank volume, V_d) between 3.8 m^3 and 8 m^3. The initial volume selected was 3.8 m^3 and the steps for the brute force method were carried out. The volume was then incremented by 0.1 m^3 and the steps were carried out again. This was repeated until the volume selected reached 8 m^3. Thus the brute force method tried 43 different designs between between 3.8 m^3

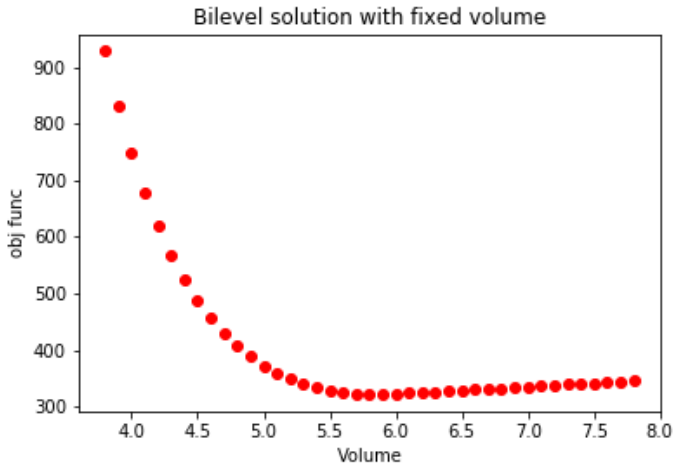

Figure 4.3: The brute force method implemented for volumes between 3.8 m^3 and 8m^3 using the objective function in Equation 4.21

and 8 m^3. The results of the brute force method are presented in Figure 4.3. From Figure 4.3 we see that the minimum objective function value occurs at a volume of 5.8 m^3 with a value of 321.869. The next two lowest objective function values occur at 5.7 m^3 and 5.9 m^3. Thus the optimal solution is between 5.7 m^3 and 5.8 m^3 or 5.8 m^3 and 5.9 m^3. When the KKT conditions are used to solve the bilevel problem using the formulation in Equation 4.26 (but with the KKT conditions only applied to the initial point as previously mentioned) the optimal volume is 5.81 m^3 with an objective function of 321.857. Thus we can see the optimal solution found by the brute-force method is almost identical to the optimal solution found by the KKT conditions, furthermore the KKT conditions provides a better solution as we would expect, as the brute-force method can only choose from a discrete set of volumes. These experimental results demonstrate that we can use the KKT conditions (despite being only necessary conditions for the inner optimization problem) to represent the inner optimizations posed in the bilevel formulation and thus solve the problem posed in Equation 4.20

4.3.2 KKT Design vs. Relaxed Design

The bilevel formulation was suggested as a more realistic design formulation for systems that have to transition between steady-states. What we would like to show are the benefits of operating using this formulation. The formulation we would compare the bilevel design to, is when the optimization problem is allowed to pick any initial and final operating point. Thus this formulation is very similar to Equation 4.20, but no inner optimization is present, thus giving the formulation in Equation 4.27. The design resulting from this formulation will be referred to as the Relaxed design. As previously stated the KKT design is 5.81 m^3 and from the formulation in Equation 4.27 the design generated (the Relaxed Design) is 4.17 m^3 with an objective function value of 308.641. Thus we can see the relaxed design is significantly smaller and provides a better objective function. Both designs are able to meet the demand change almost immediately as seen from Figure 4.4. However there are several operating differences, the most significant difference being the temperature at which Reactor 1 initially operates at as seen in Figure 4.5. We see that since the Relaxed design is able to choose the initial operating conditions, it is able to operate at a much lower initial temperature. Furthermore because the volume of the tank in the KKT design is larger, it can operate at lower concentrations as seen in Figure 4.6.

$$
\begin{aligned}
\max_{\mathbf{d},\mathbf{u}(t)} \quad & [\phi(\mathbf{d},\mathbf{x}(t),\mathbf{y}(t),\mathbf{u}(t)) - f(\mathbf{d})] \\
s.t \quad & \mathbf{z}(\mathbf{d},\dot{\mathbf{x}}(t),\mathbf{x}(t),\mathbf{y}(t),\mathbf{u}(t)) = \mathbf{0} \\
& \mathbf{h}(\mathbf{d},\mathbf{x}(t),\mathbf{y}(t),\mathbf{u}(t)) = \mathbf{0} \\
& \mathbf{g}(\mathbf{d},\mathbf{x}(t),\mathbf{y}(t),\mathbf{u}(t)) \leq \mathbf{0} \\
& \dot{\mathbf{x}}(0) = \mathbf{0} \\
& t_o \leq t \leq t_f
\end{aligned}
\tag{4.27}
$$

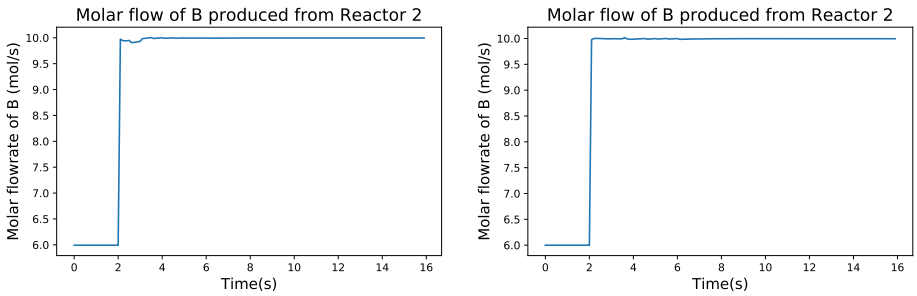

(a) KKT design (b) Relaxed design

Figure 4.4: The molar flow rate of B produced by Reactor 2 in the KKT and relaxed designs

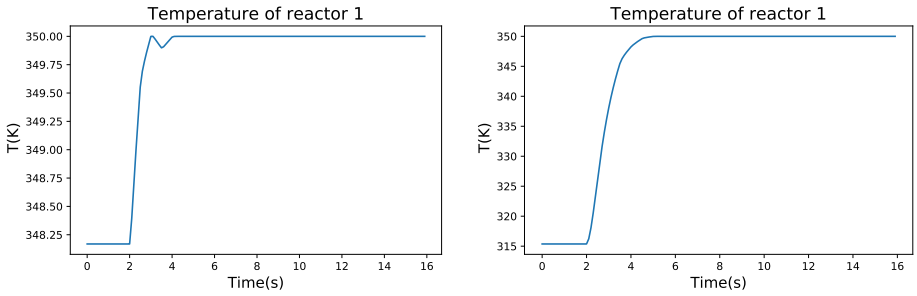

(a) KKT design (b) Relaxed design

Figure 4.5: The temperature profiles for Reactor 1 in the KKT and Relaxed designs

When we apply the KKT formulation with the volume fixed to that determined by the Relaxed design (thus the Relaxed design is forced to operate initially at the steady-state optimum) its performance is far worse as it is not able to meet demand immediately (as can be seen from Figure 4.7(a)). The new objective function value is 634.857. This is consistent with Figure 4.3, as the objective function value is between the objective function value for a volume between 4.1 and 4.2 m^3. This again shows that the KKT formulation is consistent with the brute-force method. The reason the relaxed design cannot initially meet the demand when operating at the initial optimum is because it cannot initially increase the volumetric flow rate exiting from Reactor 2 need to meet the demand. This can be seen in Figure 4.7(b), where the volumetric flow rate profile has a very similar behavior to the molar flow rate of B.

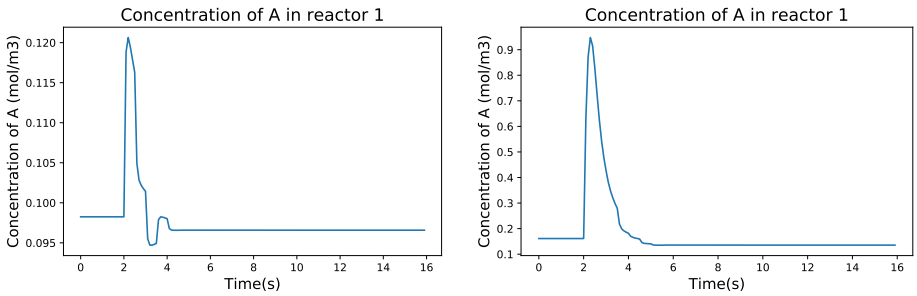

(a) KKT design (b) Relaxed design

Figure 4.6: The concentration profiles of A for Reactor 1 in the KKT and Relaxed designs

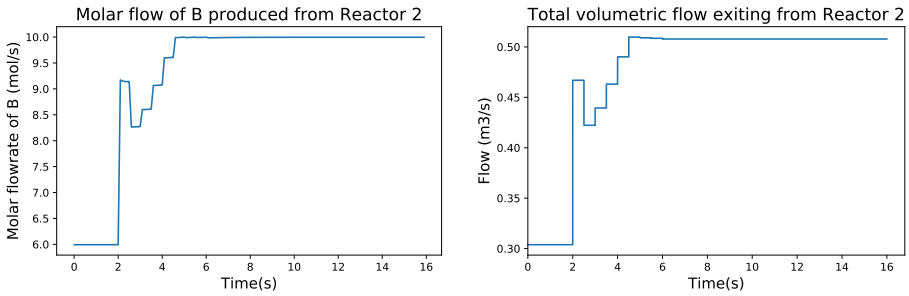

(a) The molar flow rate of B produced (b) The total flow rate from Reactor 2

Figure 4.7: Production profiles for the Relaxed design initially operating at the steady-state optimum

The reason the Relaxed design cannot meet the demand in this case is seen in comparing the control profiles between the KKT design and the Relaxed design initially at the steady-state optimum. From Figure 4.8 we see the primary difference is the Relaxed design is not able to add as much fresh feed of pure A to the Mixer as the KKT design. This is because the Relaxed design has a smaller volume, hence the concentration of A in Reactor 1 is higher than in the KKT design. In the Mixer the exiting stream of Reactor 1 is mixed with fresh feed. Thus in the Relaxed design, because of the high concentration of A in the exiting feed from Reactor 1, does not add as much feed of pure A to prevent the concentration of A in Reactor 2 from exceeding 0.3 $\frac{mol}{m^3}$, which is an operating constraint. This is seen in Figures 4.9 and

4.10 which show the concentration of A in the first and second reactors respectively for the KKT and Relaxed design initially at the steady-state optimum. From Figure 4.9 we see that the concentration in Reactor 1 for the Relaxed design at the steady-state optimum is about 30 percent higher, and consequently as seen in Figure 4.10, the Relaxed design operates at the maximum concentration in Reactor 2 for much longer.

The addition of fresh feed is necessary to meet the required volumetric flow rate to meet the demand because as seen in Figure 4.11, the concentration of B in Reactor 2 stays roughly the same throughout operation and this is why the increase in flow rate is needed to meet demand as we can't just increase the concentration of B instead. The KKT design due to it's larger volume has a lower concentration of A from Reactor 1 entering the Mixer, and thus more fresh feed can be added. The flow rate also can't be increased by adding more feed to Reactor 1 in the Relaxed design. This is because when the Relaxed design is forced to operate at the steady-state optimum, its initial operating temperature is much closer to 350 K (around 348 K) compared to when it could operate at any initial steady-state (as seen from Figure 4.5(b) where it operates at around 317 K). Thus any additional feed to Reactor 1 will cause the temperature in Reactor 1 to exceed 350 K, which is a constraint violation. A comparison of temperature profiles for Reactor 1 for the Relaxed design and the Relaxed design at the steady-state optimum can be seen in Figure 4.12.

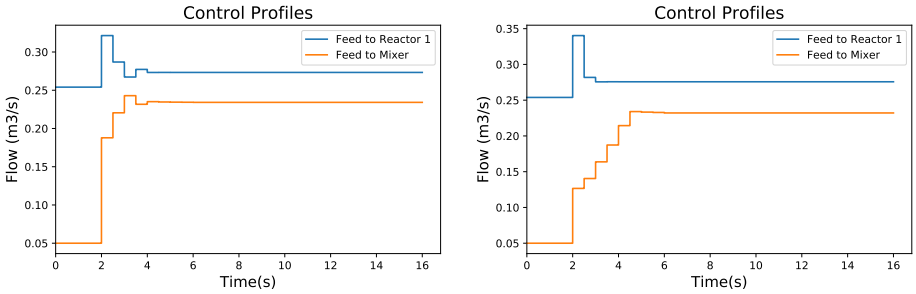

(a) KKT design (b) Relaxed Design at SS optimum

Figure 4.8: The control profiles for selected designs

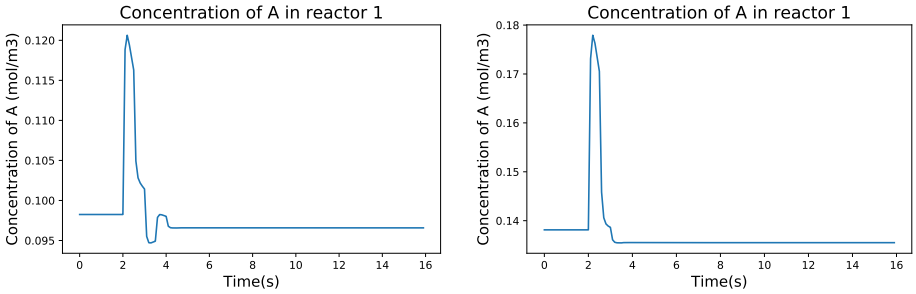

(a) KKT design (b) Relaxed Design at SS optimum

Figure 4.9: The concentration profile of A in Reactor 1 for the KKT design and the Relaxed design at the steady-state optimum

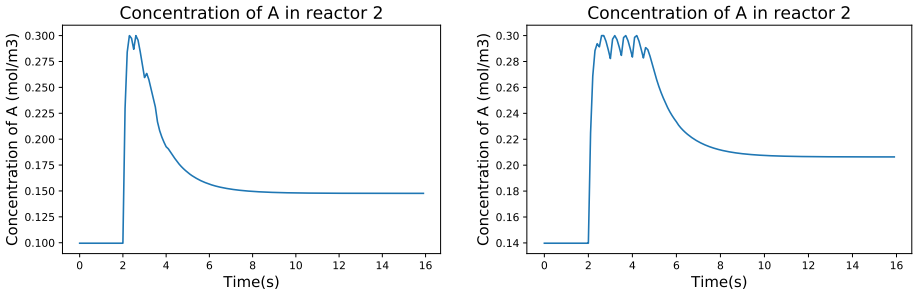

(a) KKT design (b) Relaxed Design at SS optimum

Figure 4.10: The concentration profile of A in Reactor 2 for the KKT design and the Relaxed design at the steady-state optimum

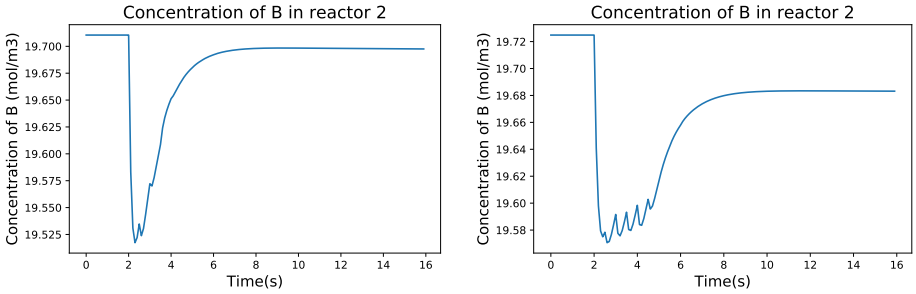

(a) KKT design (b) Relaxed Design at SS optimum

Figure 4.11: The concentration profile of B in Reactor 2 for the KKT design and the Relaxed design at the steady-state optimum

When the Relaxed design is allowed to choose the initial operating point (that's not steady-state optimal) it chooses a point where the temperature of Reactor 1 is far below 350 K. Operating at a temperature much lower than 350 K, allows the feed to Reactor 1 to be increased far more than in other designs. This is seen in Figure 4.13 where to meet the demand change, the feed to Reactor 1 is increased to levels far greater than the KKT design or when the Relaxed design has to be at the operate steady optimum (0.45 $\frac{m^3}{s}$ compared to around 0.33 $\frac{m^3}{s}$). This demonstrates that depending on the operating conditions, additional demand increases can be met either by increasing feed to the Mixer or increasing feed to Reactor 1.

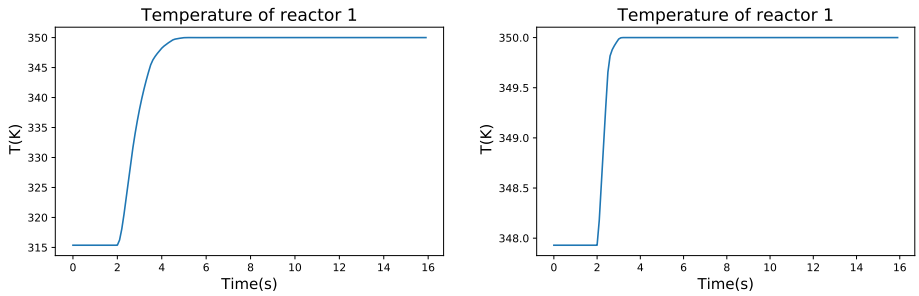

(a) Relaxed design (b) Relaxed design at SS optimum

Figure 4.12: The temperature profiles for Reactor 1 for the Relaxed design and the Relaxed design being forced to operate initally at the steady-state optimum

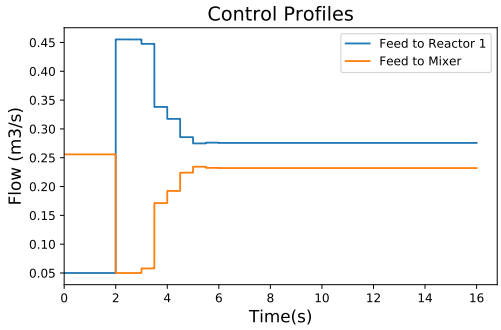

Figure 4.13: The control profiles for the Relaxed design that can choose the initial operating point

4.4 Design under Uncertainty

Now that we have established that utilizing the KKT conditions can generate a bilevel solution, and its advantages compared to a relaxed formulation, we would like to develop a more formal design problem. Uncertainty in an optimization formulation is often captured using a two-stage stochastic optimization, and this is the method that will be used in this study. In this study, six different demand scenarios will used to define the uncertainty space.

The problem formulation used in the previous section has a horizon of 16 seconds which is not very realistic for an operating scenario. In our new formulation each

scenario will be one hour long and flow rates and parameters are now in terms of minutes instead of seconds. If the dynamics are too fast, then utilizing a dynamic optimization formulation is not very important, hence we have reduced the reaction constants $k_{0,I}$ and $k_{0,II}$ to slow down the dynamics of the process. The most significant change is the objective function where instead of using set-point tracking, the objective function is now daily profit. In this formulation no additional revenue is generated for production greater than demand, thus its contribution to the objective function can be expressed in terms of the minimum function seen in Equation 4.28. However a minimum function can pose numerical difficulties so we will estimate this using a function consisting of hyperbolic tangent functions. In Equation 4.29 we present a hyperbolic tangent function that is used the calculate the revenues of the plant, where $Q_2 c_{B2}$ is the molar flow rate of B from Reactor 2 and β is a parameter that adjusts the steepness of the hyperbolic tangent function (the larger β the more Equation 4.29 behaves like a step function). For our daily profit we let the profit represent the average profit made in a day. Thus for a single 1hr scenario we must multiply the profit by 24 to get the daily profit and the capital cost of the tank represents the capital cost amortized to a day. The daily profit is expressed in Equation 4.30

$$\phi(x, Demand) = \min[x, Demand] = \begin{cases} x & x \leq Demand \\ Demand & Demand \leq x \end{cases} \tag{4.28}$$

$$\phi_{rev} = \frac{1}{2} Q_2 c_{B2} \cdot \big[1 + tanh[\beta(Demand - Q_2 c_{B2})])\big] + \frac{1}{2} Demand \cdot \big[1 - tanh[\beta(Demand - Q_2 c_{B2})]\big] \tag{4.29}$$

$$\phi = 24 \int_0^{t_f} [10\phi_{rev} - 0.01 q_{cool,1} - q_{cool,2} - 0.1 Q_{F1} - 0.1 Q_M] dt + 240 V_d \tag{4.30}$$

4.4.1 Two-stage stochastic optimization

To capture the uncertainty in the demand we use six 1hr scenarios where starting from an initial demand at steady-state, either a step up or step down in demand is made. In the demand profile, the initial demand is held for 20 minutes and then steps up or down to the final demand for the next 40 minutes. To generate the six scenarios, we use three demands, a low, medium and high demand. In this study we have chosen the demand to be 6, 8 and 10 moles of B produced per minute. The six demand profiles are generated from all possible permutations of selecting two of the demands for the demand profile. Thus in our 6 scenarios with have three demand increases and three demand decreases. The scenarios used can be seen in Figure 4.14. Each scenario will correspond to a model that uses the DAE defined by Equations 4.1 to 4.14 and the operating constraints from Equations 4.15 -4.19 (thus the the same model used in Section 4.3 with the reaction constants changed).

For the formulation of the two stage optimization, we have a common design (volume) for each scenario, which is our first stage decision variable. The objective function of two-stage stochastic optimization is the expected value of the objective function over the six scenarios. However since the capital cost will be the same for all six scenarios we can move it to outside the expected value function. Thus the overall objective function can be expressed as the expected value of the operational profit of the six scenarios plus a capital cost function. Thus defining ϕ_{op} in Equation 4.31 we can then formulate the two-stage stochastic optimization in 4.32. $\theta(t)$ represents the uncertainty profile domain and $\theta_i(t)$ is a single realization of the uncertainty. The uncertainty domain in this study is discrete, consisting of six demand scenarios. $\mathbf{x}_i(t)$, $\mathbf{y}_i(t)$ and and $\mathbf{u}_i(t)$ are the differential, algebraic and control variables for uncertainty

scenario $\theta_i(t)$.

$$\phi_{op} = 24 \int_0^{t_f} [10\phi_{rev} - 0.01q_{cool,1} - q_{cool,2} - 0.1Q_{F1} - 0.1Q_M]dt \tag{4.31}$$

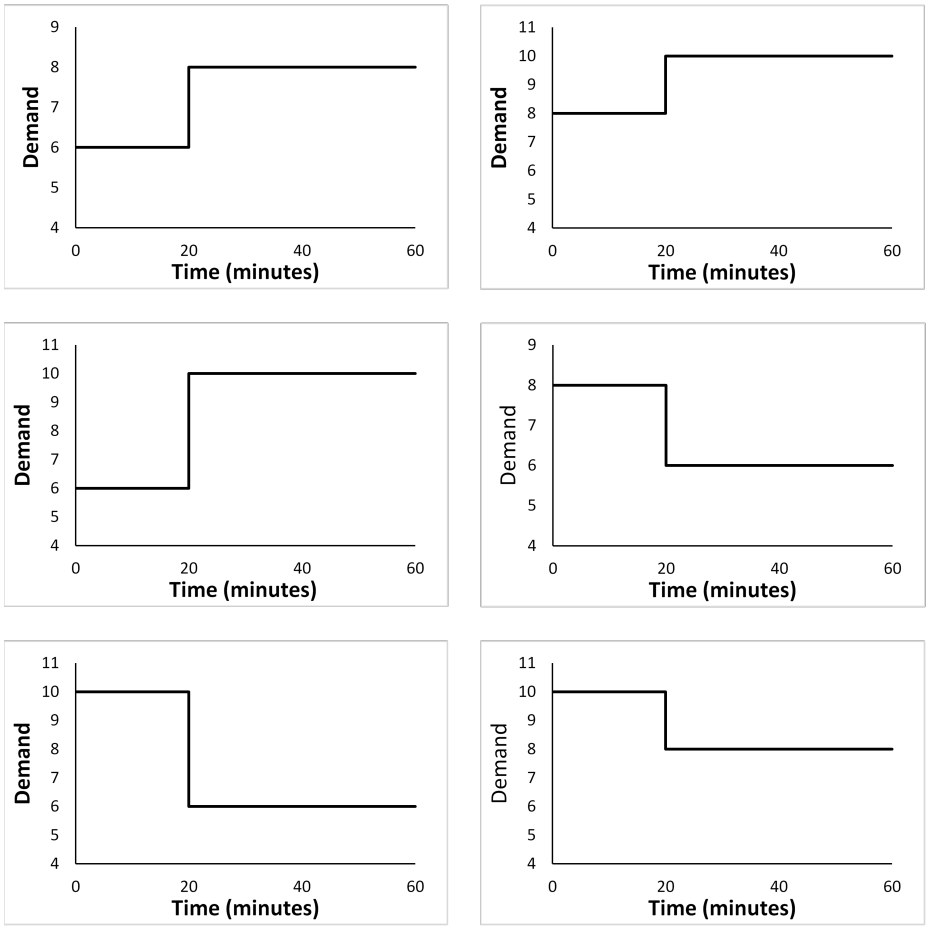

Figure 4.14: The six demand scenarios used in the two-stage stochastic optimization

$$
\begin{aligned}
\max_{\mathbf{d},\mathbf{u}_1(t)....\mathbf{u}_n(t)} \quad & \underset{\theta(t)}{E}[\phi_{op}(\mathbf{d},\mathbf{x}(t),\mathbf{y}(t),\mathbf{u}(t),\theta(t)] - f(\mathbf{d}) \\
\text{s.t} \quad & \mathbf{z}(\mathbf{d},\dot{\mathbf{x}}_i(t),\mathbf{x}_i(t),\mathbf{y}_i(t),\mathbf{u}_i(t),\theta_i(t)) = \mathbf{0} \\
& \mathbf{h}(\mathbf{d},\mathbf{x}_i(t),\mathbf{y}_i(t),\mathbf{u}_i(t),\theta_i(t)) = \mathbf{0} \\
& \mathbf{g}(\mathbf{d},\mathbf{x}_i(t),\mathbf{y}_i(t),\mathbf{u}_i(t),\theta_i(t)) \leq \mathbf{0} \\
& \dot{\mathbf{x}}_i(0) = \mathbf{0} \\
& \forall\, i \\
& i \in \{1.....n\} \\
& t_o \leq t \leq t_f
\end{aligned}
\tag{4.32}
$$

As the uncertainty set is discrete and we assume the probability of each scenario occurring is the same, the expected value of the uncertainty can be expressed in Equation 4.33. From this equation we can also see why $f(\mathbf{d}) = 240V_d$, as when the capital cost is in the expected value function it is both multiplied and divided by n, and thus remains the same.

$$
\underset{\theta(t)}{E}[\phi_{op}(\mathbf{d},\mathbf{x}(t),\mathbf{y}(t),\mathbf{u}(t),\theta(t)] = \frac{1}{n}\sum_{i=1}^{n}\phi_{op}(\mathbf{d},\mathbf{x}_i(t),\mathbf{y}_i(t),\mathbf{u}_i(t),\theta_i(t)) \tag{4.33}
$$

The formulation is Equation 4.32 is for generating the Relaxed design. For the KKT design, ϕ_{op} must include the complementarity penalty function as is seen in 4.34. Thus the two-stage stochastic formulation to generate the KKT design is seen in Equation 4.35. In Equation 4.35 $\boldsymbol{\lambda}_{\mathbf{0}i}$, $\boldsymbol{\lambda}_{\boldsymbol{f}_i}$, $\boldsymbol{\nu}_{\mathbf{0}i}$ and $\boldsymbol{\nu}_{\boldsymbol{f}_i}$ are the vectors of Lagrange

multipliers for scenario i

$$\phi_{kkt} = \phi_{op} - \rho_0[\boldsymbol{\lambda_0}^T \mathbf{g_{ss}}(\mathbf{d}, \mathbf{x}(0), \mathbf{y}(0), \mathbf{u}(0))] - \rho_f[\boldsymbol{\lambda_f}^T \mathbf{g_{ss}}(\mathbf{d}, \mathbf{x}(t_f), \mathbf{y}(t_f), \mathbf{u}(t_f))] \quad (4.34)$$

$$\begin{aligned}
\max_{\substack{\mathbf{d},\mathbf{u}_1(t)....\mathbf{u}_n(t) \\ \boldsymbol{\lambda_0}_1....\boldsymbol{\lambda_0}_n \\ \boldsymbol{\lambda_f}_1....\boldsymbol{\lambda_f}_n}} \quad & \underset{\theta(t)}{E}[\phi_{kkt}(\mathbf{d}, \mathbf{x}(t), \mathbf{y}(t), \mathbf{u}(t), \boldsymbol{\lambda_0}, \boldsymbol{\lambda_f})] - f(\mathbf{d}) \\
\text{s.t} \quad & \mathbf{z}(\mathbf{d}, \dot{\mathbf{x}}_i(t), \mathbf{x}_i(t), \mathbf{y}_i(t), \mathbf{u}_i(t), \theta_i(t)) = \mathbf{0} \\
& \mathbf{h}(\mathbf{d}, \mathbf{x}_i(t), \mathbf{y}_i(t), \mathbf{u}_i(t), \theta_i(t)) = \mathbf{0} \\
& \mathbf{g}(\mathbf{d}, \mathbf{x}_i(t), \mathbf{y}_i(t), \mathbf{u}_i(t), \theta_i(t)) \leq \mathbf{0} \\
& \nabla_{[\mathbf{x}(0),\mathbf{y}(0)\mathbf{u}(0)]}\mathcal{L}(\mathbf{d}, \mathbf{x}_i(0), \mathbf{y}_i(0), \mathbf{u}_0(t), \boldsymbol{\nu_0}_i, \boldsymbol{\lambda_0}_i, \theta_i(t)) = \mathbf{0} \\
& \nabla_{[\mathbf{x}(t_f),\mathbf{y}(t_f)\mathbf{u}(t_f)]}\mathcal{L}(\mathbf{d}, \mathbf{x}_i(t_f), \mathbf{y}_i(t_f), \mathbf{u}_i(t_f), \boldsymbol{\nu_f}_i, \boldsymbol{\lambda_f}_i, \theta_i(t)) = \mathbf{0} \\
& \dot{\mathbf{x}}_i(0) = \mathbf{0} \\
& \dot{\mathbf{x}}_i(t_f) = \mathbf{0} \\
& \boldsymbol{\lambda_0}_i \geq \mathbf{0} \\
& \boldsymbol{\lambda_f}_i \geq \mathbf{0} \\
& \forall\, i \\
& i \in \{1.....n\} \\
& t_o \leq t \leq t_f
\end{aligned} \quad (4.35)$$

In the two-stage stochastic formulation, the control variables (the feed to Reactor 1 and the feed to the Mixer) are the same as the formulation in Section 4.3 and are our second-stage decision variables. The optimization horizon for each scenario is 1hr long and there are only 5 control intervals. The first control interval is 20 minutes

long and is the duration of the system operating at the initial steady-state. The next three control intervals are 1.25 minutes long each and span the duration of the transition. The final control interval is over the remaining time in the horizon. In the production constraints of this formulation, the system must have a production rate of B greater than or equal to the demand for the duration of the first and final control interval. However during transition the production rate of B can be less than the specified demand (thus demand can be unmet during transition).

All optimizations were done using IPOPT using the CasADi module in Python 3.6 on a Dell Optiplex 7020 with an Intel core i7 processor and 16GB of RAM.

4.4.2 Results

For this section the KKT design and the Relaxed design refer to the designs generated by the two-stage stochastic optimization and not the design generated in Section 4.3 (unless mentioned explicitly). Using the two-stage stochastic optimization, both a Relaxed and KKT design were generated and the results can be seen in Table 4.2.

Design	**KKT**	**Relaxed**
Volume (m^3)	15.0683	13.7957
Daily profit	89958	90200

Table 4.2: The daily profits for designs using KKT and Relaxed formulations for a two-stage stochastic optimization using 6 different demand scenarios

The results from Table 4.2 are consistent with the results from section 4.3.2 where the KKT design requires a larger volume than the Relaxed design. The two demand scenarios where the designs differ in operation are the demand step from 6 to 10 and 8 to 10 (for no other scenario is there any unmet demand over the entire horizon for either design, i.e the demand change is met immediately). In these two scenarios demand was unmet during transition for both designs, and the operation for each

design is different.

We can see from Figures 4.15 and 4.16 that the productions profiles are different depending on the design. For the demand step of 6-10 the KKT design initially produces at a demand of 6 $\frac{mol}{hr}$ (as would be expected, as the KKT design is derived from the bilevel formulation, where the initial and final operating points are at the steady state optimum) but the Relaxed design operates initially at a higher production rate of 6.84 $\frac{mol}{hr}$ and is able to operate at a higher production rate during transition.

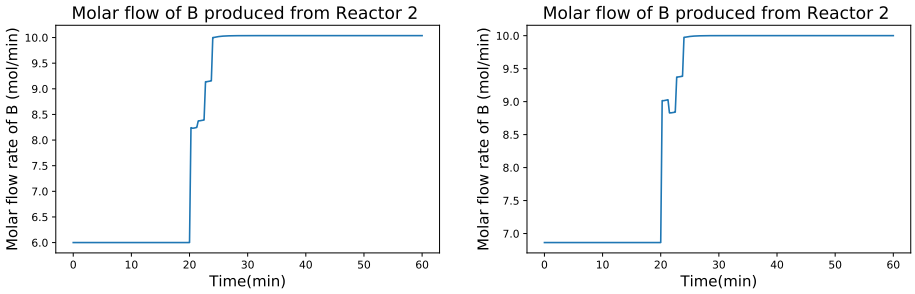

(a) KKT design (b) Relaxed Design

Figure 4.15: The production of B from reactor for a demand temp of 6 to 10

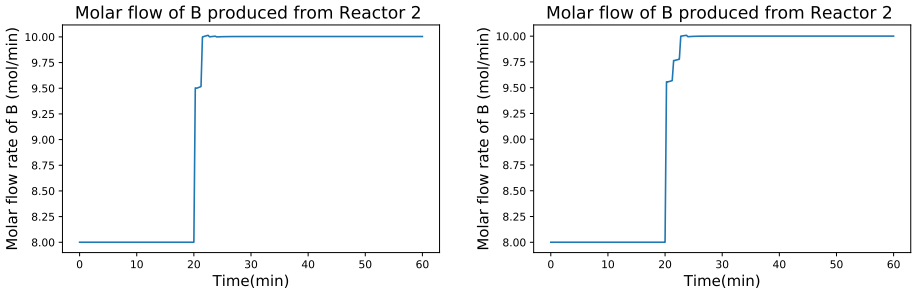

(a) KKT design (b) Relaxed Design

Figure 4.16: The production of B from reactor for a demand step of 8 to 10

To understand the trade-offs that occur in the two-stage stochastic optimization, we look at the demand step of 6-10 as this is where we see the most difference between the KKT and Relaxed designs (other than the 6-10 step and 8-10 step, the difference in operation between the KKT and Relaxed design is minimal) and this determines

the difference in volume between the KKT and Relaxed design. Based on the designs generated and the objective function 4.31 both the Relaxed and KKT optimization formulations prioritize meeting the final demand of 10 $\frac{mol}{hr}$ over reducing capital costs. This makes sense as a difference in production rate of just 0.5 $\frac{mol}{hr}$ for the last 40 minutes is 200 dollars of revenue lost. We compare this to increasing the volume by 1 m^3 (roughly the difference between the KKT and Relaxed design) and this results in a capital cost increase of 240 dollars. Thus we see that based on the economics of the objective function, meeting the final demand is what is prioritized in the optimization problem.

Given the above information, the trade-off we see is not between the final production (which the optimization will always try and meet) and capital cost, but the initial production and production during transition and capital cost. In a two-stage stochastic optimization there could be a trade-off between optimal operation in the most extreme scenario (the 6-10 step) and the design (as the optimal transition for the most extreme demand step could lead to over design and may lower the daily profit). We see this trade-off in the Relaxed design.

The Relaxed design chooses to overproduce for the 6-10 step (as seen in Figure 4.15) as when Reactor 2 overproduces it operates at a higher temperature. A limitation of the Relaxed design in Section 4.3.2 was that it could not add as much fresh feed of pure A to the Mixer during the transition without violating the maximum concentration of species A in Reactor 2. However if Reactor 2 is already operating a higher temperature the concentration of A in the feed can be higher as it is consumed at a faster rate and thus more fresh feed to the Mixer can be added to meet the final demand of 10 (which as has been stated, is of greatest benefit to daily profit). In the two-stage stochastic formulation for the Relaxed design, the increase in the operational costs due to overproducing B in the 6-10 step is offset by the reduction in capital costs as we can operate at smaller volume and still add enough feed to the Mixer to meet the

final demand. It seems overproducing allows for a smaller design while also letting the Relaxed design to meet the final demand for the 6-10 demand step.

In additional optimizations where Relaxed formulation for the two-stage stochastic optimization is forced to operate initially at a demand of 6 $\frac{mol}{hr}$ (although it does not have to be steady-state optimal, i.e KKT conditions are not enforced) for the 6-10 step, the daily profit is less than the original Relaxed formulation (where overproduction occurs) as the volume of the tanks must be increased to meet the final demand of 10 (we see that even though the operational costs are lower because we don't overproduce, it is offset by higher capital costs and has an overall lower daily profit). This demonstrates how the optimization balances the operating profit, capital costs, and ability to meet final demand. The trade-off we see is dependent on the economics of the objective function. In the Relaxed two-stage stochastic optimization, overproducing in only one scenario is offset by the reduction is capital cost for all the scenarios. However when we perform a single scenario optimization with the 6-10 demand step, we don't see overproduction, as the increased operational costs has a higher weight in the formulation (however if we increased the weight of the capital cost or lowered the weight of the operational cost we can again see the overproduction trade-off).

The trade-off between suboptimal operation during the initial and transitional periods and the capital cost illustrates why the Relaxed design is smaller than the KKT design and provides a higher daily profit. As the initial and final operating point at the KKT design have to be at the steady-state optimum, this provides less flexibility for the KKT design to trade-off operational profit and capital cost compared to the Relaxed design (which can choose the initial point and final point). Thus the Relaxed formulation is able to find operating and design paradigms that can increase the daily profit that may be infeasible for the KKT formulation. The KKT design must initially operate at the steady-state optimum (where it operates at a demand of 6 $\frac{mol}{hr}$). Because the KKT design does not overproduce, the initial concentration of A

in Reactor 2 is lower than that of the Relaxed Design, as seen in Figure 4.18. While we would expect the concentration to be lower as the KKT design volume is larger, we see that the initial concentration of A in Reactor 2 for the Relaxed design is over 50 percent higher than in the KKT design (the KKT design volume is only 7 percent higher than the Relaxed design). The size of this difference is due to the Relaxed design adding more feed to the Mixer so that it can overproduce (this increases the concentration of A in the reactor, and from the energy balance in Equation 4.8, we see this will increase the temperature at steady-state). As the KKT design initially operates at a lower concentration of A in Reactor 2, the KKT design operates at a lower temperature than the Relaxed design (this can be seen in Figure 4.17). In order to meet the final demand of 10, the volume for the KKT design has to be large enough so that the concentration of A in Reactor 2 is low enough so that enough feed can be added to the Mixer (to increase the overall flow rate) without the concentration constraint in Reactor 2 being violated. As also seen in 4.3.2, the initial steady-state optimum operates too close to maximum temperature in Reactor 1 to add additional feed to Reactor 1 to make up the flow rate needed. In the demand step of 8-10 we see both designs initially operated at the specified demand but the KKT design is able to to meet the final demand quicker and again has the higher operational profit.

We also see, as one would expect, that the control profiles are different, usually the KKT design initially uses less feed to the Mixer as this lowers the operational costs, which contributes to operating at the optimal steady-state conditions. These profiles are seen in Figures 4.19 and 4.20. We see from Figure 4.19 that the operational profiles of the KKT and Relaxed design are quite similar in transition where we see increase in fresh feed to the Mixer to meet the demand change. For all other scenarios the operation is very similar both in terms of production and control variable values for both designs. There is no overproduction in these scenarios (only the 6-10 demand step for the Relaxed design has overproduction).

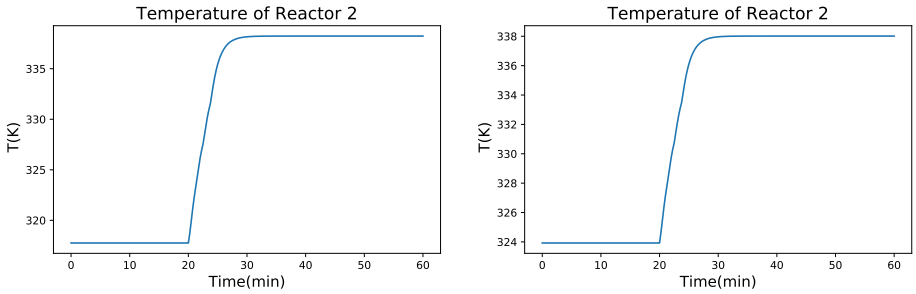

(a) KKT design (b) Relaxed Design

Figure 4.17: The temperature of Reactor 2 for the KKT and Relaxed Design

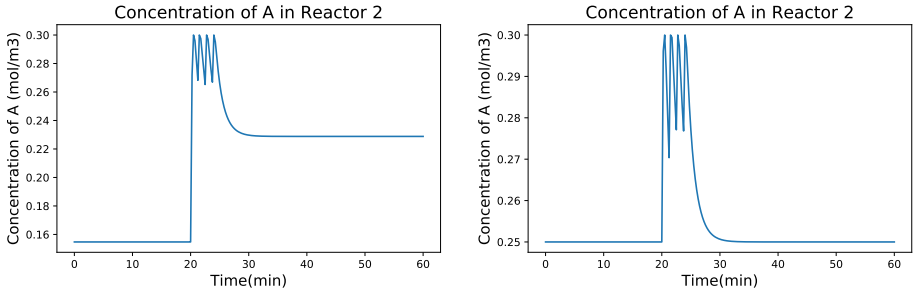

(a) KKT design (b) Relaxed Design

Figure 4.18: The concentration of A in Reactor 2 for the KKT and Relaxed Design

Looking at the daily profit it seems that the Relaxed design should be utilized based on the economics. However, like in Section 4.3.2, the prevailing idea in this study is that realistic operation under uncertainty involves operating at the optimal steady-state. Thus we should compare both designs under these conditions. We will take the 6 scenarios used in the two stage stochastic optimization and find the operating profit for each scenario when the volume is fixed at the KKT and Relaxed designs. However, both designs will be forced to initially operate at the optimal steady-state, thus the KKT conditions will be enforced for the initial point. We do not enforce the KKT conditions at the final point as this could lead to infeasible operation for the Relaxed design for the given time horizon and control interval structure. Furthermore, while in the two-stage stochastic optimization, demand had to be met before and after transition, we will not enforce this constraint for these optimizations. From the

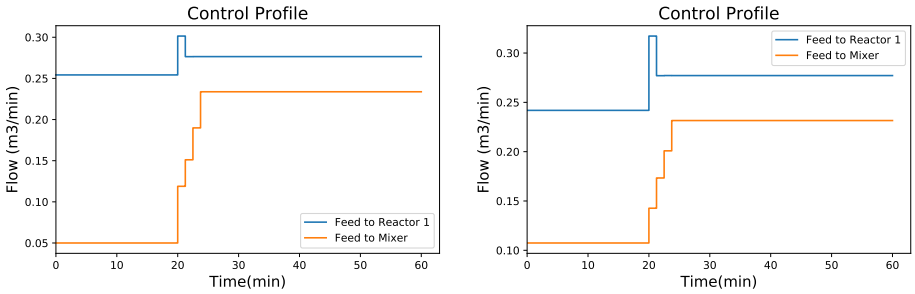

(a) KKT design (b) Relaxed Design

Figure 4.19: The control profiles for a demand step of 6 to 10

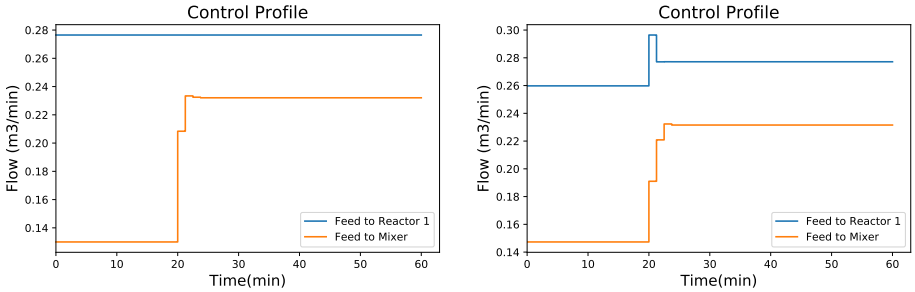

(a) KKT design (b) Relaxed Design

Figure 4.20: The control profiles for a demand step of 8 to 10

initial point, the optimization can operate under conditions where it does not meet demand. This is again due to the fact that the operation for the Relaxed design may be infeasible if we force it to meet demand. Once we have the operational profit for each scenario under each design, we will calculate a new daily profit using the equation for the objective function in Equation 4.32.

The results of this new calculation are seen in Table 4.3. As expected, the new daily profit for the KKT design is slightly improved as this formulation is a relaxation (as the KKT conditions at the endpoint are not enforced). We see that the Relaxed design under this formulation is worse. This main reason for this is because for the 6-10 demand step, the Relaxed design cannot actually meet the final demand as seen in Figure 4.21. We also see that while the Relaxed design is able to meet the the final demand in the step from 8 to 10, it transitions sub-optimally both compared to

the KKT design and the Relaxed design when it is not forced to initially operate at the steady state optimum. This is seen when we compare Figure 4.22 to Figure 4.16. We see the Relaxed design initially operating at the steady-state optimum has more unmet demand during transition compared to when the Relaxed design can choose any initial point.

Design	**KKT**	**Relaxed**
Daily profit	89974	89043

Table 4.3: The daily profits for designs using KKT and Relaxed formulation for a two-stage stochastic optimization using 6 different demand scenarios where the initial operation for each scenario is at the steady-state optimum

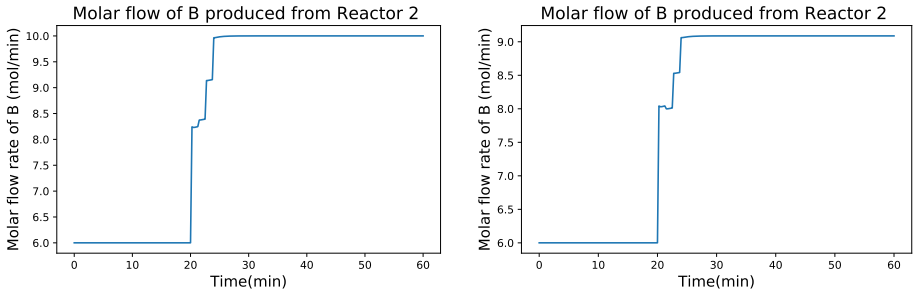

(a) KKT design (b) Relaxed Design

Figure 4.21: The production of B from Reactor 2 for a demand step of 6 to 10 when the design must initially operate at the steady-state optimum

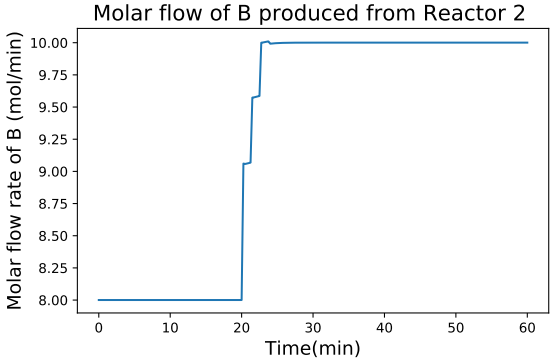

Figure 4.22: The moles of B produced for the Relaxed design for a demand change of 8 to 10 when the design must initially operate at the SS optimum

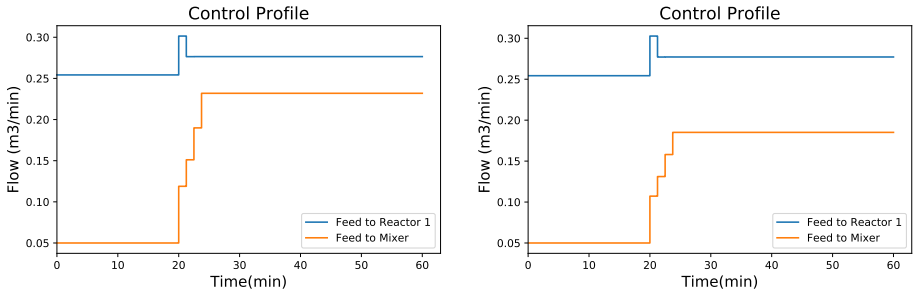

(a) KKT design (b) Relaxed Design

Figure 4.23: The control profiles for a demand step of 6 to 10 when the design must initially operate at the steady-state optimum

The Relaxed design cannot meet the final demand because, as in Section 4.3.2 not enough feed of pure A can enter the Mixer without violating the concentration limit of A in Reactor 2 thus limiting the volumetric flow rate exiting Reactor 2. This can be seen in Figure 4.23 where we can see the KKT design can add additional feed to the Mixer. Thus when the final control move is made, the concentration of A in Reactor 2 is still too high and the temperature of Reactor 2 is not high enough (as the Relaxed design operating at the steady-state optimum must initially produce at 6 $\frac{mol}{hr}$ as opposed to overproducing and thus operates at a lower temperature) to allow for the necessary feed to the Mixer to meet the needed flow rate. A comparison of the concentrations in Reactor 2 for the Relaxed and KKT design are seen in Figure 4.24. A comparison of the temperature in Reactor 2 for the Relaxed design, when any initial operating point can be chosen versus when it is operating at the steady state optimum can be seen in Figure 4.25.

The KKT design is able to meet the demand because due to the larger volume, the concentration leaving Reactor 1 is lower hence more feed can be added to the Mixer without violating the concentration constraint in Reactor 2. The reason the Relaxed design could add additional feed to the Mixer when not initially operating at the steady-state optimum was because Reactor 2 operates as a higher temperature. This because the Relaxed design, when not being forced to initially operate at the steady-

state optimum, chooses to initially over produce (6.84 $\frac{mol}{hr}$) which allows Reactor 2 to operate at a higher temperature. We also see that not only is the Relaxed design operating at the steady-state optimum not able to meet the final demand, but compared to the KKT design its overall transition is worse as it has more unmet demand during the transition period.

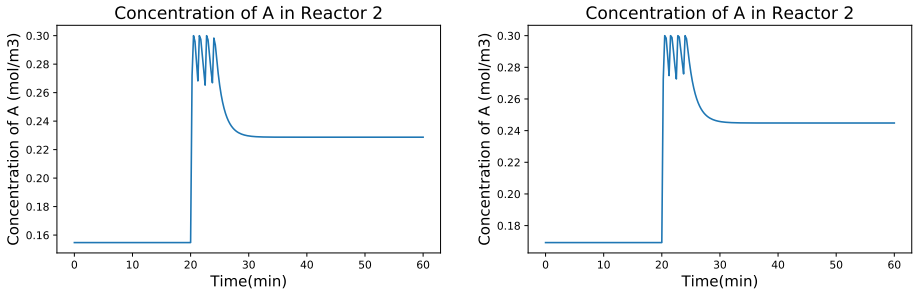

(a) KKT design (b) Relaxed Design

Figure 4.24: The concentration of A in Reactor 2 for a demand step of 6 to 10 when the design must initially operate at the steady-state optimum

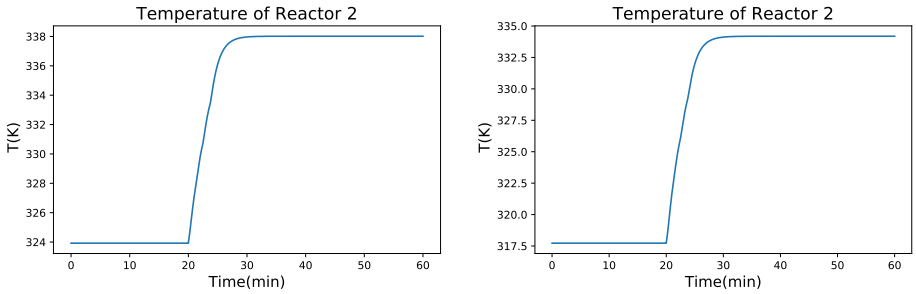

(a) Relaxed design at chosen initial steady-state (b) Relaxed Design at KKT conditions

Figure 4.25: The temperature of Reactor 2 in for the Relaxed design for different initial operating conditions

The Relaxed design can meet the final demand when the maximum concentration in Reactor 2 is increased (allowing more feed to the Mixer) or the maximum temperature in Reactor 1 is increased (allowing more feed to Reactor 1) which allows for the necessary amount of volumetric flow needed to meet the final demand. These results can be seen in Figures 4.26 and 4.27. From Figure 4.26 (b) we can see that more flow is

added to Reactor 1 and in Figure 4.26 (a) the reactor temperature is allowed to exceed 350 K (and is operating at a higher concentration). In 4.27 (a) the concentration of A in Reactor 2 is allowed to be greater than 0.3 and thus more feed can be fed to the Mixer to meet the volumetric flow rate necessary.

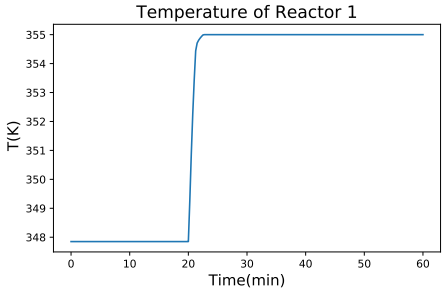

(a) Temperature profile of Reactor 1

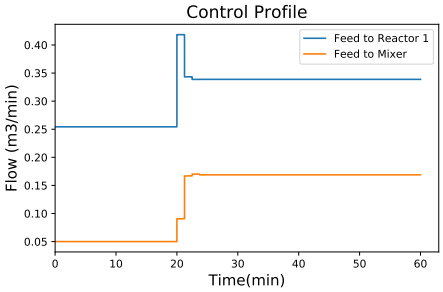

(b) Control profile

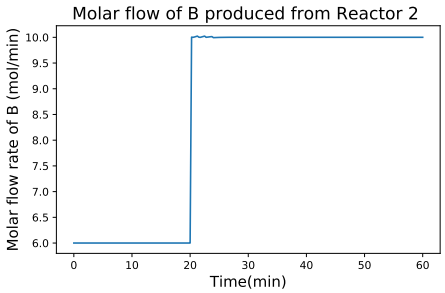

(c) Moles of B produced from Reactor 2

Figure 4.26: Profiles of selected variables for the Relaxed design when the maximum temperature of Reactor 1 is increased from 350 K to 355 K

For the Relaxed design operating initially at the steady-state optimum, if the transition is allowed to be longer, this also allows it to meet the final demand. This is as if the final control move is made when the temperature of Reactor 2 is high enough, it can add more feed of pure A to the Mixer and species A is consumed fast enough to prevent a violation of the concentration constraint. Hence if we increase the number of control intervals or make the control intervals longer the Relaxed design is able to meet the demand. This may suggest that the control intervals can be adjusted so that the Relaxed design can approach the performance of the KKT design; however the

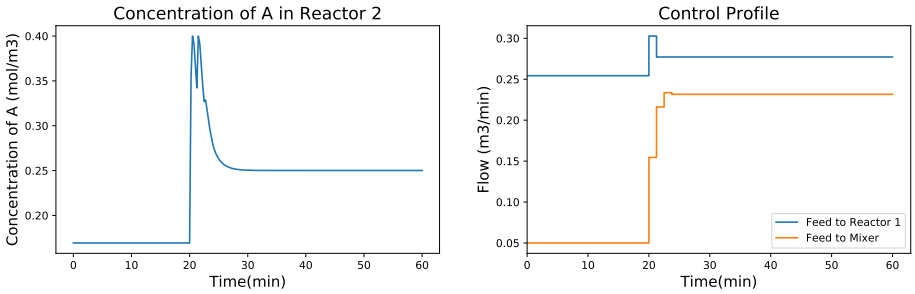

(a) Concentration profile of A

(b) Control profile

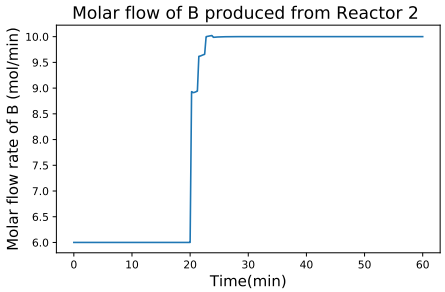

(c) Moles of B produced from Reactor 2

Figure 4.27: Profiles of selected variables for the Relaxed design when the maximum concentration of A Reactor 2 is increased from 0.3 $\frac{mol}{m^3}$ to 0.4 $\frac{mol}{m^3}$

operational performance of the KKT design is still better using the original control intervals. This is seen in Figure 4.28 and Table 4.4. In 4.28 (a) the number of control intervals was increased from 5 to 7 (2 more control intervals for transitions) and in 4.28 (b) the three control intervals during transition are increased each from 1.25 minutes to 2.5 minutes. These are both for the Relaxed design operating initially at the steady-state optimum. Figure 4.28 (c) is the original transition for the KKT design which can also be seen in Figure 4.21 (a). The operational profit for each scenario is shown in Table 4.4. From Table 4.4 and Figure 4.28 we can see that while the Relaxed design can meet the final demand in these scenarios, the transition is still worse compared to the KKT design.

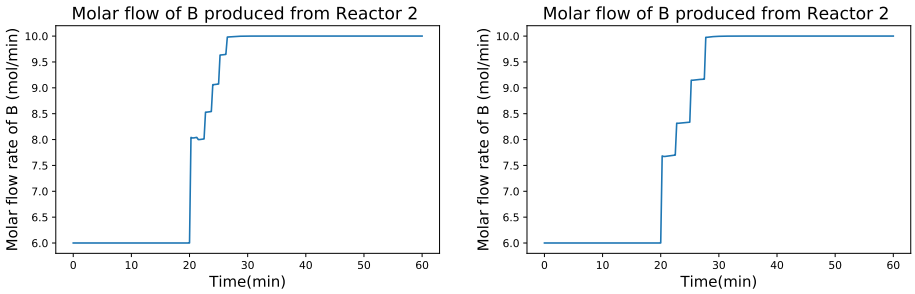

(a) 7 control intervals used for Relaxed design

(b) 5 control intervals with increased length for Relaxed design

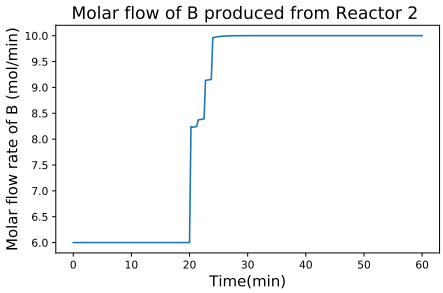

(c) 5 control intervals at original length (original formulation) for KKT design

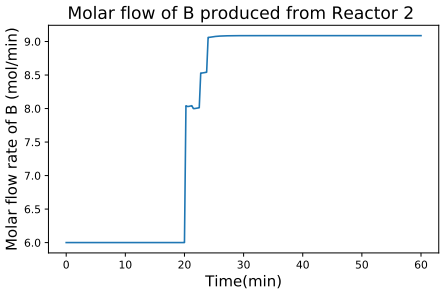

(d) 5 control intervals at original length (original formulation) for Relaxed design

Figure 4.28: The molar production of B for various designs and control intervals for the the demand scenario 6-10

Examining the impact of the number and length of control interval suggests that the Relaxed design could be made made better by creating an optimization formulation with more control intervals. As it seems that the performance during the scenario of a demand step from 6-10 was the main difference between the KKT and Relaxed design, we did a single scenario optimization with that scenario being the 6-10 demand step. We use the same objective function as in Equation 4.30, thus this demand scenario is weighted 6 times more than in the original two-stage stochastic optimization. Using this formulation, a new KKT design and Relaxed design were generated. Both design volumes are higher than the designs generated from the original two-stage stochastic optimization (as expected, as now the design only has to be optimal for a single

Control interval structure	Design	Operational Profit
7 control intervals	Relaxed	4194.55
Long control intervals	Relaxed	4162.36
Original control intervals	Relaxed	3914.98
Original control intervals	KKT	4220.41

Table 4.4: A comparison of the operational profit for demand scenario 6-10 for various designs and control interval structures

scenario). However, more importantly, it was found that increasing the number of control intervals starting with 5 control intervals (the original formulation) did not change the design. This makes sense as both designs are able to meet the final demand using only three control intervals for transition. This also suggests that using 5 control intervals in total and three for transitions in our formulation does not favor one design over the other. As well this also shows that the difference in performance due to transition (and in some the case the final production rate) between the KKT and Relaxed design cannot be accounted for in the optimization formulation simply by the structure of the control intervals (the Relaxed design does not become more similar to the KKT design simply by adding more control intervals). This shows that considering the initial and final operating state by including the KKT conditions can be an important factor in integrated design and control.

4.4.3 Frequency Studies

As we have seen in previous sections, the design (volume) of the CSTR system has a large impact on how the plant transitions from one point to another. In the formulation previously used in this study, each scenario is 1hr long and the daily profit is for a 24 hr horizon, thus 24 transitions occur over the optimization horizon. As the number of transitions increases, we would expect that the optimization is incentivized further to meet the demand as quickly as possible during transition to avoid loss in

operational profit. To study this, much like the study for control intervals, as it seems that the design is primary determined by the most extreme scenario (in this study the 6-10 demand step) we will do an optimization with only one scenario (the 6-10 demand step). We do not include a scenario where the demand steps down as from the two-stage stochastic optimization done in the previous sections, we found that these kinds of scenarios did not influence the design.

The frequency will be changed by changing the horizon over which the demand change takes place as can be seen in Figure 4.29 and Equations 4.36 and 4.37. Equation 4.36 corresponds to Figure 4.29 (a), and is the original formulation. To double the frequency we use the scenario in Figure 4.29 (b) whose horizon is half the horizon in Figure 4.29 (a). Equation 4.37 corresponds to Figure 4.29 (b), and we can see since the horizon is only 30 minutes, to get daily profit we multiply the integral calculating the operational profit by 48, thus the profit from the transition period is doubled, and this represents doubling the frequency. The ratio of the time spent at each demand is still the same regardless of the frequency, since in order to compare design at different frequencies we do not want to change the potential operational profit that can be made. This formulation was done using both the KKT and Relaxed formulation. For the KKT design, we only enforce the KKT conditions at the initial point, as with high frequencies the intervals can be quite short and steady state may simply not be achievable. We use 5 control intervals (three for transition), where the lengths of the transition intervals are 1.25 minutes (the original formulation) for all frequencies.

$$\phi = 24 \int_0^{60} [10\phi_{rev} - 0.01q_{cool,1} - q_{cool,2} - 0.1Q_{F1} - 0.1Q_M]dt + 240V_d \tag{4.36}$$

$$\phi = 48 \int_0^{30} [10\phi_{rev} - 0.01q_{cool,1} - q_{cool,2} - 0.1Q_{F1} - 0.1Q_M]dt + 240V_d \tag{4.37}$$

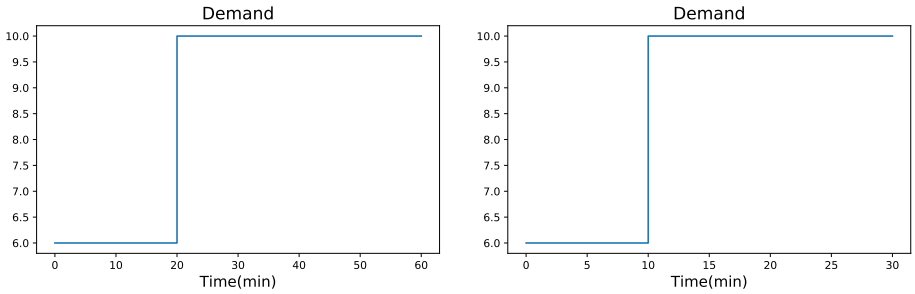

(a) Frequency = 1 (b) Frequency = 2

Figure 4.29: The demand profiles for when the frequency of the original formulation is changed

The results of this section are seen in Figures 4.30 and 4.31. For the KKT design we considered frequency changes of 1, 2, 4 and 8. For the Relaxed design we considered frequency changes of 1 and 2. In Figure 4.30 each subfigure gives the frequency of the formulation and the resulting optimal volume (V_{opt}) for a KKT design formulation. We see that as the frequency is increased, V_{opt} increases and demand is met more quickly. This is consistent with what we would expect, since the more frequent the transitions, the more important it is for demand to be met during the transitions. Thus a larger volume and capital cost can be incurred as the benefit of increasing operating profit during transition becomes more valuable. We also see that as the frequency of transitions increases, the design approaches being able to meet demand instantaneously. Thus the optimal volume as the frequency increases approaches 23.3 m^3, which is the design for a demand scenario of 6-10 when meeting the demand is enforced throughout the entire horizon including transitions (in our formulations in the previous sections we do not enforce the demand constraints during transitions). It should be noted that the dynamics of the system mean it takes about 20-30 minutes for the system to settle to steady-state, so for frequencies of 4 and 8, the system does not reach steady-state.

In Figure 4.31 we see that since the Relaxed design since can choose the initial steady-state point, it can meet demand almost immediately even for a frequency of 1. Thus

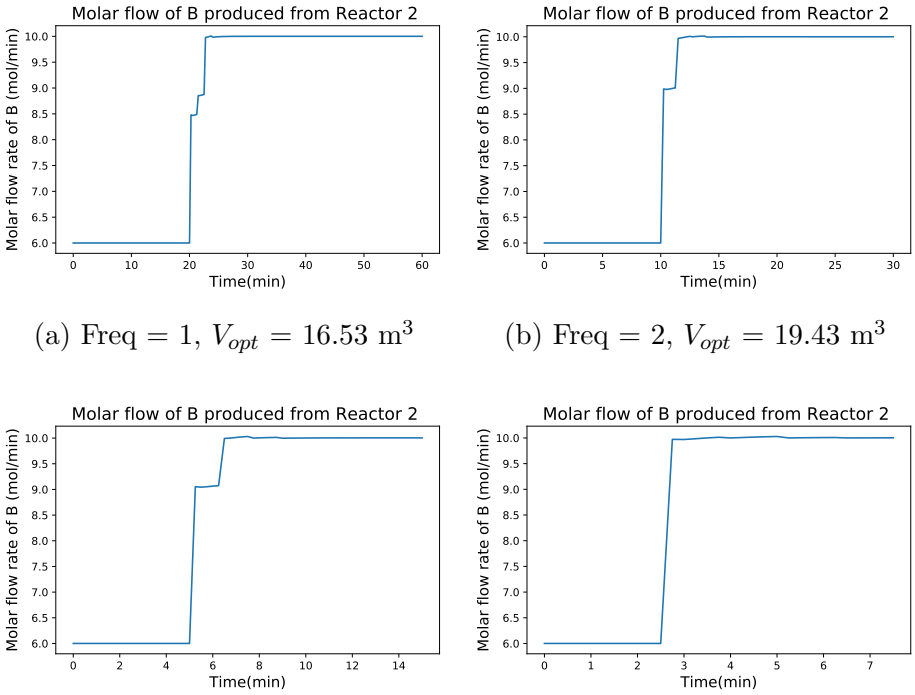

(a) Freq = 1, V_{opt} = 16.53 m^3 (b) Freq = 2, V_{opt} = 19.43 m^3

(c) Freq = 4, V_{opt} = 19.66 m^3 (d) Freq = 8, V_{opt} = 23.02 m^3

Figure 4.30: The production rate of B from Reactor 2 for changes in frequency and their corresponding optimal volumes for a demand step of 6-10 using the KKT formulation

for a frequency of 2 the demand is met immediately. As demand is met immediately by a frequency of 2 we did not increase the frequency further as the design would not change. We also see that while for a frequency of 1 the KKT and Relaxed design are similar (although as we have seen this can still make a difference in transition), as the frequency is increased the difference between the KKT and Relaxed design becomes much larger and presumably the operational performance would also differ further. Thus we see if the frequency of transitions increases, it becomes of greater importance to consider operating at steady-state optima in the optimization formulation.

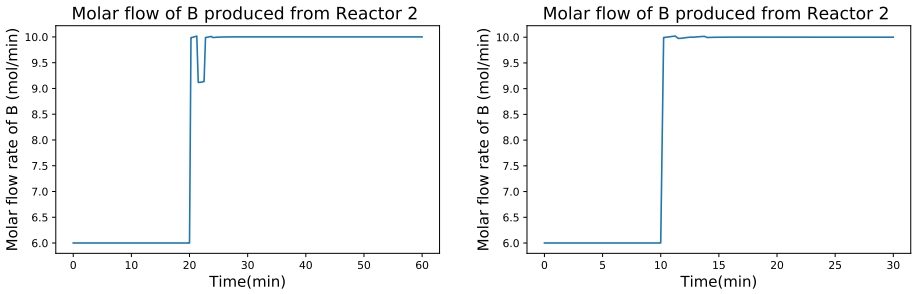

(a) Frequency = 1, $V_{opt} = 15.\ 37\ \text{m}^3$ (b) Frequency = 2, $V_{opt} = 16.17\ \text{m}^3$

Figure 4.31: The production rate of B from Reactor 2 for changes in frequency and their corresponding optimal volumes for a demand step of 6-10 using the Relaxed formulation

4.5 Conclusion and Future work

Uncertainty in market conditions suggest that for the dynamic operation of plants, the design of the plant must take into account future operating conditions while also recognizing that future conditions are uncertain. Thus a plant operating under uncertain conditions should currently be operating at the optimal operating conditions.

Finding a design in a dynamic optimization that also initially operates at the steady-state optimum results in a bilevel optimization problem. This can be collapsed into a single level optimization by incorporating the Karush-Kuhn-Tucker (KKT) conditions for the initial operating points into the optimization formulation.

The KKT conditions for the initial and final operating points were embedded in a two-stage dynamic optimization formulation to find the optimal annualized profit of a two CSTR system (the KKT formulation). This was compared to an optimization formulation where the KKT conditions are not present (the system can operate at any initial point and essentially sees future demand patterns), a Relaxed formulation. Comparing the KKT formulation and Relaxed formulation, the optimal volume of the Relaxed design is smaller than the KKT design, and has a higher daily profit. From the designs generated, we force both designs to initially operate at the steady-state

optimum for the six scenarios in the two-stage stochastic optimization. In certain cases the Relaxed design cannot meet the final demand. Furthermore in this case the KKT design provides the better daily profit. Thus for integrated design and control, a design that incorporates the beginning and ending optimal operating conditions can provide an economic advantage compared to designs that are generated where the optimization formulation behaves as if it has complete knowledge of the operating horizon. The difference between the KKT and Relaxed design and their operation may also be exacerbated by the frequency of the changes, and consideration of the KKT design may become more important.

Further applications of this study would include demonstrating the importance of considering the bilevel formulation in the integrated design and control of large scale models of chemical plants such as an air separation unit. This may be achieved by including the KKT conditions in the optimization formulation regarding these models, or utilizing the brute-force method, if the KKT conditions pose numerical difficulties.

Chapter 5

Conclusion

The studies in this thesis investigated integrated design and control for plants under uncertainty. The first study in this thesis investigated how incorporation of process dynamics in a nitrogen plant is important when considering the design of the plant under demand uncertainty. In addition to a nominal design, two-stage stochastic optimization is used to generate dynamically operable and flexible designs for the nitrogen plant. From the two-stage stochastic optimization formulation, the flexible design provides a better annualized profit than the dynamically operable design, primarily because the flexible design allows for lower operational costs. However when both designs are subject to dynamic transitions, we see that the flexible design in some cases provides less operational profit during transition and also may not be able to meet the final demand. Furthermore, incorporating plant dynamics into the optimization formulation also gave greater insight into what design compromises benefit the operation of the plant, that otherwise would not have been in seen in flexible and nominal formulations. Thus we see that accounting for dynamic operation of the plant during transition is an aspect of integrated design and control that can be very beneficial.

While the first chapter in this thesis established the benefits of considering a dynamically operable design, a limitation of that study was the dynamic optimization formulation knew the entire uncertainty profile and the plant could adjust its current behavior to account for future demands. It is more realistic that given unknown future demands, the current operation will be operating at the steady-state optimum and this poses a bilevel optimization formulation. The bilevel optimization problem can be reduced to a single level by embedding the KKT conditions for the initial and final operating point. This method is implemented for a 2 CSTR model under demand uncertainty where two-stage stochastic dynamic optimization is used to find the optimal volume of the CSTRs. An optimization formulation where the KKT condition are enforced generates a larger volume and thus has higher capital costs than a formulation where the KKT conditions are not enforced. However when both designs are forced to initially operate at the steady-state optimum for a given demand, we see that the design volume that was generated by not enforcing the KKT conditions, transitions slower and in some cases cannot meet the final demand compared to the volume generated from the KKT conditions.

Throughout this thesis we see that integrated design and control is a useful tool in investigating the design of a plant under uncertain operating conditions. The studies in this thesis have focused on elucidating the benefits of incorporating the dynamic behavior of plants in two-stage stochastic optimization formulations and the implementation of realistic operating assumptions and their effect on dynamically operable designs.

List of References

Andersson, J. A. E., Gillis, J., Horn, G., Rawlings, J. B., and Diehl, M. (In Press, 2018). CasADi – A software framework for nonlinear optimization and optimal control. *Mathematical Programming Computation*, .

Bahri, P. A., Bandoni, J. A., and Romagnoli, J. A. (1997). Integrated Flexibility and Controllability Analysis in Design of Chemical Processes. *AIChE Journal*, **43**(4), 997–1015.

Baker, R. and Swartz, C. L. E. (2008). Interior Point Solution of Multilevel Quadratic Programming Problems in Constrained Model Predictive Control Applications. *Ind. Eng. Chem. Res.*, **47**(1), 81–91.

Bansal, V., Perkins, J. D., and Pistikopoulos, E. N. (2002). A Case Study in Simultaneous Design and Control Using Rigorous, Mixed-Integer Dynamic Optimization Models. *Industrial & Engineering Chemistry Research*, **41**(i), 760–778.

Barton, P. I., Allgor, R. J., Feehery, W. F., and Galn, S. (1998). Dynamic optimization in a discontinuous world. *Industrial & Engineering Chemistry Research*, **37**(3), 966–981.

Biegler, L. T. (2007). An overview of simultaneous strategies for dynamic optimization. *Chemical Engineering and Processing: Process Intensification*, **46**(11), 1043–1053.

Biegler, L. T., Cervantes, A. M., and Wächter, A. (2002). Advances in simultaneous strategies for dynamic process optimization. *Chemical Engineering Science*, **57**(4), 575–593.

Birge, J. R. and Louveaux, F. (1997). *Introduction to Stochastic Programming*. Springer Series in Operations Research and Financial Engineering. Springer.

Cao, Y. (2011). Design for Dynamic Performance: Application to Air Separation Unit. Master's Thesis, Department of Chemical Engineering, McMaster Univeristy, Hamilton.

Cao, Y., Swartz, C. L. E., Baldea, M., and Blouin, S. (2015). Optimization-based assessment of design limitations to air separation plant agility in demand response scenarios. *Journal of Process Control*, **33**, 37–48.

Cao, Y., Swartz, C. L. E., and Flores-Cerrillo, J. (2016a). Dynamic modeling and collocation-based model reduction of cryogenic air separation units. *AIChE Journal*, **62**(5), 1602–1615.

Cao, Y., Swartz, C. L. E., and Flores-Cerrillo, J. (2016b). Optimal dynamic operation of a high-purity air separation plant under varying market conditions. *Industrial & Engineering Chemistry Research*, **55**(37), 9956–9970.

Cervantes, A. and Biegler, L. (2009). Optimization Strategies for Dynamic Systems. *Encyclopedia of Optimization*, , 2750–2757.

Chachuat, B. (2007). Nonlinear and dynamic optimization: From theory to practice.

Dimitriadis, V. D. and Pistikopoulos, E. N. (1995). Flexibility Analysis of Dynamic Systems. *Industrial & Engineering Chemistry Research*, **34**(12), 4451–4462.

Douglas, J. M. (1988). *Conceptual Design of Chemical Processes*. McGraw-Hill, New York.

Feehery, W. F. and Barton, P. I. (1999). Dynamic optimization with equality path constraints. *Industrial & Engineering Chemistry Research*, **38**(6), 2350–2363.

Figueroa, J. L., Bahri, P. A., Bandoni, J. A., and Romagnoli, J. A. (1996). Economic impact of disturbances and uncertain parameters in chemical processes - A dynamic back-off analysis. *Computers and Chemical Engineering*, **20**(4), 453–461.

Halemane, K. P. and Grossmann, I. E. (1983). Optimal process design under uncertainty. *AIChE Journal*, **29**(3), 425–433.

Hunter, J. D. (2007). Matplotlib: A 2d graphics environment. *Computing In Science & Engineering*, **9**(3), 90–95.

Ierapetritou, M. G. and Pistikopoulos, E. N. (1996). Batch plant design and operations under uncertainty. *Industrial and Engineering Chemistry Research*, **35**(3), 772–787.

Ierapetritou, M. G., Wu, D., Vin, J., Sweeney, P., and Chigirinskiy, M. (2002). Cost Minimization in an Energy-Intensive Plant Using Mathematical Programming Approaches. *Industrial & Engineering Chemistry Research*, **41**, 5262–5277.

Jamaludin, M. Z. and Swartz, C. L. E. (2017). Dynamic real-time optimization with closed-loop prediction. *AIChE Journal*, **63**(9), 3896–3911.

Lenhoff, A. M. and Morari, M. (1982). Design of resilient processing plants-I Process design under consideration of dynamic aspects. *Chemical Engineering Science*, **37**(2), 245–258.

Li, H. and Swartz, C. L. (2018). Approximation techniques for dynamic real-time optimization (DRTO) of distributed MPC systems. *Computers and Chemical Engineering*, **118**, 195–209.

Loeblein, C. and Perkins, J. (1998). Economic analysis of different structures of on-line process optimization systems. *Computers & Chemical Engineering*, **22**(9), 1257–1269.

Luus, R. (1993). Piecewise linear continuous optimal control by iterative dynamic programming. *Industrial & Engineering Chemistry Research*, **32**(5), 859–865.

Luyben, M. L. and Floudas, C. A. (1994). Analyzing the interaction of design and control-1. A multiobjective framework and application to binary distillation synthesis. *Computers and Chemical Engineering*, **18**(10), 933–969.

Miller, J., Luyben, W., Belanger, P., Blouin, S., and Megan, L. (2008a). Improving agility of cryogenic air separation plants. *Industrial & Engineering Chemistry Research*, **47**(2), 394–404.

Miller, J., Luyben, W. L., and Blouin, S. (2008b). Economic incentive for intermittent operation of air separation plants with variable power costs. *Industrial and Engineering Chemistry Research*, **47**(4), 1132–1139.

Mitra, S., Pinto, J. M., and Grossmann, I. E. (2014). Optimal multi-scale capacity planning for power-intensive continuous processes under time-sensitive electricity prices and demand uncertainty. Part I: Modeling. *Computers and Chemical Engineering*, **65**, 89–101.

Mohideen, M. J., Perkins, J. D., and Pistikopoulos, E. N. (1996). Optimal design of dynamic systems under uncertainty. *AIChE Journal*, **42**(8), 2251–2272.

Morari, M. (1983). Design of resilient processing plants-III. A general framework for the assessment of dynamic resilience. *Chemical Engineering Science*, **38**(11), 1881–1891.

Najafi, H., Najafi, B., and Hoseinpoori, P. (2011). Energy and cost optimization of a plate and fin heat exchanger using genetic algorithm. *Applied Thermal Engineering*, **31**(10), 1839–1847.

Narraway, L. T. and Perkins, J. D. (1993). Selection of process control structure based on linear dynamic economics. *Industrial & Engineering Chemistry Research*, **32**, 2681–2692.

Narraway, L. T., Perkins, J. D., and Barton, G. W. (1991). Interaction between process design and process control: economic analysis of process dynamics. *J. Proc. Cont.*, **1**, 243–250.

Nocedal, J. and Wright, S. J. (2006). *Numerical Optimization*.

Pattison, R. C., Touretzky, C. R., Johansson, T., Harjunkoski, I., and Baldea, M. (2016). Optimal Process Operations in Fast-Changing Electricity Markets: Framework for Scheduling with Low-Order Dynamic Models and an Air Separation Application. *Industrial & Engineering Chemistry Research*, **55**(16), 4562–4584.

Paules IV, G. E. and Floudas, C. A. (1992). Stochastic programming in process synthesis: A two-stage model with MINLP recourse for multiperiod heat-integrated distillation sequences. *Computers and Chemical Engineering*, **16**(3), 189–210.

Pistikopoulos, E. and Ierapetritou, M. (1995). Novel approach for optimal process design under uncertainty. *Computers & Chemical Engineering*, **19**(10), 1089–1110.

Sahindis, N. V. (2004). Optimization under uncertainty: State-of-the-art and opportunities. *Computers and Chemical Engineering*, **28**(6-7), 971–983.

Schenk, M., Sakizlis, V., Perkins, J., and Pistikopoulos, E. (2002). Optimization-based methodologies for integrating design and control in cryogenic plants. In Grievink, J. and van Schijndel, J. (Eds.), *ESCAPE-12*, p. 331.

Soliman, M., Swartz, C. L. E., and Baker, R. (2008). A mixed-integer formulation for back-off under constrained predictive control. *Computers and Chemical Engineering*, **32**(10), 2409–2419.

Swartz, C. L. E. and Stewart, W. E. (1986). A collocation approach to distillation column design. *AIChE Journal*, **32**(11), 1832–1838.

Turton, R. (1998). *Analysis, synthesis and design of chemical processes*. Prentice Hall PTR, Upper Saddle River, New Jersey.

US Department of Energy (2006). Benefits of demand response in electricity markets and recommendations for achieving them. a report to the united states congress pursuant to section 1252 of the energy policy act of 2005. Technical report.

Washington, I. (2017). Nitrogen plant model description template. Personal correspondence.

White, V., Perkins, J. D., and Espie, D. M. (1996). Switchability analysis. *Computers and Chemical Engineering*, **20**(4), 469–474.

Zhu, Y., Legg, S., and Laird, C. D. (2010). Optimal design of cryogenic air separation columns under uncertainty. *Computers and Chemical Engineering*, **34**(9), 1377–1384.

Zhu, Yu, Laird, C. D. (2011). A Multiperiod nonlinear programming approach for Operation of Air Separation Plants with Variable Powe Pricing. *AIChE Journal*, **57**(11), 3199–3209.

Appendix A

This appendix provides the DAEs that define the nitrogen plant. The DAEs are given separately for each unit of the plant, where the integrated reboiler-condenser (IRC) and distillation column are considered a single unit. For a detailed account of the derivation and construction of the DAEs that make up the nitrogen plant see Cao [2011]. The description of the variables and models for the nitrogen plant are derived from a template provided by Ian Washington .

Distillation Column and IRC

The distillation column itself consists of n_c actual distillation trays and we consider the condenser, tray $n_c + 1$ and the reboiler, tray $n_c + 2$. The sump is considered the 0^{th} tray. Below are the tables that document the parameters and variables of the DAE that makes up the distillation column and IRC. The equations shown here are for the full order model, where there is a mass and energy balance for each tray in the column. As has been previously mentioned, part of the column is modelled using spatial collocation; how the full order model is translated to a reduced model is stated at the end of Appendix A. The control variables in this unit are the liquid feed to the column from the PHX, the nitrogen gas draw (the ratio of nitrogen gas sent to the PHX for sale versus the nitrogen gas sent to the IRC). The design variable is the diameter of the column.

Distillation Column and IRC Variable Description

Index	
$i \in I$	component $I = \{1, 2, 3\}$, $1 := N_2$, $2 := O_2$, $3 := Ar$
$n \in N$	stage (tray) $N = \{0, \ldots, n_c + 2\}$
l	liquid (superscript)
v	vapor (superscript)
Example	$x_{i,n}$: liquid molar fraction for component i on stage n
Variable	**Description**
$M_{i,n}$	liquid phase molar holdup
$x_{i,n}$	liquid phase composition
$y_{i,n}$	vapor phase composition
$y^*_{i,n}$	vapor phase equilibrium composition
$z_{i,n}$	feed composition
L_n	liquid phase molar flow rate
V_n	vapor phase molar flow rate
$F^{l,v}_n$	feed molar flow rate
L_{reflux}	liquid reflux molar flow rate
L_{N_2}	liquid N2 product molar flow rate
V_{N_2}	vapor N2 product molar flow rate
r_{draw}	fraction of vapor drawn as product
r_{reflux}	liquid reflux ratio
h_n	height of liquid on tray
T_n	temperature
P_n	pressure
ΔT_{irc}	IRC temperature difference
ΔP_n	tray pressure drop
H_n	phase molar enthalpy
E_n	liquid phase energy holdup
$h_{i,n}$	component molar enthalpy
$\bar{V}^v_n$	vapor phase molar volume
ρ_n	phase molar density
$\rho_{i,n}$	component molar density
$P^{\text{sat}}_{i,n}$	vapor pressure
$\gamma_{i,n}$	activity coefficient
$K_{i,n}$	K-values
w_n	phase molar mass
a_n	Peng-Robinson EOS parameter
b_n	Peng-Robinson EOS parameter
$Q_{\text{leak},n}$	heat transfer to tray
Q	heat transferred from condenser to reboiler
$(UA)_{\text{irc}}$	lumped heat transfer coefficient
l_{reb}	liquid level in reboiler
l_{sump}	liquid level in sump
D_{col}	column diameter

Distillation Column and IRC Parameters

Parameter	**Description**
g	gravity constant
R	gas constant
w_i	molar mass
T_i^c	critical temperature
P_i^c	critical pressure
r_i	Rackett number
A_i, B_i, C_i	Antoine parameters
$A_{i,j}$	Margules interaction $i, j \in I$
$k_{i,j}$	binary interaction $i, j \in I$
ω_i	acentric parameter
p_i	parachor number
$a_i^v, b_i^v, c_i^v, d_i^v$	vapour enthalpy parameters
$a_i^l, b_i^l, c_i^l, d_i^l$	liquid enthalpy parameters
α	pressure drop parameter
β	pressure drop parameter
α_{top}	pressure drop parameter
η	tray efficiency
$(UA)_n$	leakage coefficient
$(UA)_{\text{irc}}^{\text{base}}$	base coefficient
$\bar{L}_{n_c+1}$	base condensate rate
h_{weir}	weir height
l_{weir}	weir length
S_{tray}	tray spacing
f_{active}	active tray area
$v_{\text{sump}}^{\text{cap}}$	sump capacity
L_{sump}^{ss}	controller bias
L_{reb}^{ss}	controller bias
l_{sump}^{ss}	controller set point
l_{reb}^{ss}	controller set point
K_{c_1}	sump controller constant
K_{c_2}	reboiler controller constant
T_{ambient}	ambient temperature

Distillation Column and IRC Subexpressions

$$
\begin{aligned}
P_{i,n}^{\text{sat}} &:= \exp(A_i + B_i/(T_n + C_i)) \\
\gamma_{i,n} &:= \exp\left[\textstyle\sum_{j\in I}\sum_{k\in I}(A_{ji} - 0.5A_{jk})x_{j,n}\,x_{k,n}/(R\,T_n)\right] \\
K_{i,n} &:= \gamma_{i,n}P_{i,n}^{\text{sat}}/P_n \\
\rho_{i,n}^{l} &:= \frac{P_i^c}{R\,T_i^c}\,r_i^{-[1+(1-T_n/T_i^c)^{2/7}]} \\
\rho_n^{l} &:= \textstyle\sum_{i\in I}\,x_{i,n}\,\rho_{i,n}^{l} \\
\rho_n^{v} &:= 1/\bar{V}_n^{v} \\
h_{i,n}^{l} &:= a_i^{l}\,T_n + b_i^{l} \\
h_{i,n}^{v} &:= (a_i^{v}\,P_n + b_i^{v})T_n + c_i^{v}P_n + d_i^{v} \\
w_n^{l} &:= \textstyle\sum_{i\in I}\,x_{i,n}\,w_i \\
w_n^{v} &:= \textstyle\sum_{i\in I}\,y_{i,n}\,w_i \\
f_i &:= 0.37464 + 1.54226\,\omega_i - 0.26992\,\omega_i^2 \\
b_i &:= 0.0778\,R\,T_i^c/P_i^c \\
b_n &:= \textstyle\sum_{i=1}^{n_c}\,y_{i,n}\,b_i \\
a_{i,n} &:= \tfrac{0.45724(R\,T_i^c)^2}{P_i^c}[1 + f_i\,(1 - \sqrt{T_n/T_i^c})]^2 \\
a_n &:= \textstyle\sum_{i=1}^{n_c}\sum_{j=1}^{n_c}\,y_{i,n}\,y_{j,n}(a_{i,n}\,a_{j,n})^{0.5}(1 - k_{ij}) \\
v_{n_c}^{\text{flood}} &:= C_{n_c}[(\rho_{n_c}^{l}\,w_{n_c}^{l} - \rho_{n_c}^{v}\,w_{n_c}^{v})/(\rho_{n_c}^{v}\,w_{n_c}^{v})]^{0.5} \\
C_{n_c} &:= [(0.0744\,S_{\text{tray}} + 0.0117)\log_{10}(FLV_{n_c}^{-1}) \\
&\qquad + 0.0304\,S_{\text{tray}} + 0.0153](\sigma_{n_c}/0.02)^{0.2} \\
FLV_{n_c} &:= \max\left\{0.1, \frac{L_{n_c}\,w_{n_c}^{l}}{V_{n_c}\,w_{n_c}^{v}}\left(\frac{\rho_{n_c}^{v}\,w_{n_c}^{v}}{\rho_{n_c}^{l}\,w_{n_c}^{l}}\right)^{0.5}\right\} \\
\sigma_{n_c} &:= \left(\textstyle\sum_{i\in I}\,p_i(\rho_{n_c}^{l}x_{i,n_c} - \rho_{n_c}^{v}y_{i,n_c})\right)^4 \\
\alpha_{n_c}^{\text{flood}} &:= V_{n_c}/(\rho_{n_c}^{v}A_{\text{tray}})/v_{n_c}^{\text{flood}}
\end{aligned}
$$

DAE of Distillation Column and IRC

$$
\begin{aligned}
V_{n_c}(1 - r_{\text{draw}}) - L_{n_c+1} &= 0 \\
L_{n_c+1} - (L_{\text{reflux}} + L_{N_2}) &= 0 \\
L_{\text{reflux}} - r_{\text{reflux}}\, L_{n_c+1} &= 0 \\
V_{N_2} - r_{\text{draw}}\, V_{n_c} &= 0 \\
\dot{M}_{i,0}[L_1\, x_{i,1} - L_0\, x_{i,0}) &= 0 \\
\dot{M}_{i,1} - [L_2\, x_{i,2} - L_1\, x_{i,1} - V_1\, y_{i,1}] & \\
+F_1^l\, z_{i,1}^l + F_1^v\, z_{i,1}^v] &= 0 \\
\dot{M}_{i,n} - [L_{n+1}\, x_{i,n+1} + V_{n-1}\, y_{i,n-1} - L_n\, x_{i,n} & \\
-V_n y_{i,n} + F_n^l\, z_{i,n}^l + F_n^v\, z_{i,n}^v] &= 0 \\
\dot{M}_{i,n_c+2} - [L_0\, x_{i,0} - L_{n_c+2}\, x_{i,n_c+2} & \\
-V_{n_c+2}\, y_{i,n_c+2}] &= 0 \\
\dot{E}_1 - [L_2\, H_2^l - L_2\, H_1^l - V_1\, H_1^v & \\
+F_1^l\, H_{f,1}^l + F_1^v\, H_{f,1}^v + Q_{\text{leak},n}] &= 0 \\
\dot{E}_n - [L_{n+1}\, H_{n+1}^l + V_{n-1}\, H_{n-1}^v - L_n\, H_n^l & \\
-V_n\, H_n^v + F_n^l\, H_{f,n}^l + F_n^v\, H_{f,n}^v + Q_{\text{leak},n}] &= 0 \\
V_{n_c}(1 - r_{\text{draw}}) H_{n_c}^v - L_{n_c+1} H_{n_c+1}^l - Q &= 0 \\
L_0(H_0^l - H_{n_c+2}^l) - V_{n_c+2}(H_{n_c+2}^v - H_{n_c+2}^l) + Q &= 0 \\
\textstyle\sum_{i \in I}\, x_{i,n} - 1 &= 0 \\
\textstyle\sum_{i \in I}\, y_{i,n} - 1 &= 0 \\
y_{i,n} - K_{i,n}\, x_{i,n} &= 0 \\
y_{i,n}^* - K_{i,n}\, x_{i,n} &= 0 \\
y_{i,n} - [y_{i,n-1} + \eta(y_{i,n}^* - y_{i,n})] &= 0 \\
x_{i,n_c+1} - y_{i,n_c} &= 0
\end{aligned}
$$

$$h_n - h_{\text{weir}} - 1.41[L_n/(\sqrt{g}\,\rho_n^l\,l_{\text{weir}})]^{2/3} = 0$$

$$h_n - M_n/(\rho_n^l A_{\text{tray}}) = 0$$

$$P_n - \left(\frac{R\,T_n}{\bar{V}_n^v - b_n} - \frac{a_n}{(\bar{V}_n^v - 0.414\,b_n)(\bar{V}_n^v + 2.414\,b_n)}\right) = 0$$

$$P_{n-1} - P_n - \Delta P_n = 0$$

$$\Delta P_n - \alpha\,\rho_{n-1}^v w_{n-1}^v [V_{n-1}/(\rho_{n-1}^v A_{\text{hole}})]^2 - \beta\,\rho_n^l\,w_n^l\,g\,h_n = 0$$

$$\Delta P_{n_c+1} - \alpha\,V_{n_c}^2 = 0$$

$$P_{n_c+1} - [\textstyle\sum_{i\in I} x_{i,n_c+1}\,P_{i,n_c+1}^{\text{sat}}] = 0$$

$$P_{n_c+2} - P_{\text{reb}} = 0$$

$$H_n^l - [\textstyle\sum_{i\in I} x_{i,n}\,h_{i,n}^l] = 0$$

$$H_n^v - [\textstyle\sum_{i\in I} y_{i,n}\,h_{i,n}^v] = 0$$

$$E_n - [M_n \textstyle\sum_{i\in I} x_{i,n}\,h_{i,n}^l] = 0$$

$$\Delta T_{\text{irc}} - (T_{n_c+1} - T_{n_c+2}) = 0$$

$$T_0 - T_1 = 0$$

$$Q_{\text{leak},n} - (UA)_n(T_{\text{ambient}} - T_n) = 0$$

$$Q - (UA)_{\text{irc}}\,\Delta T_{\text{irc}} = 0$$

$$(UA)_{\text{irc}}/(UA)_{\text{irc}}^{\text{base}} - (L_{n_c+1}/\bar{L}_{n_c+1})^{0.8} = 0$$

$$v_{\text{reb}} - M_{n_c+2}/\rho_{n_c+2}^l = 0$$

$$v_{\text{sump}} - M_0/\rho_0^l = 0$$

$$l_{\text{sump}} - v_{\text{sump}}/v_{\text{sump}}^{\text{cap}} = 0$$

$$L_{n_c+2} - [L_{\text{reb}}^{ss} + K_{c_2}(l_{\text{reb}} - l_{\text{reb}}^{ss})] = 0$$

$$L_0 - [L_{\text{sump}}^{ss} + K_{c_1}(l_{\text{sump}} - l_{\text{sump}}^{ss})] = 0$$

Spatial collocation of distillation column

As has been previously mentioned, to reduce the size of the model spatial collocation is used for the middle section of the column. The collocation points can be thought of as trays (however they do not need to have an integer value) and column conditions between collocation points are estimated using Lagrange polynomials. Thus we only perform mass and energy balances around the spatial collocations points (where there are fewer collocation points than trays in the distillation). Thus an example of a component balance around a collocation point is seen below:

$$\dot{M}_{i,s_k} - [\bar{L}(s_k+1)\,\bar{x}_i(s_k+1) + \bar{V}(s_k+1)\,\bar{y}_i(s_k+1) - \bar{L}(s_k)\,\bar{x}_i(s_k+1) \\ -\bar{V}(s_k)\,\bar{y}_i(s_k)] = 0$$

Where s_k is the k^{th} collocation point and s_k+1 and s_k-1 represent "one tray above" and "one tray below" the collocation point s_k. $\bar{L}$ and $\bar{V}$ are Lagrange polynomials that interpolate the collocation points for the liquid and vapour flow leaving each tray. $\bar{x}_i$ and $\bar{y}_i$ are the Lagrange polynomials for the liquid and vapour fractions for component i. These Lagrange polynomials are defined by:

$$\bar{L}(s) = \sum_{j=1}^{K+1} W_j^l(s)\,L_{s_j} \quad \bar{x}_i(s) = \sum_{j=1}^{K+1} W_j^l(s)\,x_{s_j,i}$$

$$\bar{V}(s) = \sum_{j=0}^{K} W_j^v(s)\,V_{s_j} \quad \bar{y}_i(s) = \sum_{j=0}^{K} W_j^v(s)\,y_{s_j,i}$$

Where L_{s_j} and V_{s_j} are the liquid and vapour flow at the j^{th} collocation point and $x_{s_j,i}$ and $y_{s_j,i}$ are the liquid and vapour fractions for component i at the j^{th} collocation point. $W_j^l(s)$ and $W_j^v(s)$ are Lagrange polynomial basis functions that as defined by:

$$W_j^l(s) = \prod_{\substack{z=0 \\ z\neq j}}^{K+1} \frac{s - s_z}{s_j - s_z}$$

$$W_j^v(s) = \prod_{\substack{z=0 \\ z\neq j}}^{K} \frac{s - s_z}{s_j - s_z}$$

Thus we see $\bar{L}(s_k) = L_{s_k}$ and this holds true for the other Lagrange polynomials. For further information on the spatial collocation method with regards to ASUs see [Cao *et al.*, 2016a].

Primary Heat Exchange (PHX)

The primary heat exchanger is a plate and fin heat exchanger used to cool the incoming air stream into the column and heat the product and waste streams. The heat exchanger consists of three streams, the feed of air for the compressor, the N_2 product from the top of the column and the vapor waste from the IRC. The PHX is split into two zones, in Zone 1 all three streams are vapor, and in Zone 2 the feed air stream is liquid. The full order model of the PHX divided the heat exchanger into segments where energy balances are constructed around the segment and includes the temperature of the metal wall of the PHX in that segment. However, as for the column, the size of the model is reduced by using spatial collocation for Zone 1. The collocation points are analogous to the segments in the PHX for Zone 1. In the full order model there was only one segment in Zone 2, and that remains true for the

reduced order model. The design variables in this unit are the length of Zone 1 and Zone 2.

PHX Model Variable Description

Index	
$k \in K$	zone $K := \{1, 2\}$
$j \in J$	stream $J := \{1, 2, 3\}$
	$1 :=$ cold waste, $2 :=$ cold N_2 product, $3 :=$ hot air
$n \in N_k$	The number of collocation points (Zone 1) or segments (Zone 2)
	$N_k := \{1, \ldots, n_{c,k}\}$ in zone k
$s_n \in S_k$	The set of collocation points (Zone 1) or segments (Zone 2)
	$S_k := \{s_1 \ldots s_{n_{c,k}}\}$
	For Zone 2, $n_{c,2} = 1$ and since there is no collocation $s_1 = 1$
$i \in I$	component $I := \{1, 2, 3\}$, $1 := N_2$, $2 := O_2$, $3 := Ar$
l	liquid (superscript)
v	vapor (superscript)
Variable	**Description**
E_{k,j,s_n}	energy holdup at the n^{th} collocation point
T_{k,j,s_n}	temperature at the n^{th} collocation point
T^m_{k,s_n}	metal wall temperature at the n^{th} collocation point
$T_{j,\text{in}}$	stream inlet temperature
$T_{j,\text{out}}$	stream outlet temperature
$T_{j,\text{pur}}$	purge point temperature
$(UA)_{k,j}$	lumped heat transfer coefficient
H_{k,j,s_n}	molar enthalpy at the n^{th} collocation point
$H_{j,\text{in}}$	stream inlet molar enthalpy
$H_{j,\text{out}}$	stream outlet molar enthalpy
$H_{j,\text{pur}}$	purge point molar enthalpy
$h_{k,j,s_n,i}$	component molar enthalpy at the n^{th} collocation point
$F_{k,j}$	molar flow rate
$y_{j,i}$	vapor composition
$x_{3,i}$	liquid composition
$V_{k,j}$	volume of stream in zone
V_j^{slot}	volume of fin
V_j^{layer}	volume of layer of fins
P_{k,j,s_n}	pressure at the n^{th} collocation point
$\Delta P_{k,j}$	pressure drop at the n^{th} collocation point
$P_{j,\text{in}}$	stream inlet pressure
$P_{j,\text{out}}$	stream outlet pressure
$P_{j,\text{pur}}$	purge point pressure
$\bar{V}^v_{k,j,s_n}$	vapor phase molar volume at the n^{th} collocation point

PHX Model Variable Description

Variable	**Description**
$\bar{V}^v_{k,j,s_n}$	vapor phase molar volume at the n^{th} collocation point
m_{k,s_n}	mass of metal
ρ_{k,j,s_n}	molar density at the n^{th} collocation point
$\rho_{k,j,s_n,i}$	component molar density at the n^{th} collocation point
ρ_m	specific density
a_{k,j,s_n}	Peng-Robinson EOS parameter
b_{k,j,s_n}	Peng-Robinson EOS parameter
l_1	length of zone 1
l_2	length of zone 2

PHX Model Parameters

Parameter	**Description**
ρ_m	metal wall density
C_p	aluminum heat capacity
b_j	parting sheet distance for stream j
N_j	fins per inch for stream j
n_j	number of layers for stream j
t_{fin_j}	fin thickness for stream j
t_{edge}	thickness of PHX shell
W	PHX width
H	PHX height
$n_{c,1}$	number of collocation points in zone 1
$\bar{a}^v_i, \bar{b}^v_i, \bar{c}^v_i, \bar{d}^v_i$	vapour enthalpy parameter
$e_{k,j}$	pressure drop parameter
$(UA)^{\text{base}}_{k,j}$	base coefficient
$F^{\text{base}}_{k,j}$	base flow rate

PHX Subexpressions

$$\rho^l_{2,3,1,i} := \frac{P^c_i}{R\,T^c_i}\, r_i^{-[1+(1-T_{2,3,1}/T^c_i)^{2/7}]}$$

$$\rho^l_{2,3,1} := \textstyle\sum_{i\in I}\, x_{3,i}\, \rho^l_{2,3,1,i}$$

$$\rho^v_{1,j,s_n} := 1/\bar{V}^v_{1,j,s_n}$$

$$\rho^v_{2,j,1} := 1/\bar{V}^v_{2,j,1}$$

$$\bar{h}^v_{1,j,s_n,i} := (\bar{a}^v_i\, P_{1,j,s_n} + \bar{b}^v_i)T_{1,j,s_n} + \bar{c}^v_i P_{1,j,s_n} + \bar{d}^v_i$$

$$h^v_{2,j,1,i} := (a^v_i\, P_{2,j,1} + b^v_i)T_{2,j,1} + c^v_i P_{2,j,1} + d^v_i$$

$$h^l_{2,3,1,i} := a^l_i\, T_{2,3,1} + b^l_i$$

$$h^v_{j,\mathrm{pur},i} := (a^v_i\, P_{j,\mathrm{pur}} + b^v_i)T_{j,\mathrm{pur}} + c^v_i P_{j,\mathrm{pur}} + d^v_i$$

$$h^v_{j,\mathrm{in},i} := (a^v_i\, P_{j,\mathrm{in}} + b^v_i)T_{j,\mathrm{in}} + c^v_i P_{j,\mathrm{in}} + d^v_i$$

$$h^v_{3,\mathrm{in},i} := (\bar{a}^v_i\, P_{3,\mathrm{in}} + \bar{b}^v_i)T_{3,\mathrm{in}} + \bar{c}^v_i P_{3,\mathrm{in}} + \bar{d}^v_i$$

$$h^v_{j,\mathrm{out},i} := (a^v_i\, P_{j,\mathrm{out}} + b^v_i)T_{j,\mathrm{out}} + c^v_i P_{j,\mathrm{out}} + d^v_i$$

$$h^l_{3,\mathrm{out},i} := a^l_i\, T_{3,\mathrm{out}} + b^l_i$$

$$f_i := 0.37464 + 1.54226\,\omega_i - 0.26992\,\omega_i^2$$

$$b_i := 0.0778\, R\, T^c_i / P^c_i$$

$$b_j := \textstyle\sum_{i=1}^{n_c} y_{j,i}\, b_i$$

$$a_{k,j,s_n,i} := \frac{0.45724(R\,T^c_i)^2}{P^c_i}[1 + f_i\,(1 - \sqrt{T_{k,j,s_n}/T^c_i})]^2$$

$$a_{k,j,s_n} := \textstyle\sum_{i=1}^{n_c}\sum_{r=1}^{n_c} y_{j,i}\, y_{j,r}(a_{k,j,s_n,i}\, a_{k,j,s_n,r})^{0.5}(1 - k_{ir})$$

PHX DAE

$$\dot{E}_{1,j,s_n} - (F_{1,j}(\bar{H}^v_{1,j}(s_n+1) - H^v_{1,j,s_n}) + (UA)_{1,j}(T^m_{1,s_n} - T_{1,j,s_n})) = 0$$

$$\dot{E}_{1,j,s_{n_{c,1}}} - (F_{1,j}(H^v_{j,\text{pur}} - H^v_{1,j,s_{n_{c,1}}}) + (UA)_{1,j}(T^m_{1,s_{n_{c,1}}} - T_{1,j,s_{n_{c,1}}})) = 0$$

$$\dot{E}_{1,3,s_1} - (F_{1,3}(H^v_{3,\text{in}} - H^v_{1,3,s_1}) + (UA)_{1,3}(T^m_{1,s_1} - T_{1,3,s_1})) = 0$$

$$\dot{E}_{1,3,s_n} - (F_{1,3}(\bar{H}^v_{1,3}(s_n-1) - H^v_{1,3,s_n}) + (UA)_{1,3}(T^m_{1,n} - T_{1,3,n})) = 0$$

$$\dot{E}_{2,j,1} - (F_{2,j}(H^v_{j,\text{in}} - H^v_{j,\text{pur}}) + (UA)_{2,j}(T^m_{2,1} - T_{2,j,1})) = 0$$

$$\dot{E}_{2,3,1} - (F_{2,3}(H^v_{3,\text{pur}} - H^l_{3,\text{out}}) + (UA)_{2,3}(T^m_{2,1} - T_{2,3,1})) = 0$$

$$m_k\, C_p\, \dot{T}^m_{k,s_n} - [\textstyle\sum_{j\in J} (UA)_{k,j}(T_{k,j,n} - T^m_{k,s_n})] = 0$$

$$E_{1,j,s_n} - H^v_{1,j,s_n}\, V_{1,j}\, \rho^v_{1,j,s_n} = 0$$

$$E_{2,j,1} - H^v_{2,j,1}\, V_{2,j}\, \rho^v_{2,j,1} = 0$$

$$E_{2,3,1} - H^l_{2,3,1}\, V_{2,3}\, \rho^l_{2,3,1} = 0$$

$$T_{2,j,1} - (T_{j,\text{pur}} + T_{j,\text{in}})/2 = 0$$

$$T_{2,3,1} - (T_{3,\text{pur}} + T_{3,\text{out}})/2 = 0$$

$$T_{j,\text{out}} - T_{1,j,s_1} = 0$$

$$T_{3,\text{pur}} - T_{1,3,s_{n_{c,1}}} = 0$$

$$H^v_{1,j,s_n} - [\textstyle\sum_{i\in I}\, y_{j,i}\, h^v_{1,j,s_n,i}] = 0$$

$$H^v_{j,\text{in}} - [\textstyle\sum_{i\in I}\, y_{j,i}\, h^v_{j,\text{in},i}] = 0$$

$$H^v_{j,\text{out}} - [\textstyle\sum_{i\in I}\, y_{j,i}\, h^v_{j,\text{out},i}] = 0$$

$$H^l_{3,\text{out}} - [\textstyle\sum_{i\in I}\, x_{3,i}\, h^l_{3,\text{out},i}] = 0$$

$$H^v_{j,\text{pur}} - [\textstyle\sum_{i\in I}\, y_{j,i}\, h^v_{j,\text{pur},i}] = 0$$

$$H^v_{2,j,1} - [\textstyle\sum_{i\in I}\, y_{j,i}\, h^v_{2,j,1,i}] = 0$$

$$H^l_{2,3,1} - [\textstyle\sum_{i\in I}\, x_{3,i}\, h^l_{2,3,1,i}] = 0$$

$$(UA)_{k,j} - (UA)^{\text{base}}_{k,j}(F_{k,j}/F^{\text{base}}_{k,j})^{0.8} = 0$$

$$P_{1,j,s_n} - \left(\frac{R\,T_{1,j,s_n}}{\bar{V}^v_{1,j,s_n} - b_j} - \frac{a_{1,j,s_n}}{(\bar{V}^v_{1,j,s_n} - 0.414\,b_j)(\bar{V}^v_{1,j,s_n} + 2.414\,b_j)} \right) = 0$$

$$P_{2,j,1} - \left(\frac{R\,T_{2,j,1}}{\bar{V}^v_{2,j,1} - b_j} - \frac{a_{2,j,1}}{(\bar{V}^v_{2,j,1} - 0.414\,b_j)(\bar{V}^v_{2,j,1} + 2.414\,b_j)} \right) = 0$$

$$P_{2,j,1} - (P_{j,\text{pur}} + P_{j,\text{in}})/2 = 0$$

$$P_{2,3,1} - (P_{3,\text{pur}} + P_{3,\text{out}})/2 = 0$$

$$\Delta P_{k,j} - e_{k,j} F^{0.5}_{k,j} = 0$$

$$P_{j,\text{pur}} - (P_{j,\text{in}} + \Delta P_{2,j}) = 0$$

$$P_{3,\text{pur}} - (P_{3,\text{in}} - \Delta P_{1,3}) = 0$$

$$P_{j,\text{out}} - (P_{j,\text{pur}} + \Delta P_{1,j}) = 0$$

$$P_{3,\text{out}} - (P_{3,\text{pur}} - \Delta P_{2,3}) = 0$$

$$P_{1,j,1} - P_{j,\text{out}} = 0$$

$$P_{1,j,s_n} - (\bar{P}_{1,j}(s_n - 1) - \Delta P_{1,j}/(s_{n_{c,1}} - 1)) = 0$$

$$P_{1,3,s_n} - (P_{3,\text{in}} - n\,\Delta P_{1,3}/s_{n_{c,1}}) = 0$$

In the above DAE we see the Lagrange polynomials $\bar{H}^v_{1,j}(s)$ and $\bar{P}_{1,j}(s_n - 1)$ which are the Lagrange polynomials representing the profiles of the vapor molar enthalpy and pressure respectively. These are given by the expressions:

$$\bar{H}^{v}_{1,j}(s) = \sum_{n=1}^{n_{c,1}} W_n(s)\, H_{1,j,s_n}$$
$$\bar{P}_{1,j}(s) = \sum_{n=1}^{n_{c,1}} W_n(s)\, P_{1,j,s_n}$$
$$W_n(s) = \prod_{\substack{z=1 \\ z \neq n}}^{n_{c,1}} \frac{s - s_z}{s_n - s_z}$$

Air compressor model

The air compressor consists of multiple stages. The compressor is modelled solely by algebraic equations. The discharge pressure of air feed is calculated using regression equations from data provided by Praxair Inc. The power required by the compressor is assumed to be the theoretical power required by the compressor which can be found through given equations. The surge line (so we can find the minimum flow necessary to the compressor) is also estimated using a regression equation from data provided by our industrial partner. The control variable is the air feed to the compressor. The design variable in this unit is the maximum power to the compressor.

Compressor Model Variable Description

Index	
$k \in K$	$K := \{\text{in}, \text{out}\}$
$i \in I$	component $I = \{1, 2, 3\}$, $1 := N_2$, $2 := O_2$, $3 := Ar$
$j \in J$	$J := \{1, 2, 3\}$
in	inlet
out	outlet
v	vapor
Variable	**Description**
T_k	temperature
P_k	pressure
Z_k	compressibility
$\bar{V}_k^v$	molar volume
F_{in}	molar flow rate
$\dot{V}_{\text{in}}^{\text{std}}$	standard volumetric flow rate
$\dot{V}_{\text{in}}^{\text{reg}}$	transformed volumetric flow rate for compressor map
$\dot{V}_{\text{in}}^{\text{sur}}$	volumetric flow rate at compressor surge
y_i	feed composition
α	inlet vane guide angle

Compressor Model Parameters

Parameter	**Description**
$\rho_{\text{in}}^{\text{std}}$	air molar density
n	poly index
η_p	poly efficiency
n_{stg}	number of stages
$m_{a,j}$	parameter to determine discharge pressure
$m_{b,j}$	parameter to determine discharge pressure
$m_{c,j}$	parameter to determine discharge pressure
$m_{d,j}$	parameter to determine discharge pressure
$m_{e,j}$	parameter to determine surge line

Air Compressor Subexpressions

$$b_i := 0.0778\, R\, T_i^c / P_i^c \qquad \forall\ i \in I$$

$$b := \textstyle\sum_{i=1}^{n_c} y_i\, b_i$$

$$f_i := 0.37464 + 1.54226\, \omega_i - 0.26992\, \omega_i^2$$

$$a_{k,i} := \tfrac{0.45724 (R\, T_i^c)^2}{P_i^c} [1 + f_i\, (1 - \sqrt{T_k / T_i^c})]^2$$

$$a_k := \textstyle\sum_{i=1}^{n_c} \sum_{j=1}^{n_c} y_i\, y_j (a_{k,i}\, a_{k,j})^{0.5} (1 - k_{ij})$$

$$w := \textstyle\sum_{i \in I} w_i\, y_i$$

Air Compressor Algebraic Equations

$$
\begin{aligned}
P_k - \left(\frac{R\,T_k}{\bar{V}_k^v - b} - \frac{a_k}{(\bar{V}_k^v - 0.414\,b)(\bar{V}_k^v + 2.414\,b)} \right) &= 0 \\
\dot{V}_{\text{in}}^{\text{std}} \rho_{\text{in}}^{\text{std}} - F_{\text{in}} &= 0 \\
\dot{V}_{\text{in}}^{\text{reg}} - \exp(\dot{V}_{\text{in}}^{\text{std}} \cdot 10^{-4}) \cdot 10^{-7} &= 0 \\
P_{\text{out}} - \left(a\,(\dot{V}_{\text{in}}^{\text{reg}})^3 + b\,(\dot{V}_{\text{in}}^{\text{reg}})^2 + c\,\dot{V}_{\text{in}}^{\text{reg}} + d \right) &= 0 \\
Z_k\,R\,T_k - P_k \bar{V}_k^v &= 0 \qquad \forall\ k \in K \\
Z_{\text{avg}} - (Z_{\text{in}} + Z_{\text{out}})/2 &= 0 \\
r_p^{n_{\text{stg}}} P_{\text{in}} - P_{\text{out}} &= 0 \\
H_{\text{poly}} - Z_{\text{avg}}\,R/w\,T_{\text{in}}\,n/(n-1)(r_p^{(n-1)/n} - 1) &= 0 \\
W - n_{\text{stg}}\,F_{\text{in}}\,w\,H_{\text{poly}}/\eta_{\text{poly}} &= 0 \\
T_{\text{out}} - T_{\text{in}}\,r_p^{(n-1)/n} &= 0 \\
\dot{V}_{\text{in}}^{\text{sur}} - e &= 0 \\
\log_{10}(-a) - (m_{a,1}\,\alpha^2 + m_{a,2}\,\alpha + m_{a,3}) &= 0 \\
\log_{10}(b) - (m_{b,1}\,\alpha^2 + m_{b,2}\,\alpha + m_{b,3}) &= 0 \\
\log_{10}(-c) - (m_{c,1}\,\alpha^2 + m_{c,2}\,\alpha + m_{c,3}) &= 0 \\
d - (m_{d,1}\,\alpha^2 + m_{d,2}\,\alpha + m_{d,3}) &= 0 \\
e - (m_{e,1}\,\alpha^2 + m_{e,2}\,\alpha + m_{e,3}) &= 0
\end{aligned}
$$

Turbine model

The air exiting the PHX is further cooled using a turbine. The state of the turbine is determined by a set of correlations relating the polytropic head, volumetric flow rate

and fan speed of the turbine, as well some of the theoretical calculations also seen in the compressor equations.

Turbine Model Variables

Index	
$k \in K$	$K := \{\text{in}, \text{out}\}$
Variable	**Description**
T_k	temperature
P_k	pressure
Z_k	compressibility
$\bar{V}_k^v$	molar volume
F_{in}	molar flow rate
y_i	feed composition
u	turbine fan speed

Turbine Model Parameters

Parameter	**Description**
n	polytropic index
a	speed parameter
b	speed parameter
c	head parameter
d	head parameter

Turbine Subexpressions

$$
\begin{aligned}
P_i^{\text{sat}} &:= \exp(A_i + B_i/(T_{\text{dew}} + C_i)) \\
b_i &:= 0.0778\, R\, T_i^c / P_i^c \\
b &:= \textstyle\sum_{i=1}^{n_c} y_i\, b_i \\
f_i &:= 0.37464 + 1.54226\, \omega_i - 0.26992\, \omega_i^2 \\
a_{k,i} &:= \tfrac{0.45724 (R\, T_i^c)^2}{P_i^c} [1 + f_i\, (1 - \sqrt{T_k / T_i^c})]^2 \\
a_k &:= \textstyle\sum_{i=1}^{n_c} \sum_{j=1}^{n_c} y_i\, y_j (a_{k,i}\, a_{k,j})^{0.5} (1 - k_{ij}) \\
w &:= \textstyle\sum_{i \in I} w_i\, y_i
\end{aligned}
$$

Turbine Algebraic Equations

$$
\begin{aligned}
P_k - \left(\frac{R\, T_k}{\bar{V}_k^v - b} - \frac{a_k}{(\bar{V}_k^v - 0.414\, b)(\bar{V}_k^v + 2.414\, b)} \right) &= 0 \\
u - (a\, F_{\text{in}} + b) &= 0 \\
H_{\text{poly}} - (c\, u^2 + d) &= 0 \\
Z_k\, R\, T_k - P_k \bar{V}_k^v &= 0 \\
Z_{\text{avg}} - (Z_{\text{in}} + Z_{\text{out}})/2 &= 0 \\
r_p\, P_{\text{in}} - P_{\text{out}} &= 0 \\
H_{\text{poly}} - Z_{\text{avg}}\, R/w\, T_{\text{in}}\, n/(n-1)(r_p^{(n-1)/n} - 1) &= 0 \\
T_{\text{out}} - T_{\text{in}}\, r_p^{(n-1)/n} &= 0 \\
P_{\text{out}} \textstyle\sum_i y_i / P_i^{\text{sat}} - 1 &= 0
\end{aligned}
$$

Appendix B

Parameters for 2 CSTR Model

Symbol	Description and steady-state values
$c_{A,F1}$	concentration of A in feed to Reactor 1, 20 mol/m^3
$c_{B,F1}$	concentration of B in feed to Reactor 1, 0 mol/m^3
$c_{C,F1}$	concentration of C in feed to Reactor 1, 0 mol/m^3
$c_{A,M}$	concentration of A in feed to Mixer, 20 mol/m^3
$c_{B,M}$	concentration of B in feed to Mixer, 0 mol/m^3
$c_{C,M}$	concentration of C in feed to Mixer, 0 mol/m^3
E_I/R	activation energy of main reaction, A $\rightarrow$ B, 6000 K
E_{II}/R	activation energy of side reaction, B $\rightarrow$ C, 4500 K
$k_{0,I}$	main reaction rate constant, 2.7×10^8 s^{-1}
$k_{0,II}$	side reaction rate constant, 160 s^{-1}
$q_{cool,1}$	cooling rate for the Reactor 1, m^{3}K/s
$q_{cool,2}$	cooling rate for the Reactor 2, m^{3}K/s
Q_{c1}	cooling water flow to Reactor 1, 0.7 m^3/s
Q_{c2}	cooling water flow to Reactor 2, 0.7 m^3/s
$T_{c1,in}$	inlet cooling water temperature to Reactor 1, 300 K
$T_{c2,in}$	inlet cooling water temperature to Reactor 2 , 275 K
T_{F1}	temperature of feed flow to Reactor 1, 300 K
T_M	temperature of feed flow to the Mixer, 300 K
U_{a1}	heat transfer coefficient in Reactor 1, 0.35 m^3/s
U_{a2}	heat transfer coefficient in Reactor 2, 0.35 m^3/s

Notes:

In the two-stage stochastic formulation all parameters that are rates have their time units changed from seconds to minutes.

To slow down the dynamic in the two-stage stochastic optimization rate constants $k_{0,I}$ and $k_{0,II}$ are multiplied by 0.25.

Backward Euler Method

The Backward Eueler method is a technique used in simultaneous methods to convert a DAE into a set of algebraic equations. The concept of the Backward Euler method is as follows, given the first order differential equation:

$$\frac{dx(t)}{dt} = f(x,t)$$
$$x(t_o) = x_0$$

To estimate the profile of $x(t)$ from t_o to t_f we will discretize $x(t)$ into $\frac{t_f - t_o}{h}$ values, where h is the time step between each discretized value of $x(t)$. Let the next value of $x(t)$ we calculated be x_k, $(k = 1)$ where x_k is an approximate value of $x(t_o + kh)$. Given $\frac{dx(t)}{dt} = f(x,t)$, we see that at $t = t_o + h = t_1$, the slope of the tangent line at x_1 is $f(x_1, t_1)$. If $x(t_o + h)$ is sufficiently close to $x(t_o)$ (i.e h is a small value) then the approximation of $x(t_o + h)$ (x_1) can be given as:

$$x_1 = hf(x_1, t_1) + x_0$$

Thus if we know x_0, the entire profile of $x(t)$ in terms of its discretized approximations

can be found by solving the above equation to find x_1, and then replacing x_0 with x_1 and solving the resulting equation for x_2 and so on. Backward Euler is an implicit method as x_k is expressed as a function of x_k, and thus an equation must be solved. However since we are using this to discretize a DAE, where a system of algebraic equations will have to be solved anyway, this does not pose much difficulty. Using the Backward Euler method we can convert the differential equations in the DAE into algebraic equations. Thus the DAE is converted into a set of algebraic equations and the entire optimization problem is solved as an NLP. Using Backward Euler, a dynamic optimization problem can be converted into an NLP as seen below:

$$\min_{u_o, u_1 \ldots . u_f} \int_{t_o}^{t_f} \phi(\mathbf{x}(t), \mathbf{y}(t), \mathbf{u}(t), \mathbf{p})$$

$$\text{s.t}$$

$$\mathbf{f}(\mathbf{x}(t), \mathbf{y}(t), \mathbf{u}(t), \mathbf{p}) = \dot{\mathbf{x}}(t)$$

$$\mathbf{h}(\mathbf{x}(t), \mathbf{y}(t), \mathbf{u}(t), \mathbf{p}) = 0$$

$$\mathbf{g}(\mathbf{x}(t), \mathbf{y}(t), \mathbf{u}(t), \mathbf{p}) \leq 0$$

$$\boldsymbol{\kappa}(\mathbf{x}(t_i), \mathbf{y_i}(t), \mathbf{u_i}(t), \mathbf{p}) \leq 0 \quad \forall i \in \{0, \ldots . n\}$$

$$\mathbf{x}(0) = \mathbf{x_o}$$

Where $\mathbf{x}$, $\mathbf{y}$ and $\mathbf{u}$ are the differential, algebraic and control variables respectively, and $\mathbf{p}$ are parameters in the optimization. $\mathbf{f}$ and $\mathbf{h}$ are the differential and algebraic equations that make up the differential algebraic equations (DAE) that govern the system being optimized. $\mathbf{g}$ and $\boldsymbol{\kappa}$ are the path constraints and point constraints respectively.

Using the Backward Euler method, the above formulation can be converted into an NLP as seen in the following formulation:

$$\min_{\substack{u_0,u_1....u_n \\ x_0,x_1....x_n \\ y_0,y_1....y_n}} h\sum_{k=0}^{n}\phi(\mathbf{x_k},\mathbf{y_k},\mathbf{u_k},\mathbf{p})$$

s.t

$$h\cdot\mathbf{f}(\mathbf{x_{k+1}},\mathbf{y_{k+1}},\mathbf{u_{k+1}},\mathbf{p})=\mathbf{x_{k+1}}-\mathbf{x_k}$$

$$\mathbf{h}(\mathbf{x_{k+1}},\mathbf{y_{k+1}},\mathbf{u_{k+1}},\mathbf{p})=0$$

$$\mathbf{g}(\mathbf{x_{k+1}},\mathbf{y_{k+1}},\mathbf{u_{k+1}},\mathbf{p})\leq 0$$

$$\boldsymbol{\kappa}(\mathbf{x_{k+1}},\mathbf{y_{k+1}},\mathbf{u_{k+1}},\mathbf{p})\leq 0 \quad \forall k\in\{0,....n-1\}$$

$$\mathbf{x}(0)=\mathbf{x_o}$$

$$n=\frac{t_f-t_o}{h}$$